UNIVERSITÀ DEGLI STUDI DI PADOVA

Dipartimento di Geoscienze
Direttore Prof. Fabrizio Nestola

TESI DI LAUREA MAGISTRALE IN
GEOLOGIA E GEOLOGIA TECNICA

# CRYSTALLOGRAPHIC ORIENTATIONS AND TIMING RELATIONSHIPS OF CLINOPYROXENE INCLUSIONS IN DIAMOND

*Relatore: Prof. Fabrizio Nestola*
*Correlatore: Dr. Leonardo Pasqualetto*

*Laureando: Pia Antonietta Antignani*

ANNO ACCADEMICO 2018 / 2019

*“Donec ad metam”*

(Gabriele d’Annunzio, 9.VIII.1918)

# Abstract

Diamonds are the deepest "fragments" of the primordial Earth that reach the Earth's surface after traveling a long path through the interior of our planet. This makes diamonds small time capsules, which reveal crucial information about the geological processes that occurred within the inaccessible mantle regions throughout the Earth's history.

Since diamond is almost pure carbon and chemically inert mineral, its age and crystallization environment within the Earth's mantle have been constrained over the last 50 years from the study of its inclusions. Most of the early studies on diamonds assumed that these inclusions and diamonds are syngenetic, i.e., they crystallized simultaneously and from the same genetic process. However, recent studies have challenged the paradigm of syngenesis, suggesting that the major portion of minerals included in lithospheric diamonds, instead, were formed before diamond, and are called protogenetic.

This discovery has implications for all genetic aspects of diamond, particularly the timing of its crystallization. Indeed, syngenesis has been a long-standing prerequisite for dating diamond through the study of radiogenic isotopes contained within its mineral inclusions. One of the most widely used mineral inclusion for dating diamonds is clinopyroxene, which is amenable with Sm-Nd isotope system. Nonetheless, timing relationships (i.e., the syn- *versus* protogenetic nature) between clinopyroxenes and their host diamonds are still poorly known.

In this thesis work, by investigating the crystallographic orientation relationships (CORs) between clinopyroxene inclusions and lithospheric diamonds from the Voorspoed mine (South Africa), it has been provided the clear evidence of the protogenetic origin of clinopyroxene inclusions in diamonds.

The results of this thesis work, therefore, raise questions on the real meaning of many “diamond formation ages” obtained from clinopyroxene inclusions. In order to assess the impact of a protogenetic inclusion of clinopyroxene on the validity of diamond age obtained from it, it has been used a diffusion model at consistent pressure and temperatures for diamond formation within the Earth’s mantle. This model demonstrates that chemical re-equilibration of clinopyroxene inclusions with diamond-forming media occurred over a very long geological timescale. Therefore, diamond ages obtained through the dating of clinopyroxene inclusions are likely older than the diamond crystallization event; hence, the use of clinopyroxene is not recommended for the age determination of lithospheric diamonds.

# Riassunto

I diamanti sono i frammenti più profondi della Terra primordiale che raggiungono la superficie terrestre dopo aver percorso un lungo viaggio all'interno del nostro pianeta. Ciò rende i diamanti piccole capsule del tempo in grado di rivelare informazioni cruciali circa i processi geologici avvenuti nelle aree inaccessibili del mantello durante la storia della Terra.

Dal momento che il diamante è un minerale chimicamente inerte e costituito quasi esclusivamente da carbonio, la sua età e ambiente di cristallizzazione all'interno del mantello terrestre sono stati definiti, in oltre 50 anni di ricerca, attraverso lo studio delle sue inclusioni. La maggior parte dei primi studi sui diamanti ha assunto che tali inclusioni e i diamanti fossero singenetici, ossia formatisi simultaneamente e dallo stesso processo genetico. Tuttavia, recenti studi hanno messo in discussione il paradigma della singenesi, suggerendo che la maggior parte delle inclusioni minerali rinvenute all'interno dei diamanti litosferici, invece, si sono formate precedentemente rispetto al diamante, prendendo l'appellativo di protogenetiche.

Tale scoperta ha forti implicazioni per tutto ciò che concerne la genesi del diamante, in particolare il momento della sua cristallizzazione. Infatti, la singenesi è stata considerata un prerequisito fondamentale al fine di datare il diamante attraverso lo studio degli isotopi radiogenici veicolati dalle sue inclusioni minerali. Una delle inclusioni minerali più utilizzate per datare il diamante è il clinopirosseno, il quale è databile con il sistema isotopico Sm-Nd. Nonostante ciò, le relazioni di tempo (ossia, la natura sin-*versus* protogenetica) tra i clinopirosseni e i diamanti, all'interno dei quali sono contenuti, sono ancora poco note.

Nel presente lavoro di tesi, mediante l'analisi delle relazioni di orientazione cristallografica tra inclusioni di clinopirosseno e diamanti litosferici provenienti

dalla miniera di Voorspoed (Sud Africa), è stata fornita l'evidenza della chiara natura protogenetica dei clinopirosseni nei diamanti.

I risultati del presente lavoro di tesi, pertanto, conducono inevitabilmente a domandarsi quale sia il reale significato di molte età di formazione dei diamanti ottenute dalle inclusioni di clinopirosseno. Al fine di valutare l'impatto di un'inclusione protogenetica di clinopirosseno sulla validità dell'età del diamante da essa ottenuta, è stato utilizzato un modello di diffusione alle condizioni di pressione e temperatura di formazione del diamante all'interno del mantello terrestre. Tale modello dimostra che il ri-equilibrio chimico di un'inclusione di clinopirosseno con il mezzo da cui cristallizza il diamante avviene in tempi geologici estremamente lunghi. Pertanto, le età dei diamanti ottenute tramite la datazione delle inclusioni di clinopirosseno, sono presumibilmente antecedenti rispetto all'evento di cristallizzazione del diamante stesso e, quindi, il loro uso non è raccomandato per determinare l'età dei diamanti litosferici.

# Table of contents

# Chapter 1

# Introduction

## 1.1 Why study diamond?

Diamond is one of the three polymorphs of native carbon (the other two are graphite and lonsdaleite), with atoms arranged in dense cubic crystal structure that gives it unique chemical and physical properties. These peculiarities include extreme hardness and strength, high refractive index (n = 2.4) that makes diamond the most valuable gemstone, but also high thermal conductivity and low thermal expansion, both useful in many technological applications (Tappert et al., 2011). From a geological point of view, instead, diamond is thought to be one of the oldest natural materials on our Planet, with ages that cover a period ranging from 3.6 billion to 90 million years ago (e.g., Gurney et al., 2010). Thanks to its chemical inertness and resistance, diamond also represents a hermetic container for mineral and fluid inclusions, which are encapsulated during its growth in the deep Earth's mantle. As a result, diamonds and their pristine inclusions are among the most studied samples in the Earth Science, because they provide a glimpse of the primordial Earth, recording the geological processes of the deepest mantle, like the carbon cycle (e.g., Shirey et al., 2013).

## 1.2 Diamonds from the Earth's mantle

In nature, diamond is stable under high pressure and temperature conditions that are found principally at great depth inside the Earth's mantle, below of about 130-150

km (Stachel and Harris, 2008). Outside the mantle setting, diamonds can be occasionally found within crustal rocks in high-pressure metamorphic (UHPM) terranes or meteorites that have impacted on the Earth's surface (e.g., Shirey et al., 2013).

Within the mantle, the main geological context for diamond formation is the subcontinental lithospheric mantle (SCLM) under the ancient cratons, i.e., Archean to Proterozoic continental nuclei whose crust was thickened by early geological processes of plate tectonics. This because the downward-protruding keels, which characterize the SCLM, are extremely thick (extending up to 250 km), with low geothermal gradient, as well as seismically stability at least from 2.0 Gyr (e.g., Stachel and Harris, 2008; Shirey et al., 2013). The presence of very deprived isotherms under these cratonic areas allows to graphite-diamond transition reaction to translate upward, occurring at lower depths (i.e., lower pressure) to the adjacent and hotter asthenosphere (see Figure 1.1-1.2). The area where the SCLM overlaps the diamond stability field is called "*diamond window*," which typically extends from about 140 km to 200 km in-depth, along model geothermal gradient consistent with 40 $mW/m^2$ surface heat flow (Stachel and Harris, 2009, and references therein; see also Figure 1.1-1.2). This diamond window hosts diamonds classified as gem-quality or *lithospheric*, which were studied in this thesis work, and differ from the more rare *super-deep* or *sub-lithospheric* diamonds, which, instead, crystalize at greater depth (from about 300 km in depth) in the sublithospheric mantle (e.g., Stachel and Luth, 2015).

Therefore, diamond is not only a lithospheric mineral but, potentially, it can form in all the Earth's mantle in which diamond is stable, including the mantle beneath the lithosphere-asthenosphere boundary if enough free C-bearing phase and right redox conditions are present (e.g., Shirey et al., 2013). Diamond formation in the mantle is linked to metasomatic processes that involve C-O-H bearing fluids or melts, which act as primary metasomatic agents percolating through the mantle rocks, react with them, and crystallize diamond via redox reactions (e.g., Shirey et al., 2013). The precipitation of diamond from such a C-bearing mobile phases can occur either by reduction of oxidized species (e.g., $CO_3^{2-}$ or $CO_2$) interacting with

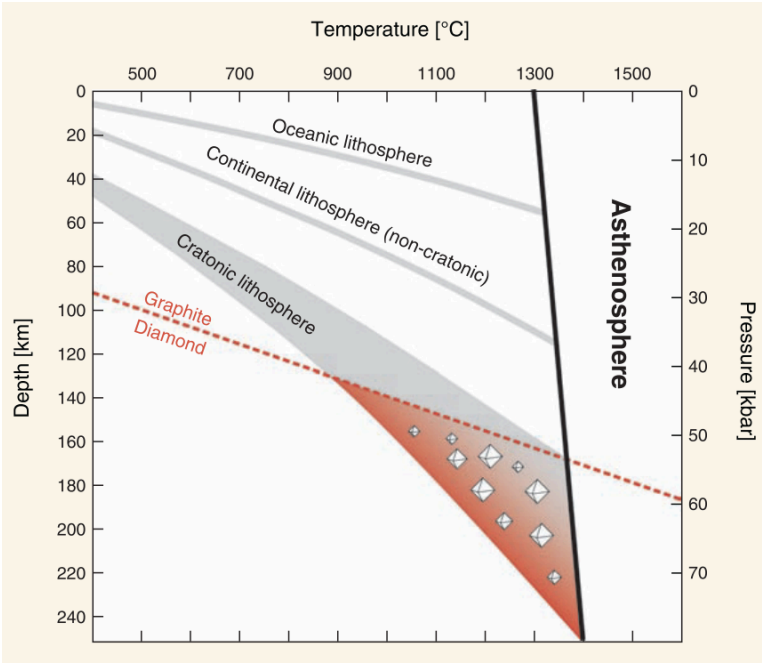


**Figure 1.1.** Phase diagram showing the cratonic lithosphere that overlaps the diamond stability field, forming the so-called "diamond window." This derived principally from the low geothermal gradient that characterizes the cratonic lithosphere, with a surface heat flow of about 40 mW/m$^2$, against the 65 mW/m$^2$ and 100 mW/m$^2$ in the case, respectively, of young continental (i.e., non-cratonic) and oceanic lithosphere (Hasterok and Chapman, 2011). The thick line is the 1300°C mantle adiabat (Hasterok and Chapman, 2011). The graphite/diamond transition reaction (red dashed line) has been recently corrected to lower pressure by Day (2012). From Tappert and Tappert (2011).

reduced wall rocks, or by oxidation of reduced species (e.g., $CH_4$), if the fluids/melts react with more oxidized wall rocks (Stachel and Luth, 2015). Alternatively, as have recently proposed Stachel and Luth (2015), diamonds can precipitate more efficiently by direct precipitation from the C-O-H fluids or melts (Stachel and Luth, 2015).

However, under the typical plume-related magmatism and relatively slow transport of diamond to the surface, it could re-equilibrate by either graphitization or more likely oxidation. The presence of diamond on the Earth's surface is then possible only thanks to very rare and explosive kimberlite or related magmas. These magmas are generated by low degree of partial melting in the deep mantle, at least at depth corresponding at the onset of the diamond stability field (i.e., at the base of SCLM or in the underlying transition zone), and are typically potassic, volatile and

MgO-rich, and not-oxidizing (e.g., Shirey et al., 2013). Due to their very rapid rise, the kimberlite can sample diamonds from the deep mantle, bringing them to the Earth's surface, where they can be found as accessory minerals in entrained peridotite or eclogite mantle xenoliths or as mineral xenocrysts if diamonds host rocks were disaggregated.

Kimberlites represent the primary source of diamonds, with 30% of them that are diamondiferous, and there is a strong relationship between them and the oldest portions of continental nuclei with melt-depleted lithospheric mantle keels (Shirey et al., 2013). This statement represents one of the essential guidelines in diamond exploration known as "*Clifford's Rule*." Contrary to what was believed in the past, the crystallization of diamond in the Earth's mantle is generally and genetically unrelated to host kimberlite magmatism (e.g., Stachel and Luth, 2015). Indeed, diamonds generally crystallized several hundreds of millions to billions of years before the kimberlitic volcanic events (e.g., Shirey et al. 2013).

Summing up, every diamond from the Earth's mantle begins its journey on the way of the Earth's surface on board of the kimberlitic magma, traveling through the Earth's mantle practically unaltered. However, because diamond is comprised mostly of carbon and is chemically inert, its structure and chemistry reveal little about its genesis and distribution within the mantle. If diamonds host fluid or mineral inclusions, from their geochemical, thermobarometric, and geochronological study, it is possible to constrain the conditions and timing of diamond crystallization. The application of the data extracted from mineral inclusions to diamond host relies on the long-standing assumption that diamond and its inclusions are syngenetic, i.e., they grew simultaneously and from the same medium. Nevertheless, recent studies have challenged the criteria used to define syngenesis, recognizing that silicate, sulfide and oxide inclusions typically considered syngenetic with diamond on the basis of their diamond-imposed morphology and supposed epitaxial relationship with diamond (e.g., Harris and Gurney, 1979), instead, crystallized before the diamond, i.e., are protogenetic (e.g., Thomassot et al., 2009; Nestola et al., 2014, 2019; Jacob et al., 2016; Milani et al., 2016). Therefore, it is vital to determine the so-called *timing relationship* between

diamond and its mineral inclusions (i.e., syngenesis *versus* protogenesis), because the protogenetic origin of inclusions in diamonds could have important implications for our understating of diamond growth within the Earth's mantle, as well as for the geological processes recorded by diamond.

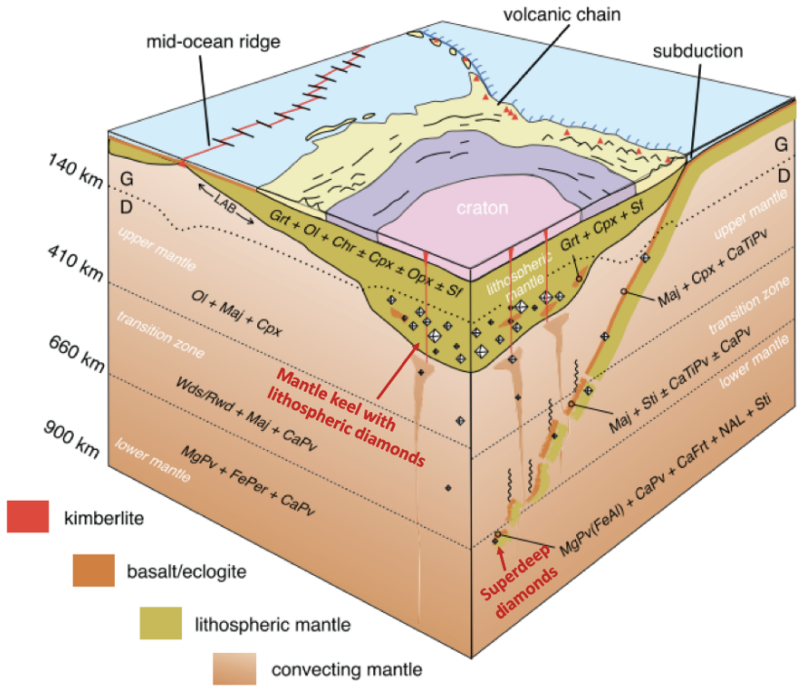


**Figure 1.2.** Block diagram showing the stable diamond regions in the Earth's mantle. G=graphite, D=diamond, LAB=lithosphere/asthenosphere boundary. Within the represented lithospheric mantle keel under continental craton are present lithospheric diamonds. The low geothermal gradient beneath the craton causes the graphite-diamond transition (black dotted line) to translates upward. In the convective mantle, instead, superdeep diamonds are formed. In the diagram are also indicated the mineralogical assemblages for peridotitic or ultramafic mantle rocks (left portion), and eclogitic or basaltic rocks (right portion), as a function of depth. These assemblages reflect the mineralogical associations found inside diamonds as mineral inclusions. Modified from Shirey et al. (2013).

## 1.3 The aim of this thesis

This thesis aims to better assess the *timing relationships* between clinopyroxene inclusions and their diamond hosts using a crystallographic approach. In detail, the crystallographic orientation relationships (CORs) between thirty-seven clinopyroxene inclusions still trapped within nine lithospheric diamonds from the Voorspoed kimberlite were analyzed (Kaapvaal craton, South Africa; see also Figure 1.3).

Clinopyroxene is one of the most important inclusions in lithospheric diamonds, and it is commonly used for dating diamond with the Sm-Nd isotopic method. Diamond age determination by dating clinopyroxene inclusions relies on the main assumption that they are syngenetic with their diamond hosts, principally based on morphological criteria. However, few studies have been carried out to discover the syngenetic *versus* protogenetic origin of these dated clinopyroxenes. If clinopyroxene inclusions are protogenetic, the reliability of the radiometric diamond ages will strongly depend on the equilibration rate of the Sm-Nd isotope system in clinopyroxene during diamond growth within the SCLM.

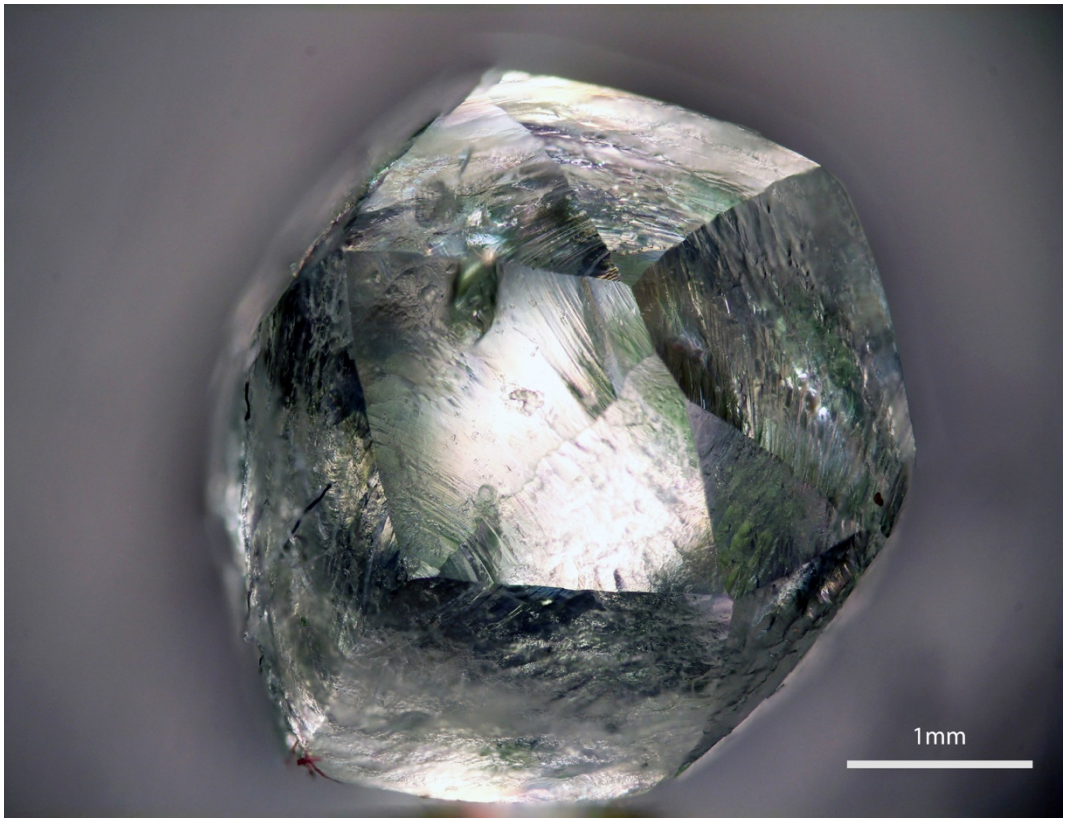


**Figure 1.3.** Diamond Lot34stone21 belonging to the inclusion-bearing diamonds studied in this thesis work. It is possible to observe the dodecahedral morphology of the diamond and the green clinopyroxene inclusions included within it.

# Chapter 2

# Inclusions hosted in diamonds

Diamonds frequently contain fluid and mineral inclusions entrapped during its growth in the Earth's mantle. Once enclosed by the host diamond, these inclusions are generally isolated from physical-chemical changes affecting rocks in the deep mantle. From the study of these inclusions, has been possible, in over 50 years of research, to constrained the environment and the conditions of diamond formation within the mantle, allowing to understand how, where, and when diamond crystallized (e.g., see reviews of Stachel and Harris, 2008; Shirey et al., 2013; Stachel and Luth, 2015).

## 2.1 Mineral inclusions

Monocrystalline gem-quality diamonds coming from the subcontinental lithospheric mantle are estimated to account for about 99% of the worldwide production, while the sublithospheric or superdeep diamonds represent the remaining 1% (Stachel and Harris, 2008). Lithospheric and sublithospheric diamonds may be recognized through the identification of their mineral inclusions. Typical inclusions that allow us to constrain the lithospheric origin are garnet, clinopyroxene, orthopyroxene, olivine, Mg-chromite, and Fe-Ni sulfides, with a minor amount of coesite and kyanite (see Table 2-1 for the abundance; Stachel et

al., 2008). Differently, the most abundant inclusions in superdeep diamonds are ferropericlase, breyite, jeffbenite, and majoritic garnet, with some other extremely rare minerals typical of the lower mantle (Nestola, 2017).

Generally, lithospheric mineral inclusions can be classified based on their composition into three suites related to their lithospheric mantle source rocks, of which two are widely dominant (Stachel and Harris, 2008):

(i) Peridotitic or P-type suite;
(ii) Eclogitic or E-type suite;
(iii) Websteritic suite.

The presence of diamonds with mineral inclusions belonging to a specific suite indicates that they crystallized within a mantle host rock with a certain paragenesis. In general, it is hugely infrequent to find two or more mineral inclusions within the same diamond host with mineral chemistry from different suites (Tappert and Tappert, 2011).

From the studies on mineral inclusions hosted in lithospheric diamonds, it has emerged that the peridotite is the primary source of lithospheric diamonds (65% of inclusion-bearing diamonds), followed by eclogitic source (33%) and a minor websteritic source (2%) (see Figure 2.1a). In general, the websteritic suite reflects a broadly pyroxenitic source, and the term websteritic is used to classify diamonds that exhibit a composition transitional between the peridotitic and eclogitic suites (Stachel and Harris, 2008). Nevertheless, it represents a secondary source paragenesis for inclusions in diamonds; therefore, the websteritic suite has been not considered for the classification of the inclusions in diamonds of this thesis work.

### *2.1.1 Peridotitic suite*

Peridotitic paragenesis inclusions are the most diffused in diamonds. Their dominance is also reflected by the frequent occurrence of peridotite xenoliths hosted in kimberlites (e.g., Tappert and Tappert, 2011).

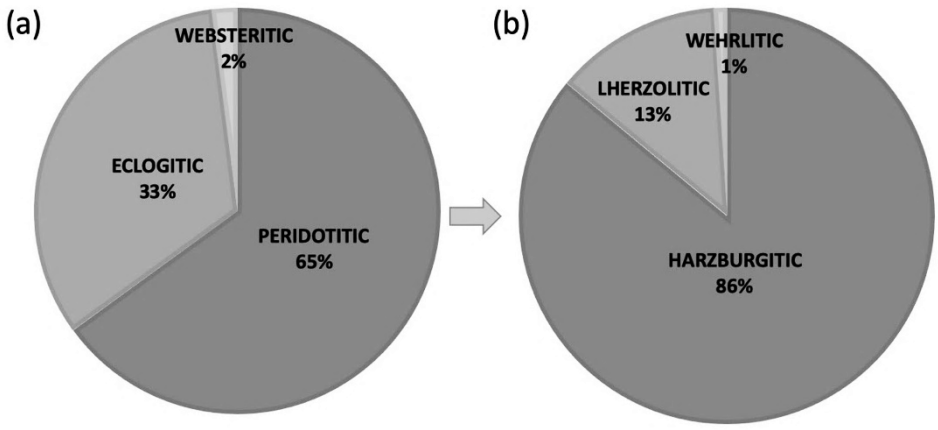


**Figure 2.1.** (a) Relative proportions of lithospheric diamond source parageneses, based on the analyses of 2844 inclusion-bearing diamonds; (b) relative proportions of peridotitic parageneses, harzburgitic (-dunitic), lherzolitic and wehrlitic, based on 685 peridotitic garnet inclusions. All data have been extracted from the database of Stachel and Harris (2008).

The peridotitic suite can be further split into harzburgitic (clinopyroxene free), lherzolitic (orthopyroxene-clinopyroxene present), and a minor wehrlitic (clinopyroxene present and orthopyroxene free) parageneses (e.g., Stachel, 2014). On a worldwide scale, peridotitic diamonds contain mineral inclusions with a predominantly harzburgitic composition (see Figure 2.1b). This fact is consistent with the high levels of chemical depletion that typify the subcratonic lithospheric mantle with respect to fertile lherzolitic mantle, as a consequence of several melt extraction events occurred during the Archean (e.g., Stachel and Harris, 2008). The minor population of lherzolitic diamonds are typically associated with metasomatic mantle re-enrichment events, triggered by the passage of fluids or melts through mantle peridotites (Stachel and Harris, 2009). Wehrlites, instead, are very uncommon diamond peridotitic source and likely related to overprints by infiltrating melts (Stachel and Harris, 2009).

The overall depleted behavior of the diamond peridotitic source is reflected in the major element composition of the inclusions having high Mg/Fe, high Cr concentrations, and low Na-Ca contents (Stachel and Harris, 2008). Accordingly, the typical mineral inclusions that compose the peridotitic suite comprise Cr-rich

pyrope garnet, high-Mg olivine and orthopyroxene, Cr-rich clinopyroxene with high diopside component and spinel with high magnesiochromite component (see Table 2-1 for relative abundance). Along with these mineral inclusions, Fe-Ni sulfides are widespread mineral inclusions found in peridotitic diamonds (Stachel and Harris, 2008).

The compositions of garnet inclusions are commonly used to classify the peridotitic diamonds into one of the three peridotitic paragenesis (i.e., harzburgitic-dunitic, lherzolitic or wehrlitic), as well as to distinguish them from eclogitic diamonds (see below). More specifically, the $Cr_2O_3$-CaO diagram for garnet inclusions reported in Figure 2.2 permits to recognize different areas related to the different inclusion paragenesis source (Grütter et al., 2004). Basically, the limit to discriminate peridotitic from eclogitic garnets is $Cr_2O_3 > 1$ wt.% (Stachel and Harris, 2008). Considering the only peridotitic garnet, the Ca-poor side of the lherzolitic field reflects depleted harzburgitic-dunitic garnets (clinopyroxene-free). However, the distinction between dunitic (pyroxene-free) and harzburgitic (orthopyroxene-present) paragenesis cannot be made using the composition of garnet. The term harzburgitic, therefore, is generally used to delineate the continuum harzburgite-dunite group in the diamond study field (Stachel and Harris, 2008). Differently, the area in the middle indicates the compositions for the lherzolitic suite, and on the Ca-rich side, there are garnets with wehrlitic composition. The distinction between these two groups is marked by the high Ca contents, which are incompatible with the presence of the orthopyroxene. In any case, werhlitic garnets are very uncommon (Stachel and Harris, 2008).

### *2.1.2 Eclogitic suite*

The studies of inclusions in diamonds and eclogitic xenoliths have revealed that eclogitic diamond source reflects an approximately basaltic bulk rock composition relatively more depleted to day-present MORB tholeiites covering the most Earth's surface beneath the oceans (Stachel and Harris, 2008). In light of this important

source compositional feature, the eclogitic inclusions can be distinguished from peridotitic inclusions by an overall lower Mg/Fe, lower Cr and higher Na, Ca, and Al contents. Garnet and clinopyroxene are the main mineral phases that compose the eclogitic suite.

Clinopyroxene generally consists of omphacite (i.e., a mixture of jadeite-aegirine and diopside end-members). Garnet, instead, is typically composed of a mixture of the three end-members grossular-almandine-pyrope. The main feature of the eclogitic garnet is the extremely low Cr-content, which allows us to recognize them from the peridotitic garnet, as shown in Figure 2.2 (Stachel and Harris, 2008). Other less diffuse mineral phases are sampled by eclogitic diamonds, namely coesite, kyanite, and rutile (Stachel and Harris, 2008; see also Table 2-1 for relative abundance). Sulfide inclusions are also very common in eclogitic inclusion suite; they are present with lower Ni content with respect to the peridotitic inclusion suite (Stachel and Harris, 2008).

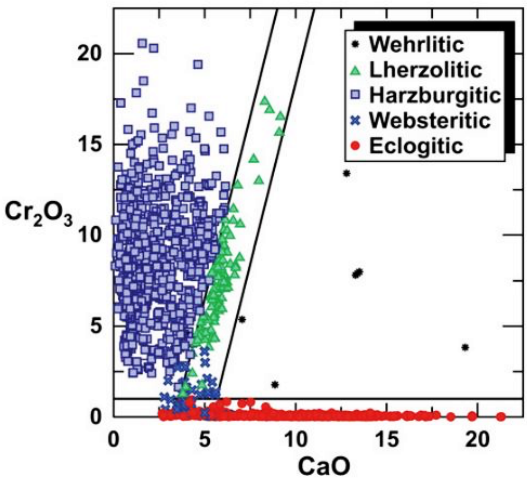


**Figure 2.2.** $Cr_2O_3$ versus CaO (wt.%) plot used for garnet inclusions classification and for indicator mineral assessment. The exact boundaries (black lines) between the three compositional fields shown in the plot have been defined by Grütter et al. (2004). The boundary between the eclogitic and peridotitic garnet inclusions has been fixed at 1wt.%. Dunitic garnets plot together with highly depleted harzburgitic garnets at very low CaO contents (<1.8 wt.%). From Stachel and Harris (2008).

**Table 2-1.** Relative abundance of mineral inclusions in lithospheric diamonds. The data derived from the database of Stachel and Harris (2008), converting the analyzed inclusion counts into percentages.

| Mineral | Percentage |
|---|---|
| Garnet | 29 |
| Sulfide | 24 |
| Mg-chromite | 14 |
| Olivine | 14 |
| Clinopyroxene | 12 |
| Orthopyroxene | 6 |
| Coesite | 0.5 |
| Rutile | 0.5 |

A preliminary identification of the nature and source paragenesis of the mineral inclusions hosted in diamonds may be optically made through the observation of the colors of the minerals, at least for those with distinct color. Particularly, garnet inclusions have a diagnostic purplish-red color when peridotitic and pale-orange to orange hue when eclogitic. Magnesiochromite inclusions are opaque, with sub-metallic luster and deep cherry red color. Clinopyroxenes, instead, usually exhibit a distinctive emerald-green color when peridotitic and pale-green color with sometimes bluish shades when eclogitic. Olivine and orthopyroxene inclusions are colorless or, if they are large inclusions, may be weakly colored. In this case, the optical recognition is challenging (Tappert and Tappert, 2011). In general, the perceived colors vary with the chemical composition and size of the inclusion. Besides, the surface features, the high refractive index, and the presence of fractures and fluids into diamonds can make difficult the optical detection of the mineral inclusions, up to blurring and obscuring the mineral inclusions. For a complete identification of mineral inclusions, more advanced analytical techniques are required, such as in-situ non-destructive Raman spectroscopy, X-ray diffractometry, and destructive detailed chemical analysis techniques (Tappert and Tappert, 2011).

The following section will discuss in more detail about the characteristics of clinopyroxene in diamonds, as it represents the mineral inclusion analyzed in this thesis work.

### *2.1.3 Clinopyroxene*

Clinopyroxene is quite recurrent mineral inclusion in lithospheric diamonds, accounting for 12% of the recovered inclusion phases (see Table 2-1; Stachel and Harris, 2008) and, together with garnet, is also one of the most commonly used mineral indicators for mining exploration.

From a crystallographic point of view, clinopyroxene has monoclinic 2/*m* point group symmetry and generally crystallizes in *C*2/*c* space group. The crystallographic data relative to clinopyroxene compositional end-members are reported in Table 2-2.

The determination of the source paragenesis for clinopyroxene inclusions, as mentioned above, can be preliminary made on the basis of color inspection, assigning emerald green inclusions to the peridotitic paragenesis, and pale-green inclusions to the eclogitic paragenesis. If the inclusion-bearing diamonds are investigated by single-crystal X-ray diffraction, as in the present thesis work (see § 4.1), the calculated unit-cell volumes may also be a useful tool to classify clinopyroxene inclusions. However, these criteria provide only a first overview of the paragenesis source in the absence of more diagnostic information. The compositional analysis (major and trace elements) yields more robust data to determine the source paragenesis and comprehend its significance. In particular, the different Cr/Al ratios can be readily used to distinguish a peridotitic Cr-diopside from an eclogitic omphacite (see Figure 2.3). More precisely, eclogitic clinopyroxene inclusions are distinct from the peridotitic ones for a Cr# (= 100Cr/[Cr+Al]) up to about 7-10% (Stachel and Harris, 2008).

**Table 2-2.** Unit cell parameters of diopside (Clark et al., 1969), hedenbergite, jadeite, and aegirine (Cameron et al., 1973). These values are measured with single-crystal X-ray diffraction at room temperature (24°C). Jadeite and aegirine are natural samples that closely approximate the end-members compositions, while hedenbergite and diopside are synthetic specimens. The abbreviations of the mineral names are based on Whitney and Evans (2010): Di=diopside; Hd=hedenbergite; Jd=jadeite; Aeg=aegirine. V = unit cell volume; *a,b,c,β* = lattice parameters. Values in parenthesis are one standard deviation.

| **Minerals** | ***a* (Å)** | ***b* (Å)** | ***c* (Å)** | ***β* (°)** | **V (Å$^3$)** |
|---|---|---|---|---|---|
| Di ($CaMgSi_2O_6$) | 9.746(4) | 8.899(5) | 5.251(6) | 105.63(6) | 438.6(3) |
| Hd ($CaFeSi_2O_6$) | 9.845(1) | 9.024(1) | 5.245(1) | 104.74(1) | 450.6(1) |
| Jd ($NaAlSi_2O_6$) | 9.423(1) | 8.564(1) | 5.223(1) | 107.56(1) | 401.8(1) |
| Aeg ($NaFe^{3+}Si_2O_6$) | 9.658(2) | 8.795(2) | 5.294(1) | 107.42(2) | 429.1(1) |

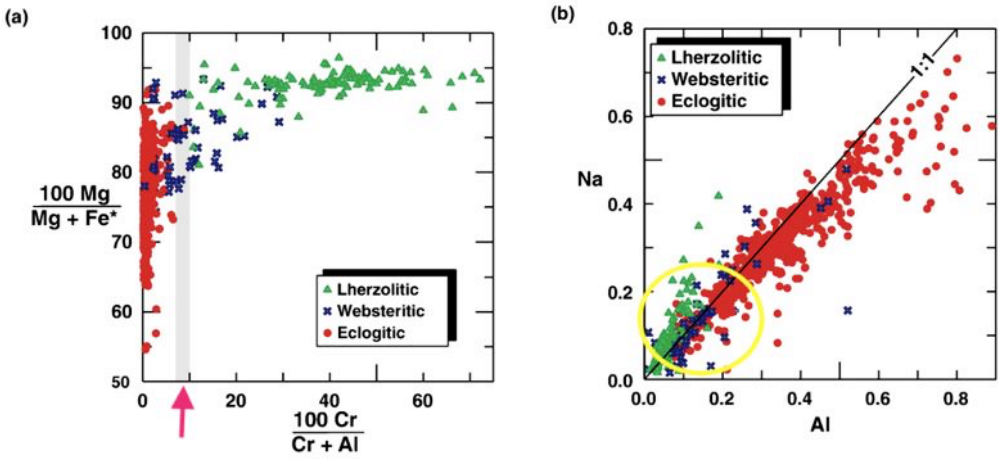


**Figure 2.3.** (a) Clinopyroxene inclusions classification in a molar Mg# (= 100Mg/[Mg+Fe]) versus molar Cr# (= 100Cr/[Cr+Al]) plot. The arrow indicates the compositional transition from eclogitic to peridotitic clinopyroxenes, which occurs at about 7 to 10% of Cr#; (b) Na versus Al plot (cation calculated on a basis of 6 oxygens per formula unit) for clinopyroxene inclusions; the linear trend between Na and Al is related to the jadeitic component of eclogitic clinopyroxenes, while Al-rich eclogitic clinopyroxenes are related to the presence of a Tschermaks component. The yellow circle indicates the presence of peridotitic clinopyroxene inclusions with low Cr-contents that overlap with Al-poor eclogitic clinopyroxenes. In both the diagrams, the websteritic suite is transitional between eclogitic and peridotitic suites. Modified from Stachel and Harris (2008).

## 2.2 Fluid inclusions

Diamond precipitation within the Earth's mantle is considered a metasomatic event induced by the circulation of carbon-rich fluids or melts, which contain either oxidized (e.g., $CO_3^{2-}$, $CO_2$) or reduced carbon species (e.g., $CH_4$). Diamonds sometimes entrap these fluids/melts during their growth, hence their preservation as fluid inclusions offers the opportunity to study the metasomatic diamond-forming fluid/melt directly (e.g., Shirey et al., 2019).

Gem-quality lithospheric diamonds or so-called octahedrally-grown diamonds (i.e., clear smooth-surfaced monocrystalline diamonds), are generally deficient in fluid inclusions, so the exact chemical nature and compositions of their forming-media is still a matter of debate (e.g., Smith et al., 2015). Most works regarding fluid inclusions in diamonds have been conducted on the so-called fibrous diamonds (e.g., Boyd et al., 1987,1992; Izraeli et al., 2001; Klein-BenDavid et al., 2014; Navon et al., 1988), which are characterized by a faster growth rate than gem-quality diamonds that allows them to entrap abundant sub-micron-sized fluid inclusions. These fluids are high-density fluids (HDFs) and range compositionally between four end-members (e.g., Weiss et al., 2009; see also Figure 2.4): hydrous-saline (rich in Cl, Na, K, carbonate, and water); high-Mg carbonatitic (rich in Mg, Ca, Fe, K, and carbonate); low-Mg carbonatitic (rich in Ca, Fe, K, Mg, and carbonate), and hydrous-silicic (rich in Si, K, Al, Fe and water).

These fluids represent an efficient metasomatic medium, highly mobile, and generally enriched in light ion lithophile (LILE) and rare earth elements (REE) (e.g., Tomlinson et al., 2009; Weiss et al., 2013). The available isotopic data of Nd, Sr, and Pb define a fluid source that varies between the "depleted" asthenospheric mantle and the ancient lithospheric mantle highly enriched in incompatible elements, including recycled old continental crust (e.g., Klein-BenDavid et al., 2014).

As long as the presence of the high-density fluids has not also been documented in gem-quality diamonds (e.g.,Weiss et al., 2014, 2015; Jablon and Navon, 2016; Nestola et al., 2018; Nimis et al., 2016; Smith et al.,2016, 2018; Krebs et al., 2019),

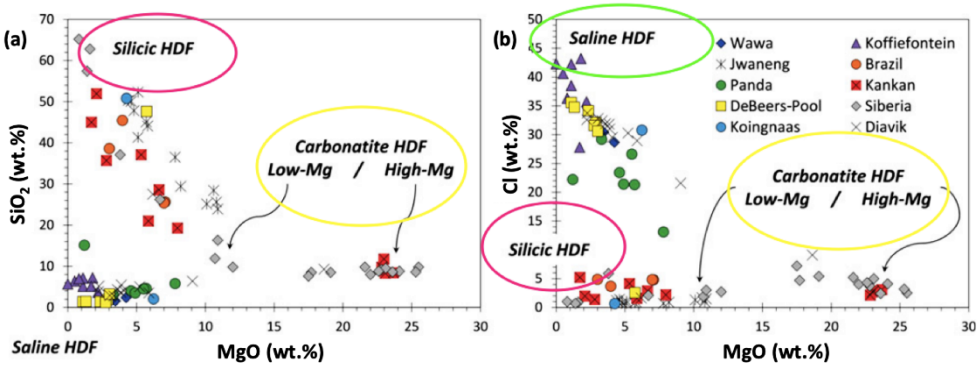


**Figure 2.4.** Composition of fluid microinclusions in fibrous diamonds worldwide. (a) $SiO_2$ versus MgO and (b) Cl versus MgO content. The data are expressed in wt.% (on a water- and carbonate-free basis). Note the clear delineation of the four compositional end-members circled in the figure. The silicic fluids and low-Mg carbonatitic fluids end-members form a continuous array (Weiss et al., 2009). HDF = high density fluid.
Data: DeBeers-Pool, Koigngnaas, and Kankan from Weiss et al., (2009,2018); Koffiefontein from Izraeli et al., (2011); Brazil from Shiryaev et al.,(2005); Diavik and Siberia from Klein Ben-David et al.,(2007,2008); Jawneng from Schrauder and Navon (1993); Panda from Tomlinson et al., (2006); Wava from Smith et al., (2012). Modified from (Shirey et al., 2019).

there was a long debate on whether these fluids could also be related to the genesis of gem-quality diamonds. Fibrous diamonds, indeed, represent only a small percentage of the mine's production worldwide and are thought to form approximately during the formation and the eruption of the kimberlite (Shirey et al., 2013). Recent studies have reported high-density fluid inclusions in non-fibrous lithospheric diamonds with carbonatitic (e.g., Weiss et al., 2014), saline (Weiss et al., 2015; Krebs et al., 2019) and silicic compositions (Nimis et al., 2016, Nestola et al., 2018). In particular, the discovery of hydrous silicic fluid films around typical mineral inclusions in gem-quality diamonds proposed that the water-rich fluids can be an efficient diamond-forming media in the lithospheric mantle, as suggested by Stachel and Luth (2015) on the basis of indirect evidence.

The previously rarity of hydrous silicic fluids in gem-quality diamonds could be ascribed to their non-easily detection since they are practically optically invisible and required high-resolution analytical techniques for their individuation, such as the micro-Raman confocal spectroscopy. Moreover, the presence of a fluid film is generally limited to the wettable surface of solid inclusions (Nimis et al., 2016).

A fluid film around mineral inclusions indicates that between the diamond host and its inclusions, there was a limited interfacial interaction. Besides, since the diffusion is much more efficient in the presence of fluids, these could enhance the diffusional exchange at mantle temperature and pressure, as well as induce dissolution/precipitation processes. Therefore, the study of mineral inclusions trapped within diamonds should take into account the presence of a fluid phase (Nimis et al., 2016).

## 2.3 Syngenesis or protogenesis?

Mineral inclusions in diamond may be distinguished based on the timings of their formation respect to their diamond host (e.g., Harris, 1968; Meyer, 1985, 1987):

i. If inclusions and diamond were crystallized at the same time, in reciprocal contact and from the same genetic process, they are called "*syngenetic*";
ii. If inclusions formed before the diamond crystallization, they are called "*protogenetic*";
iii. If inclusions were formed after the diamond crystallization, they are called "*epigenetic*."

Distinction between syngenetic and protogenetic inclusion, as summarized by Taylor et al. (2003), is not straightforward but is very important in diamond research. Indeed, the assumption of syngenesis permitted to extend all the geological information studied on the inclusions (e.g., pressure and temperature, age and geochemistry of the parent medium) to diamond (Nestola et al., 2014). Syngenesis occurs as a result of co-precipitation of the inclusion and the diamond host from the same diamond-forming fluid/melt (*mutual growth*) or by complete re-crystallization of former minerals during the growth of diamond by dissolution/re-precipitation processes (Nestola et al., 2014). Protogenetic inclusions, instead, were encapsulated by growing diamond after some time that can span from a short to

very long geological timescale (Shirey et al., 2013). Hence, the significance of the information extracted from protogenetic inclusions and its link with the diamond host requires more accurate studies on the chemical equilibria during the diamond crystallization (Nestola et al., 2014).

Unlike the syngenetic and protogenetic inclusions, the epigenetic inclusions are easily recognizable [e.g., with cathodoluminescence imaging technique (Wiggers de Vries et al., 2011), and high resolution X-ray computed tomography (Nimis, 2018)] because they result from the alteration of pre-existing inclusions or by precipitation from fluid within possible cracks inside the diamond (Nestola et al., 2014). In general, the epigenetic inclusions are linked to processes that occurred during the transport of diamond in the kimberlitic magma or after the emplacement of this latter in the crust (Stachel and Harris, 2008).

Since the 1960s, numerous studies conducted on mineral inclusions in diamonds have provided a clear picture of the mineralogical and geochemical environment in which diamond is thought to form, all based on the common assumption that the mineral inclusions and diamonds are syngenetic. Nevertheless, recent studies (e.g., Taylor et al., 2003; Nestola et al., 2014, 2017, 2019; Milani et al., 2016) have questioned the validity of criteria (see below) widely used by a good slice of scientific community to proof syngenesis, recognizing the protogenesis for some mineral inclusions that were typically considered syngenetic.

### *2.3.1 Evidence of syngenesis*

So far, the most common criterion used to proof syngenesis has been the optical observation that most of the mineral inclusions in diamond, regardless of their free-natural habit, show a pseudocubo-octahedral morphology imposed by their diamond host (e.g., Harris, 1968; Harris and Gurney, 1979; Meyer, 1985, 1987; Sobolev, 1977; see also Figure 2.5). This diamond shape imposition is considered the effect of the greater "*form energy*" of the diamond, such that it can impose its

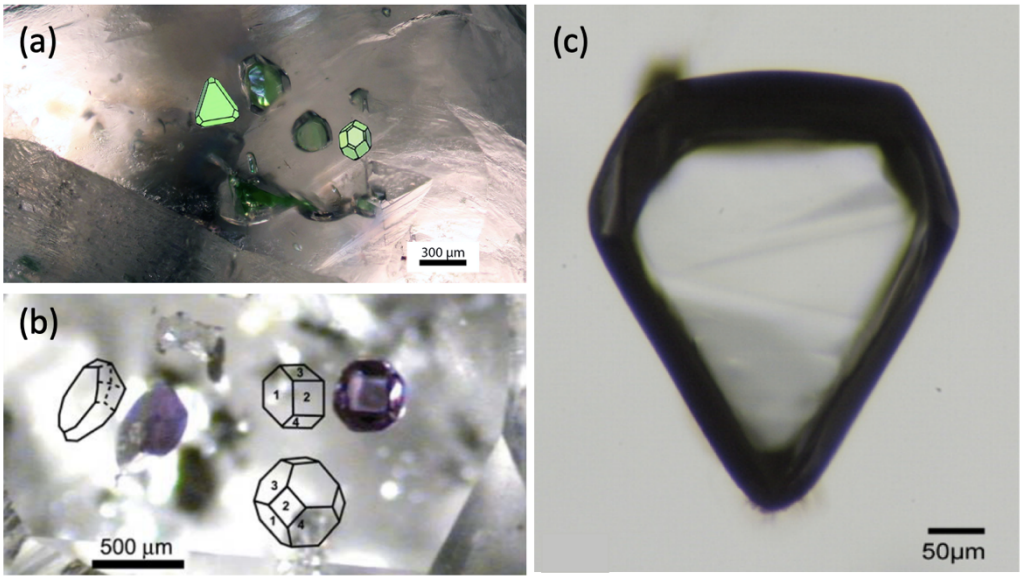


**Figure 2.5.** Examples of mineral inclusions in diamonds which show pseudocubo-octahedral morphology imposed by diamond. (a) Clinopyroxene (monoclinic) inclusions in diamond from this thesis work (Lot34stone22); (b) garnet (cubic) inclusions (modified from Taylor et al., 2003); (c) olivine (orthorhombic) inclusion (modified from Agrosì et al., 2016).

cubo-octahedral morphology upon the inclusion only during their mutual growth (Harris, 1968).

Moreover, another traditional supposed proof of syngenesis (e.g., Pearson and Shirey, 1999), has been the presence of specific crystallographic orientation relationships (CORs) between inclusions and their diamond hosts (i.e., coincidence of crystallographic planes and/or crystallographic directions), considered to be the evidence of an epitaxial growth. The first crystallographic pioneering work that reported the CORs between inclusions and diamonds was that of Mitchell and Giardini (1953), in which the authors showed the presence of two olivine inclusions with specific CORs with their diamond hosts. This observation was initially supposed to reflect a possible epitaxial relationship (Hartman, 1954). Successively, many other studies interpreted the presence of specific CORs as evidence of an epitactic growth between olivine inclusions and diamond (Frank-Kamenestky, 1964; Futergendler and Frank-Kamenetsky, 1961; Orlov, 1977), regardless of failure to find a real dominant preferred crystallographic orientation between them (Nestola et al., 2014).

Another criterion used to support syngenesis, but still argued, is the observation by cathodoluminescence technique of interrupted growth zone of diamond around an inclusion (i.e., non-luminescent diamond CL halo), based on the assumption that the diamond growth zoning pattern around the inclusions should be different depending on their syn- *versus* protogenetic nature (e.g., Bulanova 1995). Wiggers de Vries et al. (2011) applied the cathodoluminescence technique (CL) combined with electron back-scatter diffraction (EBSD) - using focused ion beam- scanning electron microscope (FIB-SEM) - in order to investigate the three-dimensional diamond growth zoning pattern near its inclusions. The presence of magnesiochromite inclusions showing a specific crystallographic orientation to their diamond host has been used to proof a potential epitaxial relationship between inclusions and diamond host. Nonetheless, the authors did not exclude a more complex growth history of the inclusion-diamond host system because of the presence of three-dimensional diamond zonation near magnesiochromite inclusions, which suggests both syngenetic and protogenetic features (Wiggers de Vries et al., 2011).

### *2.3.2 Evidence of protogenesis*

Conversely to syngenesis, until a couple of decades ago, very few studies invoked a protogenetic origin for mineral inclusions in diamonds. The first ones that severely questioned the morphology criterion used to proof syngenesis were Taylor et al. (2003), which interpreted the sinusoidal REE patterns of harzburgitic garnet inclusions with cubo-octahedral shape, as the evidence of a multi-stage geochemical evolution (i.e., partial melting followed by a metasomatic enrichment and probably a final partial melting phase) occurred prior to diamond entrapment. This complex genetic history apparently indicates a protogenetic origin of the garnets, regardless of their morphology (Taylor et al., 2003). Nevertheless, as argued by Stachel et al. (2004), the same REE patterns obtained by Taylor et al. (2003) can also be produced if the garnet crystallization occurred by reaction

between refractory mantle peridotite and C-saturated and LREE-enriched diamond-forming fluids, allowing a syngenetic origin of garnet in a metasomatic environment (Stachel et al., 2004).

The protogenetic nature of mineral inclusions in diamonds was also suggested for sulfide inclusions analyzed by Thomassot et al. (2009) with a geochemical approach based on the study of C and N stable isotopes. Furthermore, the same interpretation was given by Jacob et al. (2016), which identified Fe-Ni-sulfide inclusions that experienced a crystal-plastic deformation before their entrapment by the diamond (Jacob et al., 2016).

A more robust proof that the morphological criterion should not be used as an unambiguous evidence of syngenesis for mineral inclusions in diamonds has been supplied by recent crystallographic studies on more than seventy octahedral shaped olivine inclusions trapped in more than thirty-five diamonds coming from the Kaapvaal (South Africa) and Siberian (Russia) cratons (Nestola et al., 2014; Milani et al., 2016). The authors investigated the CORs between olivine inclusions and diamond hosts by single-crystal X-ray diffraction technique, observing the absence of specific orientations between the inclusion-host pairs. They also reported the presence of clusters of iso-oriented olivine inclusions within individual diamonds. These clusters were interpreted as remaining fragments of original olivine monocrystals that were partially dissolved during or before the growth of their diamond host from a carbon-bearing fluid/melt phase, i.e., at least these inclusions are protogenetic (Nestola et al., 2014; see also Figure 2.6). During the entrapment process, these diamonds could impose their morphology on olivine inclusions by a fluid-present interface diffusion process acting at the diamond-olivine interface. In order to minimize the surface energy, the olivine gets the morphology of diamond cavity (i.e., negative-crystal morphology) (Nestola et al., 2014; Agrosì et al., 2016). In further analyses on the same samples, stepped figures were detected at the diamond-olivine interface by X-ray tomography (Agrosì et al., 2016), along with fluid films by micro-Raman confocal spectroscopy (Nimis et al., 2016), in support of the scenario proposed by Nestola et al. (2014) and, thus, of the protogenesis.

Other recent works have applied the same crystallographic approach and

demonstrated the protogenesis for other mineral inclusions commonly included in diamonds, namely clinopyroxene (Nestola et al., 2017), magnesiochromite (Nimis et al., 2019) and garnet (Nestola et al., 2019), coming from different kimberlite worldwide. In all these works, the authors found the presence of clustered iso-oriented inclusions within individual diamonds and the overall absence of specific orientations for the inclusion-diamond host pairs, interpreting that they belonged to original monocrystals and, hence, are protogenetic, as previously suggested for olivine inclusions.

In more detail, the interpretation of the absence of specific orientations in order to constrain the timing relationships for mineral inclusions in diamonds (i.e., syngenesis *versus* protogenesis) is complicated and controversial. As underlined by Bruno et al. (2016), the lack of a systematic preferential orientation between diamonds and their inclusions is not sufficient to rule out syngenesis, as long as the variation of the interfacial energies (i.e., the energy required to create an interface) between diamond and the inclusions are not determined for any crystallographic orientation. The variation of the interfacial energies at different orientations for the typical silicate inclusions is thought to be small for the development of any preferred orientation, despite the timing of crystallization of the inclusion with respect to its diamond host (Nestola et al., 2014; Bruno et al., 2016). For the olivine inclusions, the above-outlined scenario was confirmed by the *Ab initio* calculation of interfacial energies for specific crystallographic orientations of the olivine with respect to diamond, which revealed almost equal and low adhesion energies (i.e., the energy gained once an interface is formed) for all the olivine/diamond interfaces. This discovery implies that olivine and diamond have an extremely low chemical affinity, and a preferential orientation between them cannot be developed, even during an eventual epitaxial growth of the olivine with diamond. Other silicate inclusions (e.g., coesite, garnet, pyroxene) in diamond could have similar behavior to that of the olivine (Bruno et al., 2016).

Summing up, the above-mentioned recent studies have suggested that many mineral inclusions commonly included in lithospheric diamonds can be protogenetic, although they present a diamond-imposed morphology. They also

have demonstrated that the preferred crystallographic orientations observed by many authors in the past for inclusion-diamond pairs (e.g., Mitchell and Giardini 1953) have no statistical significance and chemical-physical meanings. Indeed, as underlined by Nestola et al. (2014) and Griffiths et al., (2016), the number of investigated samples is of paramount importance to provide a statistically reliable crystallographic data for the interpretation of the CORs between diamond and its inclusions. In addition, in the absence of clear evidence of protogenesis, like clusters of iso-oriented inclusions within the same diamond host with any orientation relationship with diamond, the crystallographic data shall be interpreted with caution (e.g., Bruno et al., 2016).

The crystallographic approach proposed by Nestola et al. (2014) provided a powerful tool for resolving the ongoing debate on syngenesis *versus* protogenesis. So far, crystallographic studies on mineral inclusions in diamonds were mainly conducted on olivine and garnet inclusions (Nestola et al., 2014, 2019b; Milani et al., 2016). Therefore, systematic works to verify the protogenetic *versus* syngenetic nature of other typical mineral inclusions in diamonds, like clinopyroxene, are scarce or lacking. The protogenetic nature of mineral inclusions cannot be ignored when interpreting the data collected from them, mainly the geochronological information used to retrieve the age of diamond.

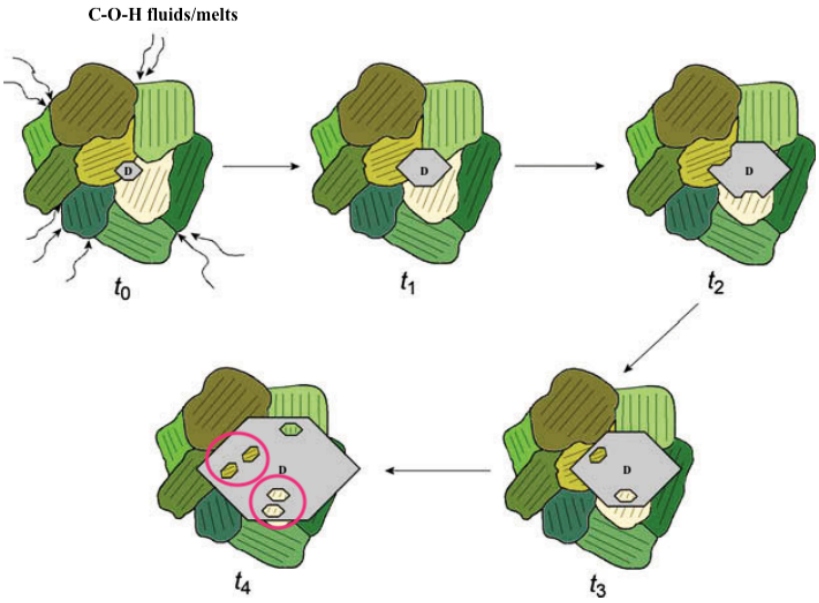


**Figure 2.6.** Mechanism of diamond-forming process proposed by Nestola et al. (2014) to explain the observed diamond-olivine crystallographic relationships. The diamond (gray) growth starts from a C-O-H fluids or melts percolating through pre-existing olivine-rich mantle peridotitic rock at high pressure and temperature ($t_0$). These fluids/melts may lead to a selective partial dissolution of pre-existing olivine crystals (different shades of green) during the growth of diamond ($t_2$) that, in turn, can result in the entrapment of the dissolving olivines as multiple inclusions within the diamond ($t_3$). These inclusions will show different crystallographic orientations if derived from different crystals, or similar orientations if they are relict fragments of former single crystals, as highlighted by circled olivine inclusions in the figure ($t_4$). Modified form Nestola et al. (2014).

## 2.4 Radiometric dating and the age of diamond

The age of diamond is of paramount importance in the Earth Science because it constrains the temporal evolution of the deep mantle processes recorded by it, such as the cycling of volatiles in the Earth (e.g., Shirey et al., 2013). Determination of how much old is a rock or mineral, like diamond, is a matter of geochronology science, which studies the radiogenic isotope systems. Before discussing how diamond can be date, some basic geochronology principles will be treated in general

terms in the following discussion, according to Dickin (2005) and Faure (2005), from which all formula presented in this section have been extracted.

An isotope of a specific chemical element is simply the same element with a different number of neutrons in its atomic nucleus. When this nucleus has an excess or deficiency of neutrons is unstable and, in order to reach a lower energy state, undergoes a process of radioactive decay, which produces a new isotope, along with the emission of particles (α- and/or β-rays) and radiant energy (γ-rays). The original unstable isotope is called radioactive *parent* isotope, and the new resulting isotope is referred to as the radiogenic *daughter* isotope. The naturally occurring decay schemes are different, but the most important for geological dating purposes are alpha (α) and beta (β) decay, which affect the number of protons, neutrons, or both, of an atom.

In a closed system (e.g., a mineral or rock), according to the *law of radioactive decay* (Rutherford and Soddy, 1902), an original unstable isotope of one element decays to a radiogenic daughter isotope of another element at a rate expressed by the so-called *decay constant* ($\lambda$). The decay constant is specific for each radionuclide and experimentally determined; it represents the probability that an unstable nuclide will decay within a stated unit of time. The inverse function of the decay constant defines the *half-lives*, i.e., the time that a half amount of parent nuclide in a sample spends to decays to its daughter nuclide. Isotope system, like uranium-lead, samarium-neodymium, lutetium-hafnium, rubidium-strontium, and rhenium-osmium, are called long-lived because they are characterized by very long *half-lives* to be used to study geological materials with ages from 4.6 billion years ago (i.e., the age of the Earth; see Table 2-3).

The age *t* of a rock or mineral can be obtained using the following *chronometer equation*:

$$\mathrm{D} = \mathrm{D}_0 + \mathrm{N}(e^{\lambda t} - 1), \tag{2.1}$$

where D is the number of radiogenic daughter atoms produced by the decay of a parent radionuclide in rock or mineral since its formation *t* years ago; N is the

number of parent atoms that have remained at any time t, and $D_0$ is the number of radiogenic daughter atoms initially present in the system at time $t$=0.

The modern mass spectrometers can measure the small differences in the parent and daughter isotopes that have been trapped in minerals or rocks by measuring the isotopic ratios. Therefore, every term of equation 2.1 is normalized to a non-radiogenic isotope of the same element as the daughter nuclide, S, which is not produced by radioactive decay and, hence, remains constant through time. The resulting equation is:

$$\left(\frac{D}{S}\right)_t = \left(\frac{D}{S}\right)_0 + \left(\frac{N}{S}\right)_t (e^{\lambda t} - 1). \quad (2.2)$$

When the present-day $(D/S)_t$ and $(N/S)_t$ isotopic ratios are determined for two or more rocks or minerals, these define a straight line called *isochron,* because all points on that line represent rock or mineral systems that have the same age $t$ and initial value of radiogenic daughter isotopes $(D/S)_0$. The slope ($e^{\lambda t}$-1), and $y$-intercept $(D/S)_0$, of this line, can be determined by a statistical procedure of least-square regression. The age of rocks or minerals is determined from the slope of this *isochron*, assuming that the decay constant of the parent nuclide is precisely known.

The interpretation of the obtained numerical value of $t$ depends on some assumption about the geological history of the rocks and minerals being dated. These assumptions are:

i. The radioactive decay has occurred in a closed system from time $t$=0 until present time $t$, i.e., the values of parent and daughter isotopes have changed only as a result of radioactive decay;

ii. All rock and mineral samples are *cogenetic*, i.e., they have been in isotopic equilibrium at the time of their formation $t$=0; thus, they have inherited the same initial isotope ratio.

**Table 2-3.** Summary of half-lives and decay constants of long-lived decay systems employed for old geological materials, like diamond, with age up to billions of years. Data have been extracted from Dickin, 2005.

| Radioactive parent isotope | Daughter isotope | Decay constant | Half-life |
|---|---|---|---|
| $^{238}U$ | $^{206}Pb$ | $1.55125 \times 10^{-10}$ | 4.5 Gyr |
| $^{235}U$ | $^{207}Pb$ | $9.8485 \times 10^{-10}$ | 703.8 Myr |
| $^{147}Sm$ | $^{143}Nd$ | $6.54 \times 10^{-12}$ | 106.0 Gyr |
| $^{40}K$ | $^{40}Ar$ | $5.81 \times 10^{-11}$ | 11.9 Gyr |
| $^{87}Rb$ | $^{87}Sr$ | $1.402 \times 10^{-11}$ | 49.4 Gyr |
| $^{186}Re$ | $^{187}Os$ | $1.666 \times 10^{-11}$ | 41.6 Gyr |
| $^{176}Lu$ | $^{176}Hf$ | $1.867 \times 10^{-11}$ | 37.1 Gyr |

Theoretically, all minerals or rocks could be dated using radiogenic isotopes if the assumptions mentioned above are satisfied. The key limitations are mainly due to the low abundance of radioactive nuclides in mineral structures and/or low instrumental sensitivity.

## *2.4.1 How can diamonds be dated?*

So far, it has not been possible to date diamond directly by radiogenic isotope systems because it is composed mainly of carbon, which has a half-life too short (atmospheric $^{14}C$ decays to $^{14}N$ with a half-life of 5.700 years) for dating diamonds that typically have ages up to billions of years (e.g., Gurney et al., 2010). The only reliable method to obtain the age of diamond is by dating its mineral inclusions because they are the principal carrier phases of radiogenic isotopes in diamonds, like those reported in Table 2-3, with long *half-lives*, and hence useful for dating the old diamonds (e.g., Pearson and Shirey, 1999).

Extensive reviews about the methodologies and results of radiometric dating of mineral inclusions in diamonds have been presented in the last two decades (e.g., see reviews by Pearson, 1999; Stachel and Harris, 2008; Gurney et al., 2010; Shirey

et al., 2013). According to these reviews, the best suited isotopic systems for dating mineral inclusions are uranium-lead (U-Pb), lead-lead (Pb-Pb), and rhenium-osmium (Re-Os) for sulfide inclusions; samarium-neodymium (Sm-Nd) and rubidium-strontium (Rb-Sr) for garnet and clinopyroxene inclusions, and argon-argon (Ar-Ar) for clinopyroxene inclusions, this latter reliable only for dating kimberlite eruption (e.g., Stachel and Harris, 2008, and references therein).

So far, the majority of worldwide diamonds have been dated by using Re-Os and Sm-Nd isotope systems. The high sensitivity of mass spectrometer for Re and Os elements, along with the relatively high Re and Os concentrations in sulfides, has always permitted to determine age on single diamonds (e.g., Pearson et al., 1998; Richardson et al., 2001, 2004; Aulbach et al., 2009; Smit et al., 2010). Otherwise, the application of Sm-Nd method, due to minimum mass necessary for instrumental sensitivity, required large single inclusions, or the combination of groups of inclusions with similar optical features and/or composition, from the same or different diamonds (e.g., Richardson et al., 1984; Richardson, 1986; Richardson et al., 1990; Richardson and Harris, 1997; Richardson et al., 2004, 2009). However, the use of groups of mineral inclusions for dating diamonds was severally criticized as producing an "average diamond age" (e.g., Koornneef et al., 2017; Navon, 1999). Thanks to recent experimental advancements have made it possible to use the Sm-Nd method to individual small (> 40 μm) silicate inclusions with very low concentration of Nd, i.e., down to >10 pg (Koornneef et al., 2017; Timmerman et al., 2017).

## *2.4.2 Sm-Nd dating method*

Sm and Nd are rare earth elements (REEs) commonly hosted as trace elements in the crystal structure of clinopyroxene, which in turn is an important mineral inclusion in lithospheric diamonds (see § 2.1). The contents of Sm and Nd in clinopyroxene inclusions found within lithospheric diamonds is on the order of a

few ppm, allowing diamond age determination. Table 2-4 reports some typical abundance of Sm and Nd in clinopyroxene inclusions hosted in diamonds.

As all the isotope systems, Sm-Nd decay scheme obeys the *law of radioactive decay* explained above, with $^{147}Sm$ representing the radionuclide that undergoes spontaneous α decay to stable $^{143}Nd$, with a half-life of about 106 Gyr ($\lambda$=6.54 x $10^{-12}$ $yr^{-1}$; see Table 2-3). The variations in the abundances of radiogenic $^{143}Nd$ are conventionally expressed with respect to non-radiogenic $^{144}Nd$. Therefore, by replacing the appropriate parent and daughter isotopes of Sm and Nd into equation 2.2, the following *isochron equation* is obtained:

$$\left(\frac{^{143}\mathrm{Nd}}{^{144}\mathrm{Nd}}\right)_t = \left(\frac{^{143}\mathrm{Nd}}{^{144}\mathrm{Nd}}\right)_0 + \left(\frac{^{147}\mathrm{Sm}}{^{144}\mathrm{Nd}}\right)_t (e^{\lambda t} - 1). \qquad (2.3)$$

The equation 2.3 can be used for dating diamonds applying the isochron method explained above to two or more separate, i.e., non-touching, cogenetic inclusions (or composites of cogenetic inclusions) in diamonds (e.g., Richardson et al., 1990; see also Figure 2.7).

Alternatively, to Sm-Nd isochron method, it is possible to use the equation 2.3 to apply the so-called Nd model age introduced after DePaolo and Wasserburg (1976). In general, the Nd model age assumes that the Nd isotopic composition of the undepleted mantle-forming the Bulk Silicate Earth equals that of the so-called chondritic uniform reservoir (CHUR). Therefore, the Bulk Silicate Earth isotope evolution line, or isotope growth curve, defines the initial Nd isotopic composition of continental igneous rocks $(^{143}Nd/^{144}Nd)_0$. If the present-day $(^{143}Nd/^{144}Nd)_t$ and $(^{147}Sm/^{144}Nd)_t$ isotopic ratios of a crustal rock sample are known (i.e., measurable by mass spectrometer), a model age for the formation of that rocks from the Bulk Silicate Earth (i.e., the timing of segregation from the mantle of the melt that produced the rock) is defined by the intersection of the Nd evolution line defined by the crustal sample with the evolution line of the considered geochemical reservoir. Nd model age can also be calculated assuming the depleted mantle (DM) as a reference geochemical reservoir. When the Nd model age is applied for dating

diamond, the sample is generally constituted by single grain or composite of cogenetic grains (e.g., Richardson et al., 2004).

Nd model ($T_{CHUR/DM}$), is mathematically expressed by the following equation derivable from the equation 2.3:

$$T_{CHUR/DM} = \frac{1}{\lambda} \ln \left[ \frac{\left(\frac{^{143}Nd}{^{144}Nd}\right)_t^{sample} - \left(\frac{^{143}Nd}{^{144}Nd}\right)_t^{CHUR/DM}}{\left(\frac{^{147}Sm}{^{144}Nd}\right)_t^{sample} - \left(\frac{^{147}Sm}{^{144}Nd}\right)_t^{CHUR/DM}} \right]. \quad (2.4)$$

Richardson et al. (1984) were the first ones to use the Nd model age to obtain the time of formation of South African diamonds by dating garnet inclusions (Stachel and Harris, 2008; see also Figure 2.8). This study of Richardson et al. (1984) is a landmark paper of diamond research field because it reported the first Paleoarchean Sm-Nd ages on garnet inclusions in lithospheric diamonds, demonstrating the antiquity of diamonds with respect to their kimberlitic magma host.

**Table 2-4**. Sm and Nd (wt. ppm) compositions (median, average, standard deviation, minimum, and maximum value) in peridotitic and eclogitic clinopyroxene inclusions in diamonds. Data have been extracted from the database of Stachel et al. (2004).

| | **Median** | **Average** | **St. Dev.** | **Min** | **Max** |
|---|---|---|---|---|---|
| Peridotitic clinopyroxene | | | | | |
| Nd | 1.36 | 2.84 | 3.69 | 0.74 | 9.42 |
| Sm | 0.49 | 1.61 | 2.50 | 0.30 | 6.06 |
| Eclogitic clinopyroxene | | | | | |
| Nd | 4.43 | 5.41 | 3.27 | 2.13 | 13.00 |
| Sm | 1.30 | 1.38 | 0.89 | 0.52 | 3.00 |

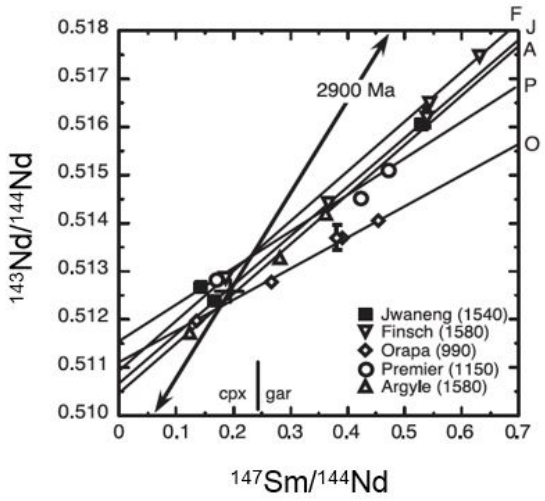


**Figure 2.7.** Example of Sm-Nd isochron method applied to eclogitic clinopyroxene (lowest Sm/Nd) and garnet (higher Sm/Nd) inclusions. The isotopic data for each mine (designated with the different solid symbols in the isochron diagram) were obtained from distinct groups of silicate inclusions extracted from separate diamonds. Isochron ages are indicated in parenthesis (after Richardson et al., 1999). Modified from Richardson et al., 2004.

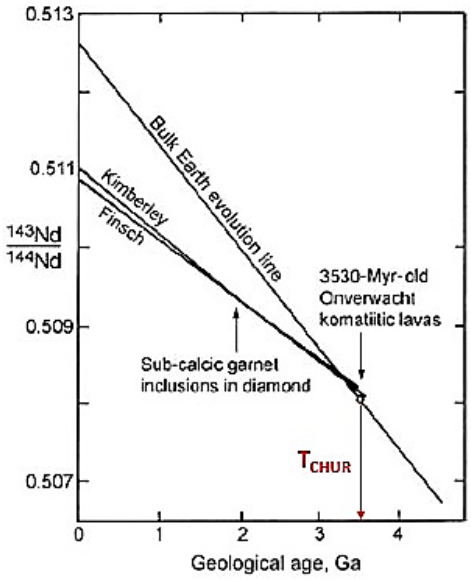


**Figure 2.8.** Example of Nd model age calculations applied to garnet inclusions in order to date diamonds coming from the Finsch and Kimberley mines studied by Richardson et al., 1984. Three samples were analyzed, each consisting of a composite of several hundred harzburgitic garnet inclusions. The intersection of the evolution line defined by the garnet inclusions with the Bulk Earth evolution line, defines the $T_{CHUR}$ indicated by the arrow (3200 ± 100 Myr). Modified from Richardson et al. (1984).

### *2.4.3 Syngenetic versus synchronous*

One of the main issues when it is interpreting the age information obtained from mineral inclusions, either isochron or model ages, is whether this age is effectively those of diamond formation. A long-standing condition for diamond dating has been that there is a syngenetic relationship between diamond and dated mineral inclusions, and, thus, that the age obtained from an inclusion indicates how long this inclusion was encapsulated within the diamond, giving the timing of diamond formation (e.g., Gurney et al., 2010). However, based on recent scientific evidence discussed in § 2.3, now we know that some mineral inclusions are protogenetic, i.e., they had formed before diamond crystallization. Nonetheless, a protogenetic inclusion can equally retain the same age as diamond in which it was passively enclosed. If this occurs, the protogenetic inclusions are terminated synchronous, not syngenetic (Nestola et al., 2017).

The possibility to use a protogenetic inclusion for dating diamond depends on the moment at which the isotopic system was closed to parent and daughter atoms mobility of specific isotope system (e.g., Sm-Nd). The measured age through isotopic dating system, in fact, is the closure age, i.e., when minerals have "stopped" diffusion of chemical elements with the surroundings (e.g., fluid, melt, or other minerals). As the system becomes close, the radiometric "clock" starts.

This can occur in two situations (Nestola et al., 2017):

i. When the minerals are encapsulated in diamonds. The crystal structure of diamond ensures slow diffusion so that the mineral inclusions are protected from any outside diffusional inter-action;

ii. When, during cooling, the minerals reached their closure temperature ($T_c$) for a specific decay system (e.g., Sm-Nd isotope system in garnet and clinopyroxene) and the diffusion of the isotopic components becomes infinitely slow (Ganguly and Tirone, 1999).

Conversely to a closed system, in an open system, the minerals isotopically inter-diffuse with fluids, melts, and other minerals of the external environment, such that the radiometric clock repeatedly resets or re-equilibrates with the surroundings until the system becomes closed through one of the two cases explained above. The rate at which this isotopic re-equilibration occurs is called *equilibration time* and is a function of temperature, elemental diffusivity, and effective grain size of the mineral of interest (e.g., Nestola et al., 2019).

The concept of closure temperature in solids was formally introduced by Dodson (1975) for a geochronological system, providing a mathematical formulation for its calculation on the basis of size and geometry of the mineral grain used for dating, as well as the cooling rate of the host rock and the diffusion kinetic properties of the decay system in the mineral of interest (Ganguly and Tirone, 2009). This formulation has been recently extended by Ganguly and Tirone (1999), and the general concepts and formulations of closure temperature can be found in the recent review of Ganguly and Tirone (2009). The closure temperature of the Sm-Nd system in clinopyroxene with diopside composition have been determined using the Dodson formulation (Dodson, 1973) considering diffusion at solid-state, a spherical crystal of 1 mm in diameter and cooling rate between 1 and 100°C/Myr. The resulting closure temperature for Nd in clinopyroxene is between 1000 and 1150°C (diffusion data from Van Orman et al., 2001,2002), i.e., within the range of temperature values for diamond formation within the subcontinental lithospheric mantle ranging from 900 to 1400°C (Stachel and Harris, 2008).

In the presence of fluids, diffusion of chemical species is much more efficient than at solid-state, also for the Sm-Nd isotope systems, which it has long been assumed to be a slowly diffusing system, especially in clinopyroxene (e.g., Ganguly and Tirone, 1999). Actually, there is much evidence of the metasomatic nature of the diamond-forming fluids (see § 2.3), which act as an infinite reservoir for diffusional exchange (Nestola et al., 2019). In the case of clinopyroxene inclusions in contact with a metasomatic fluid or melt forming diamond in the upper lithospheric mantle, free diffusion of Sm-Nd is, therefore, expected at the typical temperatures of lithospheric diamond formation.

If the diffusion rate for Sm and Nd in clinopyroxene is slow and the diamond-forming event is speedy, the diamond could entrap protogenetic mineral inclusions that did not have sufficient time to reach a full isotopic equilibration with the diamond-forming medium. In this case, the obtained age predates the diamond formation age. However, the time required by diamond to crystallize in the lithospheric mantle is yet poorly constrained (Jacob et al., 2014). Monocrystalline lithospheric diamonds show episodic growth and resorption features (e.g., Gress et al., 2018). If these episodic growth events were sufficiently long, on the order of hundreds or thousands of years, the equilibration time for a protogenetic inclusion might have been enough to lead them to reach the full chemical equilibrium with the metasomatic fluid or melt from which diamond precipitated. In this case, the protogenetic inclusion records the time of encapsulation in diamond; therefore, it can be considered synchronous with diamond (Nestola et al., 2017, 2019).

For garnet inclusions, limits for Sm-Nd equilibration have been recently calculated using a numerical modeling of chemical diffusive equilibration between a protogenetic garnet and diamond-forming fluids/melts, as a function of pressure, temperature, and grain size. The model showed that, in order to obtain the age of diamond from a protogenetic garnet, the inclusion must be smaller than 0.1 mm, and diamond must have formed at temperature higher than 1000°C (Nestola et al., 2019).

Therefore, the key point is the determination of the equilibration times also required by clinopyroxene to equilibrate for Sm and Nd isotope system with the diamond-forming fluids/melts at the condition of diamond crystallization within the subcontinental lithospheric mantle.

# Chapter 3

# Samples

## 3.1 Geological setting

The inclusion-bearing diamonds analyzed in this thesis work come from the Voorspoed kimberlite, diamondiferous mine, which belongs to the South-Eastern Terrane structural unit of the Kaapvaal Craton, South Africa (e.g., Howarth and Skinner, 2012; see also Figure 3.1). The Kaapvaal Craton, together with the Zimbabwe Craton, is one of the two Archean nuclei that constitute the biggest Kalahari Craton, which hosts the worldwide most economic diamondiferous kimberlites (Griffin et al., 2003).

### *3.1.1 Voorspoed mine (South Africa)*

The Voorspoed mine is placed in the Free State province of South Africa, 190 km south-west of the gold city of Johannesburg (Howarth and Skinner, 2012; De Wit et al., 2016; see also Figure 3.1). Voorspoed is a Group-II kimberlite (orangeite) pipe, with an emplacement age of 131.9 Myr (Phillips et al., 1998,1999). It forms the eastern-most limit of the Group II Kroonstad Kimberlite Cluster (see Figure 3.1), which consists of six pipes, including Voorspoed, and several intrusive

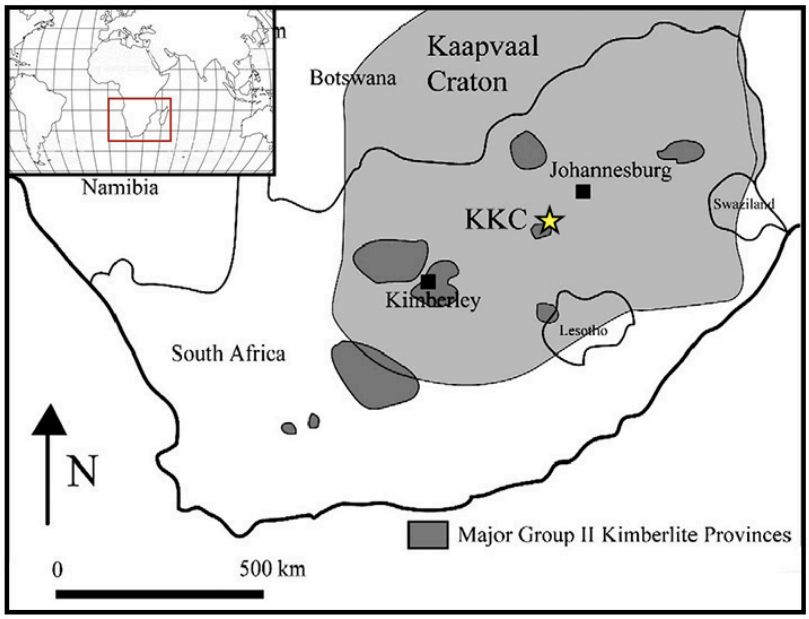


**Figure 3 1.** Map of South Africa showing the localization of the Voorspoed kimberlite pipe (star) from which the inclusion-bearing diamonds analyzed in this thesis work were extracted. The map also shows the position of the Kroonstad Kimberlite Cluster (KKC) and other Group II Kimberlite Clusters (dark gray fields) on the Archean Kaapvaal Craton (light gray field). Modified from G.H. Howarth et al. (2011).

kimberlite dikes and sills (Howarth and Skinner, 2012). Group II kimberlite term refers to a specific group of rocks defined as ultrapotassic, peralkaline, and volatile-rich ($H_2O$-rich), with abundant phlogopite macrocrysts and phenocrysts (Mitchell, 1995). The Group II Kroonstad Kimberlite Cluster was emplaced through the Witwatersrand Block of the Kaapvaal Craton and within the surrounding Phanerozoic Karoo Supergroup rocks about 145 Myr ago (De Wit et al., 2016). The only economic pipes of the Kroonstad Kimberlite Cluster are Voorspoed and Lace (Crown), the latter located approximately 9 km south-west of the Voorspoed kimberlite (Field et al., 2008).

The Voorspoed kimberlite pipe is similar in size and morphology to typical South African kimberlite pipes, but with a peculiar pipe infilling (Howarth and Skinner, 2012). In detail, the pipe of Voorspoed is oval-shaped, and the infill is composed of a combination of volcaniclastic and likely pyroclastic kimberlite units indicating two different magma sources, each with distinct diamond populations (De Wit et al., 2016, and references therein). The Voorspoed kimberlite was

discovered in 1906 by H.S. Harger and mined until 1912 when it was declared uneconomic (Howarth and Skinner, 2012). Subsequent, the De Beers company acquired the mine in 1912 and reactivated the mining production in 2006. Between 2006 and 2012, some of 2.6 Mct were produced from 11 Mt, at an average grade of 24 carats per hundred tons (De Beers annual reports). Diamonds historically recovered from the Voorspoed kimberlite were described as hard and difficult to cut (Wagner, 1914, cited in Field et al., 2008). The actual diamond production is characterized by colorless to near-colorless stones, and, among the fancies, there are yellow diamonds and a small proportion of pink diamonds. Large stones, up to 10.4 ct, and Type II diamonds (i.e., without any measurable nitrogen impurities) are commonly recovered from the Voorspoed mine (De Wit et al., 2016). Dodecahedral diamonds, mostly distorted, dominate, while octahedral diamonds are rare (Field et al., 2008).

The data reported in the literature about the diamonds and mantle-xenoliths from the Voorspoed kimberlite pipe are little. So far, the analyses conducted on inclusion-bearing diamonds from the Voorspoed mine have indicated both a lherzolitic and eclogitic affinity in term of inclusions paragenesis, with an unusually low abundances of harzburgitic inclusion suite with respect to the diamond populations in the kimberlites on the Kaapvaal Craton, and many other kimberlites worldwide (Viljoen et al., 2018). The study of Nestola et al. (2018) yielded the first geothermobarometric data for Voorspoed diamonds, suggesting a pressure of diamond formation of 5.2 GPa (~ 160 km), calculated using the elastic geobarometry on a kyanite inclusion, and an FTIR N-aggregation residence temperature of about 1120 °C (Nestola et al., 2018).

## 3.2 Analyzed samples

The inclusion-bearing diamonds analyzed in this thesis work were collected from the run-of-mine production of the Voorspoed mine. The sample suite was composed of thirty-seven clinopyroxene inclusions hosted in nine unpolished and colorless monocrystalline gem-quality diamonds, ranging in size from ~ 2 to ~ 5 mm. All

samples were preliminary characterized at the microscope in order to detect the most suitable inclusions for the single-crystal X-ray diffraction analyses. From a morphological point of view, the studied diamonds are mostly irregularly-shaped or rounded (resorbed) dodecahedron stones. They contain several clinopyroxene inclusions, ranging in size from ~ 50 to up ~ 500 μm. Besides, the monoclinic clinopyroxene inclusions are characterized by flattened or elongated diamond-imposed cubo-octahedral morphologies or elongated and distorted curvilinear contour (see Figure 3.2). Within each single diamond, it was possible to measure from one to eleven clinopyroxene inclusions. In detail, in eight of the nine studied diamonds were analyzed multiple inclusions of clinopyroxene. To preliminary constrain the paragenesis affinity of the clinopyroxene inclusions, it was examined the color of the inclusions, and were used the unit-cell volumes calculated by single-crystal X-ray diffraction (see § 4.1). More precisely, it was assumed that eclogitic clinopyroxenes (omphacite) have a unit-cell volume defined in the range between 420 and 425 $Å^3$ and a pale-green color, whereas peridotitic clinopyroxenes (Cr-diopside) have a unit-cell volume varying from 430 to 435 $Å^3$ and an emerald-green color. As discussed in § 2.1.3, more detailed chemical analyses are required to precisely determine the paragenesis of clinopyroxene inclusions. In Table 3-1 is reported a list of the samples investigated in this thesis work.

**Table 3-1.** List of the diamonds from the Voorspoed kimberlite (South Africa) and their inclusions analyzed in this thesis work. The paragenesis affinity of the clinopyroxene inclusions is indicated as P-type for peridotitic (lherzolitic) and E-type for eclogitic. The carat weights of the samples are also reported.

| Diamond | Carat weight | Inclusion | Paragenesis affinity |
|---|---|---|---|
| Lot41stone1 | 0.10 | Lot41stone1_inc1 | E-type |
| | | Lot41stone1_inc2 | E-type |
| | | Lot41stone1_inc3 | E-type |
| | | Lot41stone1_inc4 | E-type |

(*continued on next page*)

**Table 3-1** (*continued*).

| | | | | |
|---|---|---|---|---|
| | Lot41stone2 | 0.19 | Lot41stone2_inc1 | P-type |
| | | | Lot41stone2_inc2 | P-type |
| | | | Lot41stone2_inc3 | P-type |
| | | | Lot41stone2_inc4 | P-type |
| | Lot34stone2 | 0.11 | Lot34stone2_inc1 | P-type |
| | | | Lot34stone2_inc2 | P-type |
| | | | Lot34stone2_inc3 | P-type |
| | Lot34stone18 | 0.23 | Lot34stone18_inc1 | P-type |
| | | | Lot34stone18_inc2 | P-type |
| | | | Lot34stone18_inc3 | P-type |
| | | | Lot34stone18_inc4 | P-type |
| | Lot34stone21 | 0.16 | Lot34stone21_inc1 | P-type |
| | Lot34stone22 | 0.20 | Lot34stone22_inc1 | P-type |
| | | | Lot34stone22_inc2 | P-type |
| | | | Lot34stone22_inc3 | P-type |
| | | | Lot34stone22_inc4 | P-type |
| | Lot22stone36 | 0.22 | Lot22stone36_inc1 | P-type |
| | | | Lot22stone36_inc2 | P-type |
| | | | Lot22stone36_inc3 | P-type |
| | | | Lot22stone36_inc4 | P-type |
| | | | Lot22stone36_inc5 | P-type |
| | | | Lot22stone36_inc6 | P-type |
| | | | Lot22stone36_inc7 | P-type |
| | | | Lot22stone36_inc8 | P-type |
| | | | Lot22stone36_inc9 | P-type |
| | | | Lot22stone36_inc10 | P-type |
| | | | Lot22stone36_inc11 | P-type |
| | Lot10stone21 | 0.41 | Lot10stone21_inc1 | P-type |
| | | | Lot10stone21_inc2 | P-type |
| | Lot8stone4 | 0.28 | Lot8stone4_inc1 | P-type |
| | | | Lot8stone4_inc2 | P-type |
| | | | Lot8stone4_inc3 | P-type |
| | | | Lot8stone4_inc4 | P-type |
| **Total** | **9 diamonds** | **1,91 ct** | **37 inclusions** | |

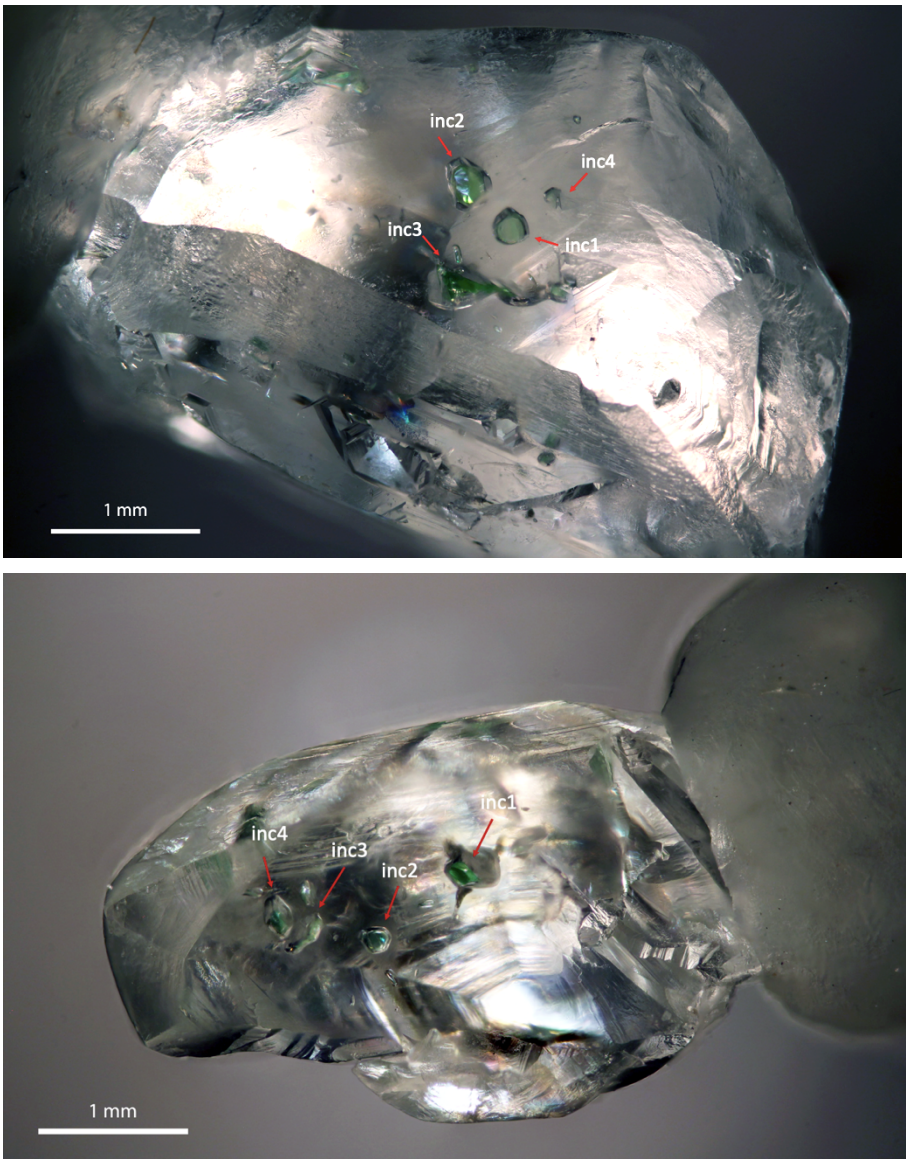


**Figure 3.2.** Diamonds Lot34stone22 (upper) and Lot41stone1 (bottom) from the Voorspoed kimberlite, South Africa. These diamonds, with their green clinopyroxene inclusions (indicated by red arrows), represent the typical lithospheric diamonds investigated in this thesis work.

# Chapter 4

# Experimental methods

## 4.1 Single-Crystal X-Ray Diffraction (SCXRD)

The crystallographic orientations of the studied clinopyroxene inclusions in each diamond were determined by *in-situ*, non-destructive, single-crystal X-ray diffraction (SCXRD), by adapting the methods developed to high-pressure studies of single-crystals in diamond-anvil cells (e.g., Nestola et al., 2011). The analyses were performed using a Rigaku Oxford Diffraction SuperNova single-crystal diffractometer, equipped with a Dectris Pilatus 200 K area detector and a Mova X-ray micro-source, installed at the Department of Geosciences, University of Padua, Italy. In order to minimize the absorption effects due to the large size of the host diamond, the instrument worked at 50 kV and 0.8 mA using a monochromatized MoKα radiation (λ = 0.71073 Å). The beam spot was about 120 μm, and the distance between sample and detector was 68 mm. This configuration allows to analyze individual inclusions still trapped in their diamond hosts down to 5 μm (Angel and Nestola, 2016).

The diffraction analyses followed the same methodological approach by Milani et al. (2016). Accordingly, the first step was the optical centering of each clinopyroxene inclusion under the X-ray beam for diffraction measurements. From the examination of the observed diffracted intensities and comparison of these with predicted spot intensities, inclusions that did not carefully centered in the X-ray

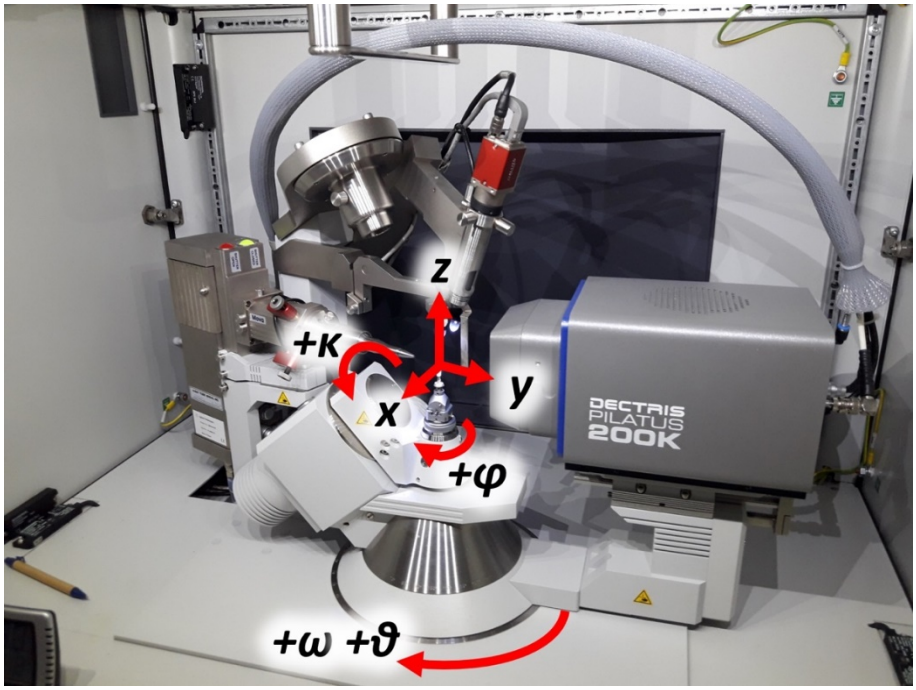


**Figure 4.1.** Rigaku Oxford Diffraction SuperNova single-crystal diffractometer used in this thesis work to study inclusions of clinopyroxene still trapped in their diamond hosts. From right to left of the figure are shown the Dectris Pilatus 200 K area detector, the conventional goniometer head at the top which diamonds were mounted by wax, and the X-ray micro-source. In the figure are also superimposed the 4 circles (ω, *k*, θ, φ) that define the kappa geometry of the goniometer, along with the axes of the Cartesian coordinate system of the diffractometer as defined by Busing and Levy, 1967.

beam were identified and corrected by moving diamond. After this alignment procedure, the measurement of the orientation of each inclusion was performed with a 360° scan along the phi-axis of the goniometer (see Figure 4.1), with a frame width of 1°. The exposure time was in the range of 15-30 seconds per frame, depending on the inclusion size. The processing of the measured frames or diffraction pattern were operated with the Crysalis software from Rigaku Oxford Diffraction. For each frame, the positions of the diffraction peaks, which correspond to reflections generated by crystallographic planes that satisfy the *Bragg's Law*, were automatically indexed by the software. This indexing procedure allows to unambiguously determine which diffraction peaks in the data set belong to clinopyroxene and which to the diamond host. An example of the result of a single diffraction measurement is reported in Figure 4.2.

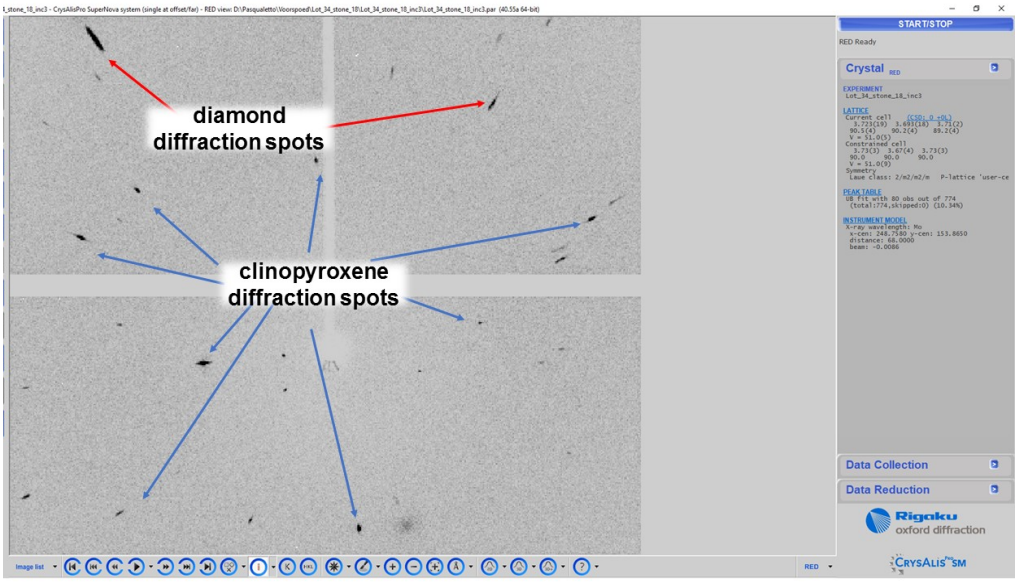


**Figure 4.2.** The image shows a typical diffraction pattern collected by single-crystal X-ray diffractometer used in this thesis work on inclusions still trapped within diamonds. The different diffraction spots (indicated by the arrows) were assigned to clinopyroxene and diamond using Crysalis software (Rigaku Oxford Diffraction). From the analysis of these spots were determined the unit-cell parameters of both diamond and clinopyroxene and hence their UB matrices, which in turn were used to determine the orientations of the inclusions relative to the diamond host.

Once all diffraction peaks were indexed, these were used by the software to determine the orientation matrices, or so-called UB matrices, of each clinopyroxene inclusion and its diamond host simultaneously. Therefore, for each measured inclusion, the output datum is a couple of UB matrices, one relative to the inclusion and the other one to the diamond host. All the collected UB matrices are reported in Appendix B. In technical terms, the UB matrix specifies the orientation of crystallographic axes of each crystal (inclusion or diamond) with respect to a set of coordinate axes associated with the diffractometer (see Figure 4.1). In other words, the UB matrix provides the information relative to the lattice parameters ($a,b,c,\alpha,\beta,\gamma$) that individuate the unit cell of a crystal and its orientation with respect to the phi-axis coordinate system of the diffractometer (Busing and Levy, 1967). Since the diffractometer coordinate system, with respect to which the UB matrices of each inclusion-diamond host pair is the same, by mathematical manipulation of them, it is possible to calculate the relative crystallographic orientations between the inclusions and their diamond hosts.

## 4.2 OrientXplot calculations

The UB matrices of each inclusion-diamond host pair were elaborated using the dedicated free available software OrientXplot (Angel et al., 2015), which allowed to calculate and display the relative crystallographic orientations between clinopyroxene inclusions and their diamond hosts (see Figure 4.3). The information about how this software working is reported below and has been extracted from the "Users Manual" of OrientXplot (Angel et al., 2015).

OrientXplot software uses the input UB matrices determined by SCXRD directly to determine, by mathematical approach, the absolute orientations between each inclusion-diamond host pair, i.e., the angles between the crystallographic axes of the diamond host and those of its inclusion(s). Nonetheless, in order to correctly determine the orientations of the inclusions relative to diamonds, it has to remove the ambiguities in indexing the diffraction patterns resulting from the symmetry of both the inclusion and the host. For example, olivine has an orthorhombic *mmm* point group symmetry, which makes the [100] direction equivalent to [-100], [010] equivalent to [0-10], and [001] equivalent to [00-1]. As a consequence, it is impossible by any physical measurement method to determine any difference between these symmetrically-equivalent crystallographic directions. Similar ambiguities characterize the crystallographic orientations of diamond and clinopyroxene, which have cubic *m*3*m* and monoclinic 2/*m* symmetry point group, respectively. If these ambiguities are not correctly considered, the distribution of the crystallographic orientations between the inclusions and diamond host will appear more random than it truly is (see Figure 4.3).

The symmetry operators that describe the possible symmetrically-equivalent orientations, preserving a right-handed description of the unit-cell axes of a crystal with a specific symmetry point group, do not include any inversion symmetry, including mirrors. Therefore, the symmetry ambiguities are described by the point sub-group 2 for clinopyroxene and 432 for diamond. OrientXplot, thus, eliminates the symmetry ambiguities by rotating the input UB matrix of each clinopyroxene

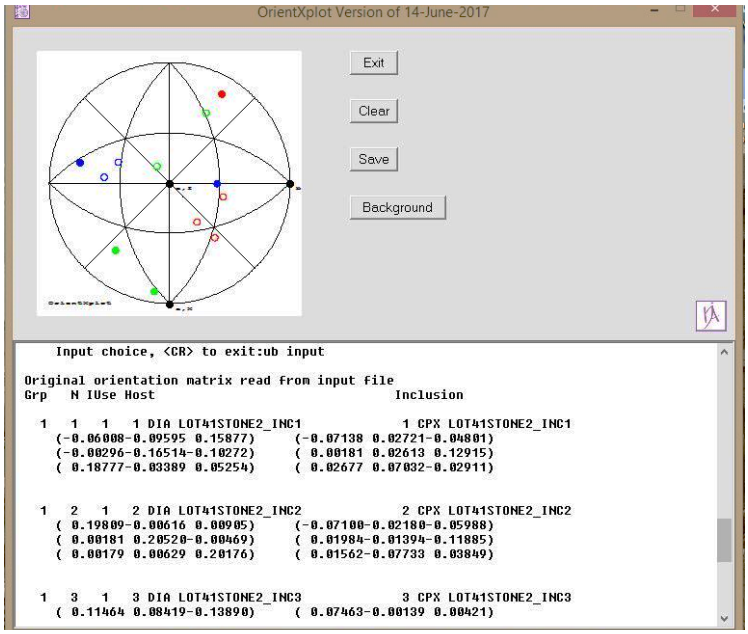


**Figure 4.3**. Graphic window of the user interface of OrientXplot software (Angel et al., 2015), showing the plotting window (top), with the stereographic projection relative to diamond Lot41stone2 analyzed in this thesis work, obtained without any treatment of the UB matrices for symmetry ambiguities; and the integrated command-line (bottom), where a list of some input UB matrices is visible. The left-hand column reports the UB matrices of the diamond host, while the right-hand column displays the UB matrices of each clinopyroxene inclusions.

inclusion by the symmetry elements of diamond point sub-group 432, oriented to coincide with the unit-cell axes of the diamond host (as determined by its UB matrix). This mathematical procedure generates 24 possible symmetrically-equivalent crystallographic orientations of clinopyroxene relative to its diamond host. For each of these 24 relative orientations, there are 2 symmetrically-equivalent orientations of the clinopyroxene because of its symmetry. Therefore, in total, are produced 24 x 2 = 48 symmetrically and physically indistinguishable descriptions of the orientation relationships between the monoclinic clinopyroxene and its cubic diamond host (see Figure 4.4).

OrientXplot provides two ways to choose one of these 48 symmetrically-equivalent orientations for each inclusion-host pair:

i. The first method requires to select the orientation that puts a specific inclusion direction (indicated by user), called *primary axis*, within the

asymmetric unit of the host, along with a specific *secondary axis* (user-specified) of the inclusion closest to the *c*-axis of the host;

ii. The second method is analogous to the first, but with the difference that the *primary axis* of the inclusion has to be chosen closest to a user-specified crystallographic direction of the host.

The resulting crystallographic orientations of each inclusion relative to its diamond host are then plotted on a stereographic projection, which has the *x*-, *y*-, and *z*-axes coincident with the principal crystallographic axes of the diamond host *a*, *b*, and *c* (see Figure 4.3, 4.4). The results are independent of the choice of one of the two methods mentioned above. Besides, if the diamond contains multiple inclusions, the stereographic projection also clearly shows the orientation relationships between the different inclusions since these are oriented to the same host reference orientation.

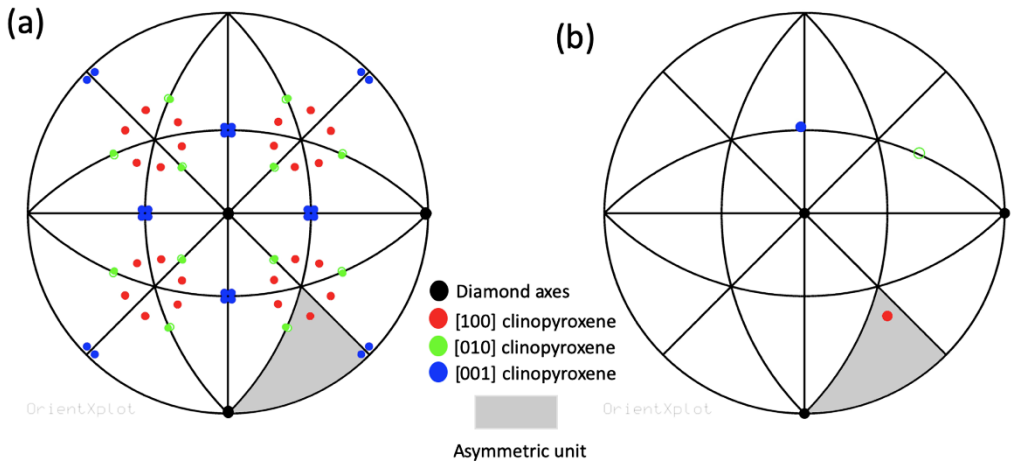


**Figure 4.4.** (a) Stereographic projection showing the 48 possible symmetrically equivalent orientations of clinopyroxene Lot34stone21_inc1 in diamond Lot34stone21. All inclusion axes poles (red, green, and blue dots) are duplicated in the upper and lower hemisphere. Only one of these 48 possible orientations have to be selected; otherwise the orientation of clinopyroxene axes will appear more random than it really is. (b) The same stereographic projection obtained after selecting one of the possible orientations for the inclusion, using one of the two symmetry criteria explained in the text, with the clinopyroxene *a*-axis selected as *primary axis* falling within the asymmetric unit of diamond host (gray area), and the clinopyroxene *b*-axis chosen as *secondary axis* closest to *c*-axis of diamond. The orientation of the *c*-axis is automatically constrained for a right-handed system. Empty symbols are directions plotting in the lower hemisphere.

## 4.3 Micro-Raman Spectroscopy

Micro-Raman spectroscopy is a non-destructive experimental technique that permits to detect liquid and gaseous compounds, solid phases, as well as solute species in fluid inclusions based on the vibrational behavior of ions or groups of bonded ions (Frezzotti et al., 2012). In this thesis work, clinopyroxene inclusions still trapped in their diamond hosts were investigated using a Thermo Scientific™ DXR™ Raman Microscope at the Department of Geoscience (University of Padua, Italy). In detail, the micro-Raman measurements were conducted out on the rims of the inclusions in order to detect the possible presence of a fluid film.

Reflected and transmitted light optics were used in order to determine the analysis positions. The analyses were performed using a 10x objective with 2.2 $cm^{-1}$ spectral resolution and ~ 1 μm spatial resolution, using a 532-nm excitation laser source at a power of 10 mW. The unpolarized Raman spectra were collected in the frequency range extended from 50 to 3573 $cm^{-1}$ μm. In order to maximize the signal to noise ratio, each measurement was repeated from 4 to 16 times, using an exposure time between 10 and 60 s, and then merged at the end of the analysis. A focusing on the inclusion rims was obtained by acquiring a set of distinct Raman spectra along different traverses perpendicular to the diamond/inclusions interface, at steps ranging from 1 to 2 μm. The spectrum which gives the strongest signal from the inclusion/diamond interface was selected for qualitative analysis. Spectral fitting was performed using the Thermo Scientific™ OMNIC Spectral Software. Raman spectra of all the investigated samples are available in Appendix C.

# Chapter 5

# Results

## 5.1 Crystallographic orientations of clinopyroxene inclusions in diamonds

The crystallographic orientation relationships (CORs) between the thirty-seven clinopyroxene inclusions and their nine diamond hosts measured in this thesis work are plotted in Figure 5.1. For all clinopyroxene inclusions, one unambiguous orientation was chosen in order to eliminate the symmetry ambiguities arising from the symmetry of both diamond and clinopyroxene. In detail, it was used the first symmetry criterion explained in § 4.2, with *a*-axis of each clinopyroxene inclusion chosen as the primary axis plotted within a specific asymmetric unit of the diamond host. The *b*-axis of the clinopyroxene was selected as the secondary axis plotted closest to the *c*-axis of the diamond host. Clinopyroxene *c*-axis, then, was automatically constrained for a right-handed system. The angles between the crystallographic axes of each diamond host and each clinopyroxene inclusion, calculated using OrientXplot software (Angel et al., 2015), are reported in Table 5-1. The uncertainty associated with these angular values is not higher than 2-3° (Nestola et al., 2014; Nimis et al., 2019).

As a whole, clinopyroxene inclusions showed no preferred orientations relative to their diamond hosts. The apparent clustering of the [100] crystallographic directions of clinopyroxene inclusions within the asymmetric unit of the diamond

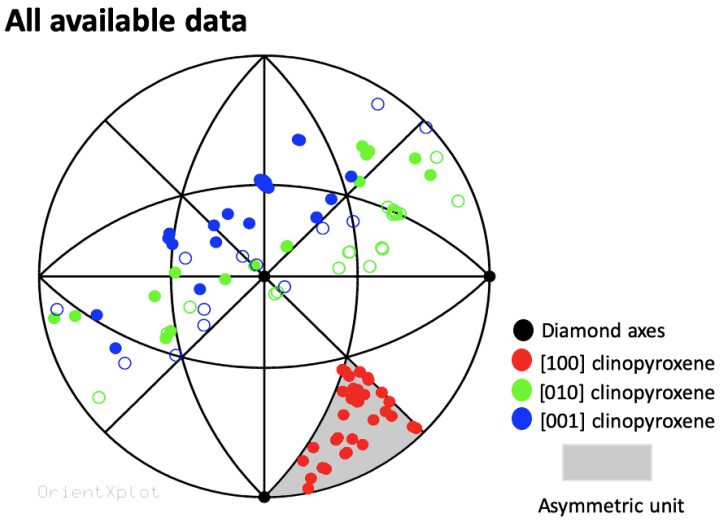


**Figure 5.1.** Stereogram showing the overall crystallographic orientations, relative to their diamond hosts, of the 37 clinopyroxene inclusions in 9 Voorspoed diamonds from this thesis work. The *a*-axes of the clinopyroxene inclusions are distributed over the entire asymmetric unit of the diamond host (gray area) according to the chosen symmetry criterion explained in the text. Empty symbols are directions plotting in the lower hemisphere. Data show any specific orientation of the clinopyroxene axes with respect to the diamond host axes.

host (the gray area of the stereogram in Figure 5.1), arises from the chosen symmetry criterion, and it does not link with real orientation preference.

Although this lack of a dominant preferred orientation between the clinopyroxene inclusions and their diamond hosts, in five diamonds, were found some inclusions of clinopyroxene having a similar crystallographic orientation to each other. Each of these diamonds showed one cluster of similarly oriented clinopyroxenes, with the other clinopyroxene inclusions that exhibited angular misorientations well beyond the measured uncertainties. In detail, samples Lot41stone1, Lot34stone2, and Lot36stone22, each presents a couple of clinopyroxene inclusions with angular mismatches up to only 3°, i.e., within one experimental uncertainty (see Figure 5.2 and Table 5-1). Similarly, in samples Lot34stone18, and Lot34stone22 were observed clinopyroxene inclusions in the same diamond, which shared a similar crystallographic orientation but with any specific orientation relative to their diamond hosts (see Figure 5.3 and Table 5-1).

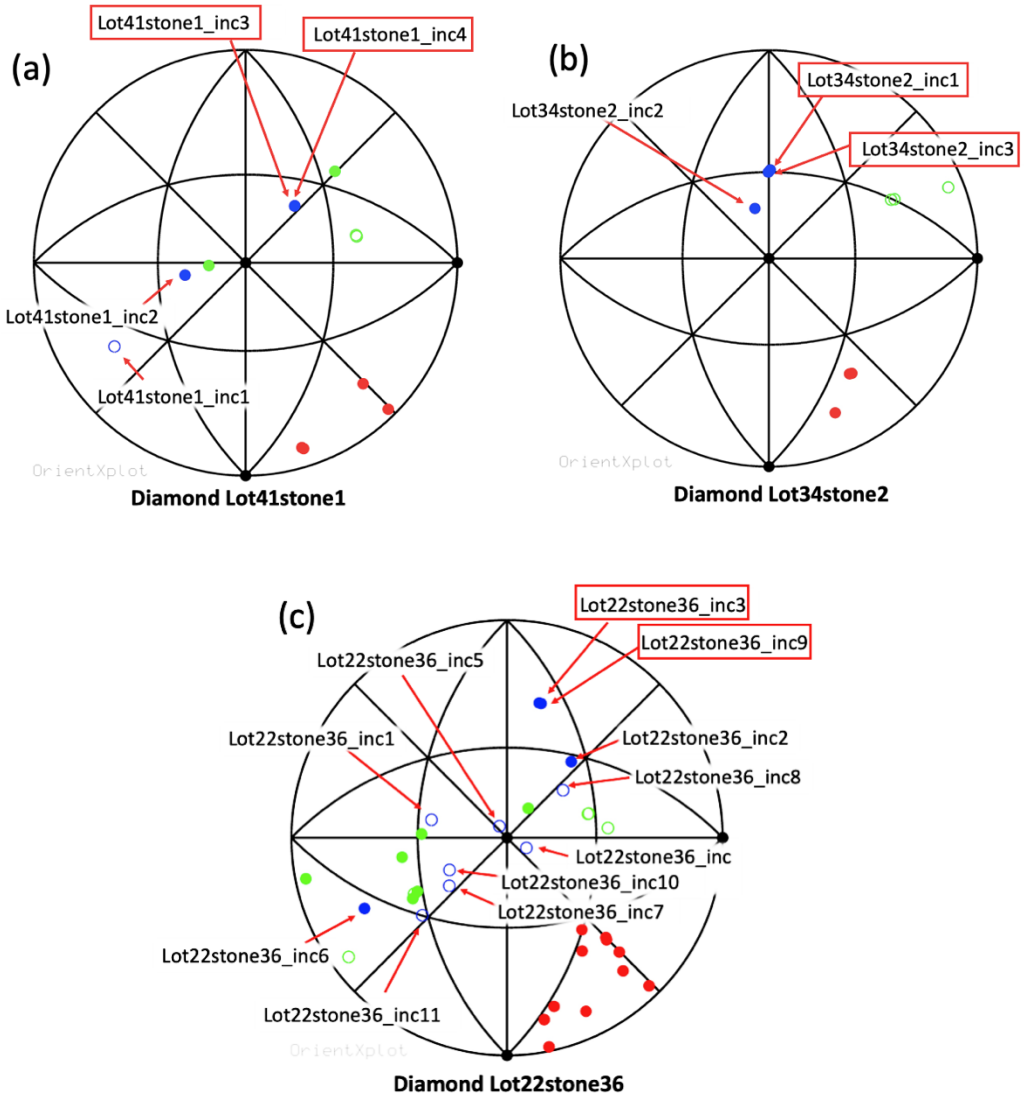


**Figure 5-2.** Stereograms showing the crystallographic orientations, relative to their diamond hosts, of multiple clinopyroxene inclusions (indicated with red arrows) in diamonds Lot41stone1 (a), Lot34stone2 (b), and Lot22stone36 (c). The red rectangles highlight the iso-oriented inclusions that are present in each of these diamonds, and which have angular mismatches up to only 3°. It is possible to see that the poles of the crystallographic axes (dots) of these inclusions practically fall at the same dot point. The other inclusions show angular misorientations to each other well beyond experimental uncertainties. For all angular values see Table 5-1. Symbols as in Figure 5.1.

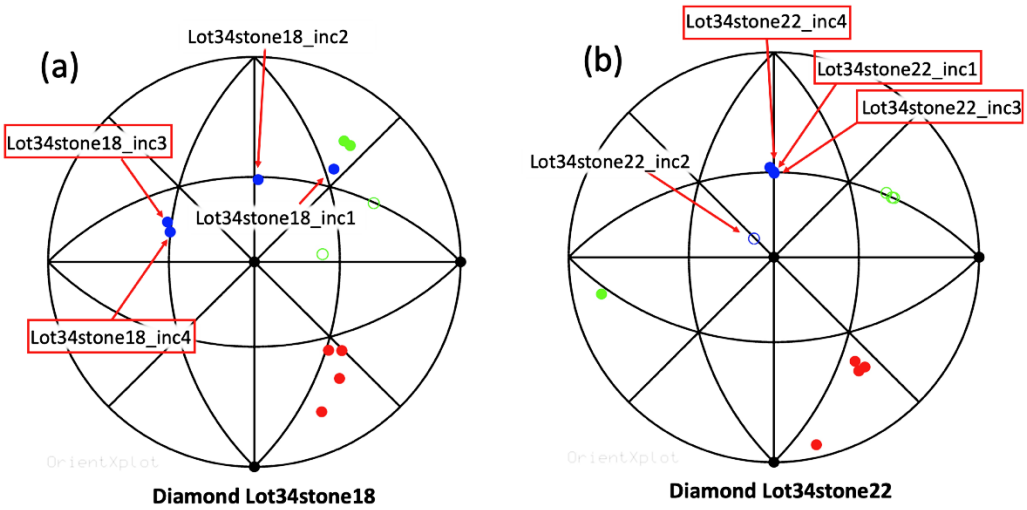


**Figure 5.3.** Stereograms showing the crystallographic orientations, relative to their diamond hosts, of multiple clinopyroxene inclusions (indicated with red arrows) in diamonds Lot34stone18 (a), and Lot34stone22 (b). The red rectangles highlight the iso-oriented inclusions that are present in each of these diamonds, and which have angular mismatches up to 6°, i.e., within two experimental uncertainties. The other inclusions show angular misorientations to each other well beyond experimental uncertainties. For all angular values see Table 5-1. Symbols as in Figure 5.1.

In the remaining three multiple inclusion-bearing diamonds, Lot41stone2, Lo10stone21, and Lot8stone4, clinopyroxene inclusions showed no specific orientations relative to the diamond hosts (see Figure 5.4 and Table 5-1). The only diamond sample with one single measured clinopyroxene inclusion, Lot34stone1, presented no specific crystallographic relationship with its diamond host and was used to test the number of possible symmetrically equivalent orientations for one single clinopyroxene inclusion in diamond using OrientXplot software (Angel et al., 2015; see also Table 5-1 for angular values and Figure 4.4 in § 4.2).

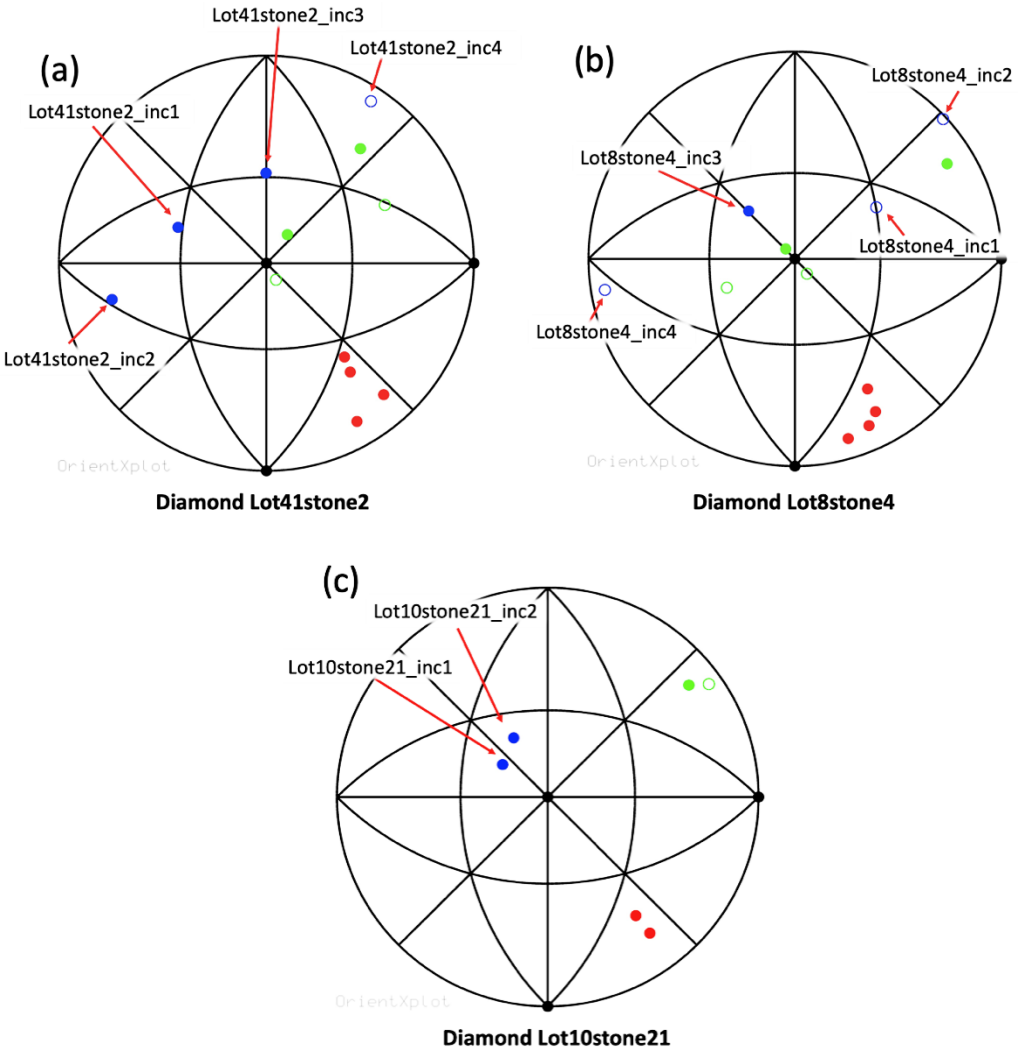


**Figure 5.4.** Stereograms showing the crystallographic orientations, relative to their diamond hosts, of clinopyroxene multiple inclusions (indicated with red arrows) in diamonds Lot41stone2 (a), Lot8stone4 (b), and Lot10stone21 (c), which show no specific orientation relationships with respect to their diamond hosts and angular misorientations to each other well beyond experimental uncertainties. For all angular values see Table 5-1. Symbols as in Figure 5.1.

**Table 5-1.** Angles (degree) between the three axes of clinopyroxene *a, b*, and *c*, and three axes of diamonds $a_1$, $a_2$, and $a_3$ for the 37 inclusions of clinopyroxene studied in this thesis.

| | **Clinopyroxene axes** | | ***a*** | | | ***b*** | | | ***c*** | |
|---|---|---|---|---|---|---|---|---|---|---|
| | **Diamond axes** | $a_1$ | $a_2$ | $a_3$ | $a_1$ | $a_2$ | $a_3$ | $a_1$ | $a_2$ | $a_3$ |
| **N** | **Samples** | | | | | | | | | |
| 1 | Lot41stone1_inc1 | 45 | 47 | 77 | 88 | 110 | 20 | 60 | 143 | 107 |
| 2 | Lot41stone1_inc2 | 45 | 46 | 88 | 130 | 52 | 62 | 83 | 123 | 33 |
| 3 | Lot41stone1_inc3 | 19 | 73 | 84 | 102 | 35 | 123 | 119 | 66 | 39 |
| 4 | Lot41stone1_inc4 | 18 | 72 | 85 | 102 | 38 | 123 | 117 | 64 | 39 |
| 5 | Lot41stone2_inc1 | 48 | 56 | 61 | 137 | 53 | 71 | 107 | 135 | 49 |
| 6 | Lot41stone2_inc2 | 30 | 61 | 83 | 108 | 79 | 19 | 79 | 160 | 75 |
| 7 | Lot41stone2_inc3 | 45 | 55 | 67 | 115 | 37 | 115 | 137 | 89 | 47 |
| 8 | Lot41stone2_inc4 | 44 | 49 | 81 | 81 | 83 | 169 | 148 | 57 | 94 |
| 9 | Lot34stone2_inc1 | 43 | 57 | 68 | 113 | 35 | 114 | 139 | 89 | 46 |
| 10 | Lot34stone2_inc2 | 25 | 67 | 78 | 112 | 23 | 94 | 115 | 95 | 28 |
| 11 | Lot34stone2_inc3 | 42 | 56 | 68 | 114 | 36 | 113 | 136 | 88 | 45 |
| 12 | Lot34stone18_inc1 | 27 | 67 | 77 | 94 | 53 | 143 | 132 | 55 | 61 |
| 13 | Lot34stone18_inc2 | 41 | 56 | 70 | 114 | 37 | 114 | 135 | 87 | 44 |
| 14 | Lot34stone18_inc3 | 49 | 58 | 59 | 137 | 53 | 73 | 110 | 135 | 50 |
| 15 | Lot34stone18_inc4 | 52 | 52 | 62 | 141 | 56 | 72 | 104 | 134 | 47 |
| 16 | Lot34stone21_inc1 | 41 | 55 | 67 | 114 | 35 | 114 | 135 | 92 | 47 |
| 17 | Lot34stone22_inc1 | 47 | 56 | 70 | 117 | 39 | 115 | 138 | 90 | 45 |
| 18 | Lot34stone22_inc2 | 14 | 77 | 86 | 78 | 165 | 81 | 101 | 101 | 165 |
| 19 | Lot34stone22_inc3 | 43 | 57 | 69 | 114 | 34 | 114 | 137 | 91 | 45 |
| 20 | Lot34stone22_inc4 | 43 | 56 | 66 | 112 | 35 | 114 | 138 | 92 | 47 |
| 21 | Lot22stone36_inc1 | 11 | 79 | 89 | 82 | 141 | 53 | 99 | 129 | 140 |
| 22 | Lot22stone36_inc2 | 20 | 75 | 78 | 93 | 40 | 130 | 126 | 60 | 49 |
| 23 | Lot22stone36_inc3 | 49 | 50 | 67 | 102 | 49 | 137 | 151 | 77 | 65 |
| 24 | Lot22stone36_inc4 | 41 | 60 | 64 | 54 | 143 | 95 | 85 | 80 | 169 |
| 25 | Lot22stone36_inc5 | 14 | 78 | 81 | 79 | 168 | 87 | 97 | 94 | 173 |
| 26 | Lot22stone36_inc6 | 44 | 46 | 87 | 105 | 79 | 19 | 65 | 149 | 73 |
| 27 | Lot22stone36_inc7 | 47 | 48 | 73 | 67 | 132 | 52 | 66 | 119 | 142 |
| 28 | Lot22stone36_inc8 | 25 | 65 | 83 | 65 | 134 | 127 | 111 | 63 | 143 |
| 29 | Lot22stone36_inc9 | 50 | 50 | 66 | 100 | 48 | 137 | 152 | 78 | 65 |
| 30 | Lot22stone36_inc10 | 43 | 50 | 78 | 64 | 134 | 55 | 74 | 119 | 146 |
| 31 | Lot22stone36_inc11 | 49 | 56 | 122 | 89 | 48 | 44 | 56 | 129 | 56 |
| 32 | Lot10tone21_inc1 | 39 | 54 | 78 | 129 | 39 | 81 | 107 | 112 | 30 |
| 33 | Lot10stone21_inc2 | 42 | 56 | 70 | 126 | 35 | 94 | 120 | 107 | 36 |
| 34 | Lot8stone4_inc1 | 17 | 73 | 84 | 76 | 126 | 141 | 114 | 50 | 130 |
| 35 | Lot8stone4_inc2 | 32 | 62 | 80 | 82 | 84 | 169 | 135 | 43 | 91 |
| 36 | Lot8stone4_inc3 | 35 | 62 | 71 | 122 | 33 | 82 | 114 | 113 | 36 |
| 37 | Lot8stone4_inc5 | 25 | 66 | 83 | 95 | 95 | 8 | 81 | 170 | 94 |

## 5.2 Micro-Raman analyses

Clinopyroxene inclusions in seven of the nine studied inclusion-bearing diamonds were analyzed with micro-Raman confocal spectroscopy (see § 4.3). In Table 5-2 is reported the list of the investigated diamond samples and relative inclusions. In Figure 5.5 and 5.6., it is possible to observe some examples of the typical Raman spectra collected from the rims of clinopyroxene inclusions. Figure 5.7 reports an example of the Raman spectrum collected from clinopyroxene inclusions, which can be easily recognized by the Raman peak in the 600-700 $cm^{-1}$ spectral region (Frezzotti et al., 2012). In Figure 5.8, instead, is shown an example of the traverse collected perpendicular to the diamond/inclusions interface. Raman spectra of all the investigated samples are reported in Appendix C.

Several of the studied clinopyroxene inclusions showed a Raman-active rim, which gives a distinct signal unrelated to either the diamond or clinopyroxene. In detail, two broad vibrational bands, indicative of a non-crystalline material, at 617-659 $cm^{-1}$ and 759-805 $cm^{-1}$ spectral region, were measured on the rims of thirteen clinopyroxene inclusions (see Table 5-2 and Figure 5.5-5.6, 5.8). These two broad peaks are similar to those reported by Nimis et al. (2016) and Nestola et al. (2018) around mineral inclusions in lithospheric diamonds and assigned to pyrosilic acid $Si_2O(OH)_6$ dimers and orthosilicic $Si(OH)_4$ acid monomers in an aqueous fluid, respectively (Zotov and Keppler, 2002). Besides, the two broad peaks, in some samples, were found accompanied by a shoulder near the upper end of the measured spectral range (3573 $cm^{-1}$) and considered to be the ~ 3600 $cm^{-1}$ O-H stretching band of water (Ratcliffe and Irish, 1982; see also Figure 5.5).

A strong first-order peak characterizes the Raman signal from the host diamonds at ~ 1333 $cm^{-1}$ ($sp^3$ bonds), along with several weak bands related to second-order peaks (~ 1850, 2020, 2460, and 2670 $cm^{-1}$; Windl et al., 1993), to N-H stretching (~ 3100-3400 $cm^{-1}$; e.g., Goss et al., 2014), to $sp^2$ amorphous carbon ( ~ 1520-1580 $cm^{-1}$; Prawer and Nemanich, 2004), and likely to trans-polyacetylene (~1420-1440 $cm^{-1}$, and 1270 $cm^{-1}$; Ferrari and Robertson, 2004). Weak Raman bands, in the ~

1040-1070 $cm^{-1}$ interval, were also observed in spectra taken on the rim of the inclusions, similar to those observed by Nimis et al. (2016) in the 950-1100 $cm^{-1}$ region and ascribed to the diamond host.

**Table 5-2**. List of the diamond samples and relative clinopyroxene inclusions studied in this thesis work with micro-Raman confocal spectroscopy, along with data for the observed Raman-active fluid films around the inclusions. The dashes (—) mean that any reliable Raman-active fluid rim was obtained from the inclusion.

| **Diamond** | **Inclusion** | **Raman shift ($cm^{-1}$)** | **Intensity** | **Raman shift ($cm^{-1}$)** | **Intensity** |
|---|---|---|---|---|---|
| Lot41stone1 | 1 | 621 | 121 | 778 | 67 |
| | 2 | — | — | — | — |
| | 3 | — | — | — | — |
| | 4 | 648 | 41 | 791 | 28 |
| Lot41stone2 | 1 | 629 | 386 | 769 | 284 |
| | 2 | 633 | 135 | 759 | 86 |
| | 4 | 617 | 128 | 761 | 80 |
| Lot34Stone2 | 1 | 634 | 202 | 776 | 154 |
| | 2 | 659 | 1015 | 805 | 769 |
| | 3 | 633 | 320 | 777 | 248 |
| Lot34stone18 | 1 | 653 | 371 | 793 | 277 |
| | 2 | 653 | 190 | 787 | 135 |
| Lot34stone21 | 1 | 627 | 63 | 764 | 42 |
| Lot34stone22 | 1 | — | — | — | — |
| | 2 | 642 | 74 | 781 | 53 |
| | 3 | 641 | 1035 | 780 | 753 |
| Lot10stone21 | 1 | — | — | — | — |
| | 2 | — | — | — | — |
| *Median* | | 634 | | 778 | |
| *Average* | | 638 | | 780 | |
| *St.dev.* | | 14 | | 15 | |
| *Maximum* | | 659 | | 805 | |
| *Minimum* | | 617 | | 759 | |

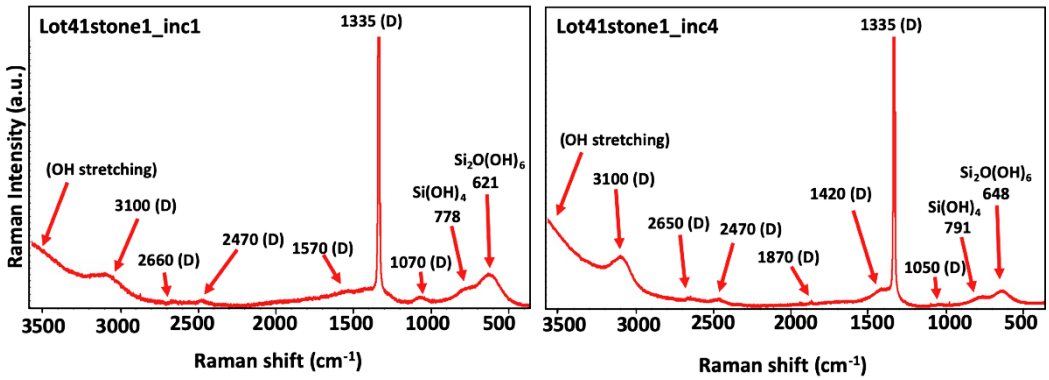


**Figure 5.5.** Examples of Raman spectra of fluid film that is present around the studied clinopyroxene inclusions. The two represented Raman spectra are related to the inclusions Lot41stone1_inc1 and Lot41stone1_inc4 in diamond Lot41stone1. D = diamond. The diamond peaks at ~ 1333 $cm^{-1}$ are truncated.

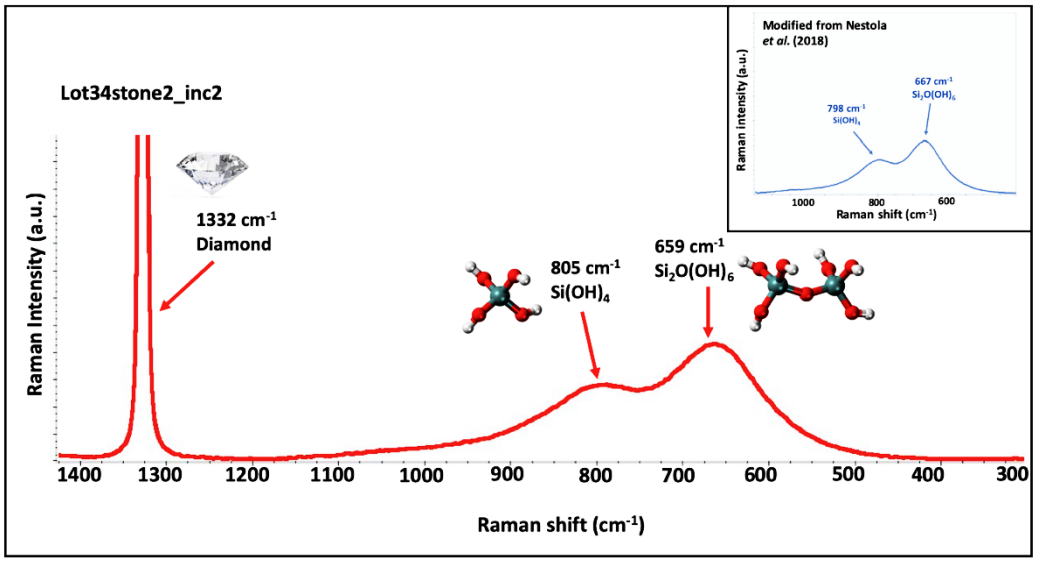


**Figure 5.6.** Detail of the Raman spectrum collected from the rim of inclusion Lot34stone2_inc2 in diamond Lot34stone2, which clearly shows the two broad peaks indicative of the presence of hydrous silicic fluid. In the upper-right edge of the figure is shown part of the Raman spectrum collected by Nestola et al. (2018) for a comparison with the Raman peaks related to fluid film measured in this thesis work. The diamond peak at ~ 1333 $cm^{-1}$ is truncated.

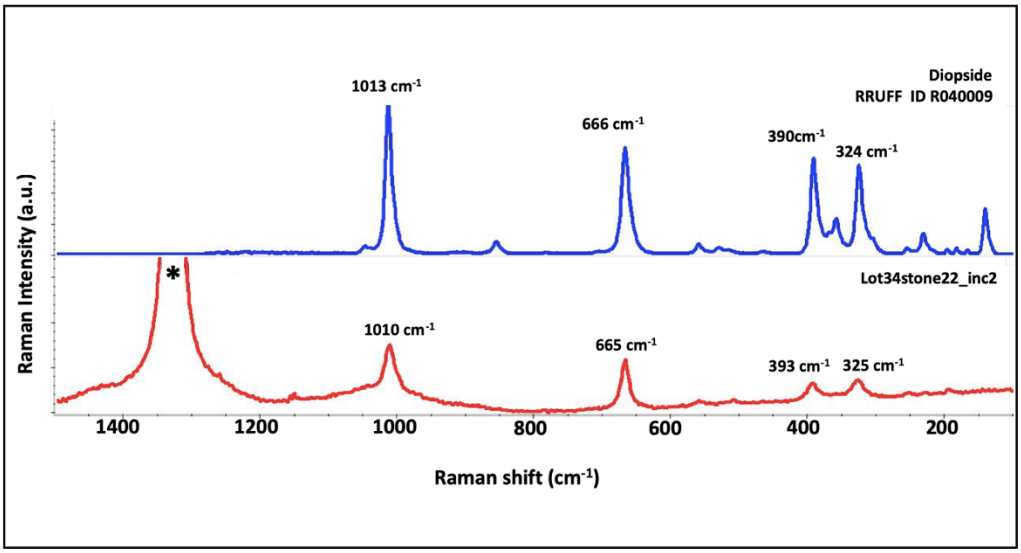


**Figure 5.7.** Raman spectrum collected from clinopyroxene inclusion Lot34stone22_inc2 in diamond Lot34stone22. The upper reference Raman spectrum is from the RRUFF Raman minerals database. Raman band of the diamond host at ~ 1333 $cm^{-1}$ is marked with asterisk and is truncated.

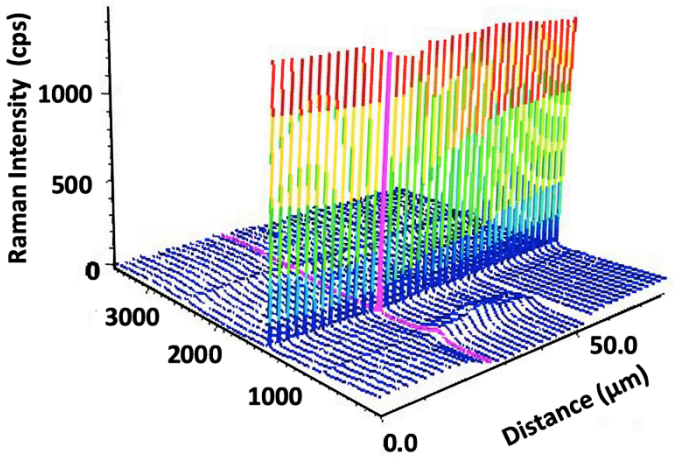


**Figure 5.8.** Series of 40 Raman spectra collected at 2-µm step across diamond/clinopyroxene interface (Lot34stone22_inc3). The spectrum at 0 µm shows the contributions from both the clinopyroxene inclusion and diamond host. The signal of clinopyroxene, approaching the interface, is substituted by those of the fluid (broad peaks at 641 $cm^{-1}$ and 780 $cm^{-1}$), which in turn disappears moving further away from the inclusion. The strong diamond peaks at ~ 1333 $cm^{-1}$ are ubiquitous along the traverse.

# Chapter 6

# Discussion

The crystallographic orientation relationships (CORs) between clinopyroxene inclusions and diamonds investigated in this thesis work have established that clinopyroxene has no preferred crystallographic orientations relative to diamond host. This finding implies, by definition, the lack of epitaxial relationships between clinopyroxene inclusions and their diamond hosts. Regardless of this overall pattern of random orientations, multiple clinopyroxene inclusions with similar orientation were observed within some of the studied diamonds. Besides, most of the analyzed clinopyroxenes, including those forming the clusters of iso-oriented inclusions within the same diamond host, show a diamond-imposed cubo-octahedral morphology ("negative crystals"), traditionally used as a proof of syngenesis (e.g., Harris, 1968).

These results are consistent with those obtained in recent detailed crystallographic studies done on a large number of olivine (Nestola et al., 2014; Milani et al., 2016), and garnet inclusions (Nestola et al., 2019) coming from different localities, where no specific orientations between the mineral inclusions with respect to diamond hosts, were found, along with clusters of iso-oriented inclusions within single diamonds. In the case of clinopyroxene inclusions, so far, only Nestola et al. (2017) have reported the CORs for a single clinopyroxene-diamond pair from a unique diamond-bearing peridotite xenolith from the Finsch kimberlite (Kaapvaal Craton, South Africa). In more detail, the diopside inclusion does not have any orientation relationship with respect to its diamond host but was

iso-oriented with a clinopyroxene of identical chemistry located at around 0.1 mm outside the diamond.

As suggested by Nestola et al. (2014), multiple inclusions having the same crystallographic orientation in the same diamond host, but which do not show any specific crystallographic orientation relative to diamond, regardless of the their diamond-imposed morphology, can be explained only if each group of these similarly oriented inclusions are fragments of pre-existing, i.e., protogenetic, monocrystal, which was partially dissolved and re-shaped by diamond-forming fluids or melts (Nestola et al., 2014).

The hydrous silicic fluid film found around several of the studied clinopyroxene inclusions, comprising the iso-oriented inclusions in single diamonds, is the same that Nimis et al. (2016), and Nestola et al. (2018) have recently detected out on silicate and oxide inclusion rims and interpreted as the relic of the diamond-forming fluid, by virtue of its ubiquity around inclusions in lithospheric diamonds (Nimis et al., 2016). Its presence suggests that between the inclusions and the growing diamond host, there was a limited interfacial interaction. However, due to the extreme thinness of this fluid film, with a maximum measured thickness of ~1.5 μm (Nimis et al., 2016), from a mechanical point of view, it cannot influence the crystallographic orientations of the mineral inclusions within their diamond hosts. Therefore, the observed random orientations between clinopyroxene inclusions and diamonds do not have any link with the fluid film. The absence of a preferred orientations between clinopyroxene inclusions and diamonds, as indicated by theoretical and experimental observations on adhesion and interface energies, derived from the fact that there is not any thermodynamic advantage for silicate inclusions to growth with specific crystallographic orientation with respect to diamond, regardless of their timing of formation (Bruno et al., 2016). Nonetheless, the presence of the iso-orientation of multiple clinopyroxene inclusions within the same diamond is clear evidence of protogenesis, confirming the conclusions previously drawn by Nestola et al. (2017) for the single clinopyroxene inclusion in a diamond from the Finsch kimberlite, South Africa (see Figure 6.1).

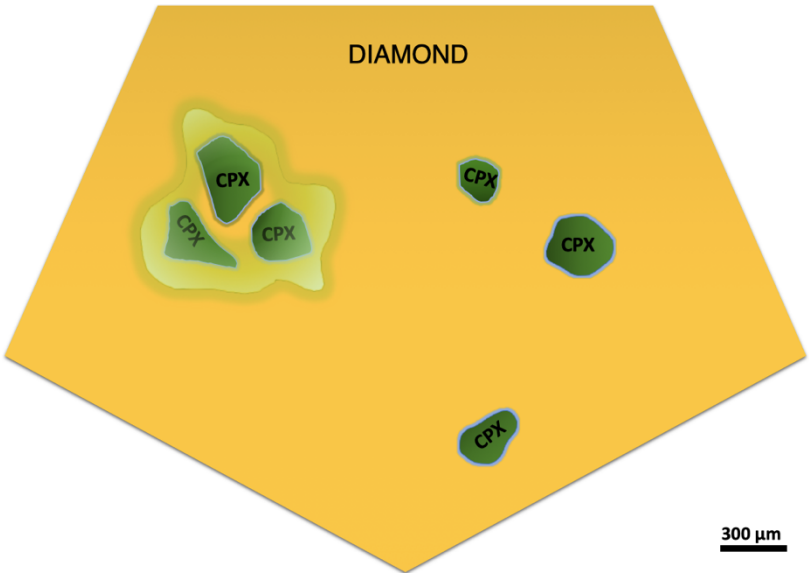


**Figure 6.1.** Possible diamond-clinopyroxene growth relationship proposed for the inclusion-bearing diamonds studied in this thesis work, according with the growth mechanism proposed for other mineral inclusions from previous studies (e.g., Nestola et al., 2014, 2017, 2019). The host diamond (yellow) contains multiple clinopyroxene inclusions (green), whose irregular shapes are simplified and inspired by those observed in the analyzed inclusions of clinopyroxene hosted in Voorspoed diamonds. In detail, the cartoon shows the presence of six inclusions of clinopyroxene with different crystallographic orientations. Among these inclusions, there is one cluster of three clinopyroxene inclusions (upper-left side of the diamond host) that share a similar crystallographic orientation and are interpreted as fragments of pre-existing clinopyroxene monocrystal (green halo), which was partially dissolved during the growth of diamond. Besides is represented the fluid film (light blue) found around the inclusions. The size of the fluid film is not real, but its low thickness, with respect to the sizes of the inclusions, indicates that mechanically it cannot influence the crystallographic orientations of the clinopyroxenes. Modified from Nestola et al., 2017.

# Chapter 7

# Conclusions

## 7.1 Timing relationships between clinopyroxene inclusions and host diamonds

The resulting data from this thesis work indicate that most, but not all, the clinopyroxene inclusions in diamonds from the Voorspoed kimberlite (Kaapvaal Craton, South Africa), existed before the diamond in which they are hosted and, hence, are protogenetic by definition [1]. This conclusion is consistent with the interpretations previously designated for other typical mineral inclusions in lithospheric diamonds from different localities (e.g., Thomassot et al., 2009; Nestola et al., 2014, 2017, 2019; Jacob et al., 2016; Milani et al., 2016), remarking that the commonly-observed cubo-octahedral shape imposition on inclusions alone cannot be considered a proof of syngenesis, and that protogenesis can be assumed as the main timing relationship between diamond and its inclusions [2].

At the same time, the recognition that clinopyroxene inclusions in diamond may often be protogenetic, rather than syngenetic, raises doubts on the reliability of many geochemical, geothermobarometric, and geochronological data extracted from these inclusions and applied to diamond. Mostly, the “diamond formation ages” based on the Sm-Nd dating method commonly applied to clinopyroxene inclusions claimed to be syngenetic with diamond on the basis of their diamond-

imposed morphology, could be mistaken if incomplete isotope re-equilibration, between these dated inclusions and the diamond-forming fluids/melts, does occur [3].

## 7.2 Implications for the age of diamonds

Thanks to the collaboration with Jacob D.E. from the Department of Earth and Planetary Science, Macquarie University, Australia, the time required by a protogenetic clinopyroxene inclusion to reach the full Nd isotope equilibration with diamond-forming fluid/melt, i.e., the equilibration time, was estimated by using a model of chemical diffusion between a fluid and an ideal free-defect clinopyroxene, as a function of temperature, pressure, and grain size. The model was calculated along cratonic geotherms consistent with lithospheric diamond formation and using the slowest diffusion coefficient reported in the literature for Sm and Nd in clinopyroxene (Van Orman et al., 2001, 2002), which was corrected for the effect of pressure on the activation volume. All details of the diffusion model are reported in Appendix A.

The results of the model are illustrated in Figure 7.1, while in Table 7-1 are reported the equilibration times, extracted from the model, for clinopyroxene inclusions of different sizes, considering mantle conditions corresponding with the typical 40 $mW/m^2$ cratonic geotherm. For the results related to other cratonic geotherms, see Table A-1 reported in Appendix A.

The diffusion model indicates that in the case of a 0.1 mm clinopyroxene grain under high-temperature conditions of 1400°C, corresponding to 6.4 GPa on 40 $mW/m^2$ cratonic geotherm, a full chemical equilibration with the diamond-forming medium would occur within ~ 44 kyr (see Figure 7.1 and Table 7-1). Considering the more typical temperature conditions for lithospheric diamond formation of 1100°C, corresponding to 5 GPa, and again a grain size of 0.1 mm, clinopyroxene will equilibrate in a much longer time of ~ 68 Myr (see Figure 7.1 and Table 7-1).

Under the same conditions, but with a larger clinopyroxene grain of 0.5 mm, the equilibration times further increased by about two orders of magnitude, occurring within ~ 1.1 Myr and ~ 1.7 Gyr, respectively (see Figure 7.1 and Table 7-1).

Phenomena like dissolutions and precipitations upon interaction with fluid, as well as the presence of lattice defects, which characterize crystals in nature, could result in faster diffusion rates, i.e., in shorter equilibration times. Nonetheless, at the typical cratonic mantle conditions for lithospheric diamond growth, which lie around the average temperature value of 1160 ± 110°C (Stachel and Harris, 2009), the times required for a clinopyroxene inclusions to reach isotopic resetting with the diamond-forming media are very long on geological timescale (see Figure 7.1, Table 7-1, and Table A-1 in Appendix A). Then, it is possible to conclude that the use of clinopyroxenes for dating diamond, because they would likely not equilibrate for Sm and Nd with the diamond-forming fluid/melt, i.e., they are not synchronous with the diamond host, is not recommended [4].

**Table 7-1.** Calculated maximum times for equilibration of clinopyroxene grains of different size with a diamond-forming fluid at pressure-temperature conditions corresponding to 40 mWm-$^{2}$ cratonic geotherm from Hasterok and Chapman (2011). Data outside the temperature range of 900–1400°C were excluded because such thermal conditions cannot occur along realistic geothermal gradients for diamond stability within lithospheric mantle.

| **Geotherm temperature** | **Clinopyroxene grain size** | | |
|---|---|---|---|
| *40 mWm$^{-2}$* | *0.1 mm* | *0.5 mm* | *1 mm* |
| 900°C | 7.6 x $10^{10}$ yrs | 1.9 x $10^{12}$ yrs | 7.6 x $10^{12}$yrs |
| 1000°C | 1.7 x $10^{9}$ yrs | 4.3 x $10^{10}$ yrs | 1.7 x $10^{11}$ yrs |
| 1100°C | 6.8 x $10^{7}$ yrs | 1.7 x $10^{9}$ yrs | 6.8 x $10^{9}$ yrs |
| 1200°C | 4.2 x $10^{6}$ yrs | 1.1 x $10^{8}$ yrs | 4.2 x $10^{8}$ yrs |
| 1300°C | 3.7 x $10^{5}$ yrs | 9.3 x $10^{6}$ yrs | 3.7 x $10^{6}$ yrs |
| 1400°C | 4.4 x $10^{4}$ yrs | 1.1 x $10^{6}$ yrs | 4.4 x $10^{6}$ yrs |

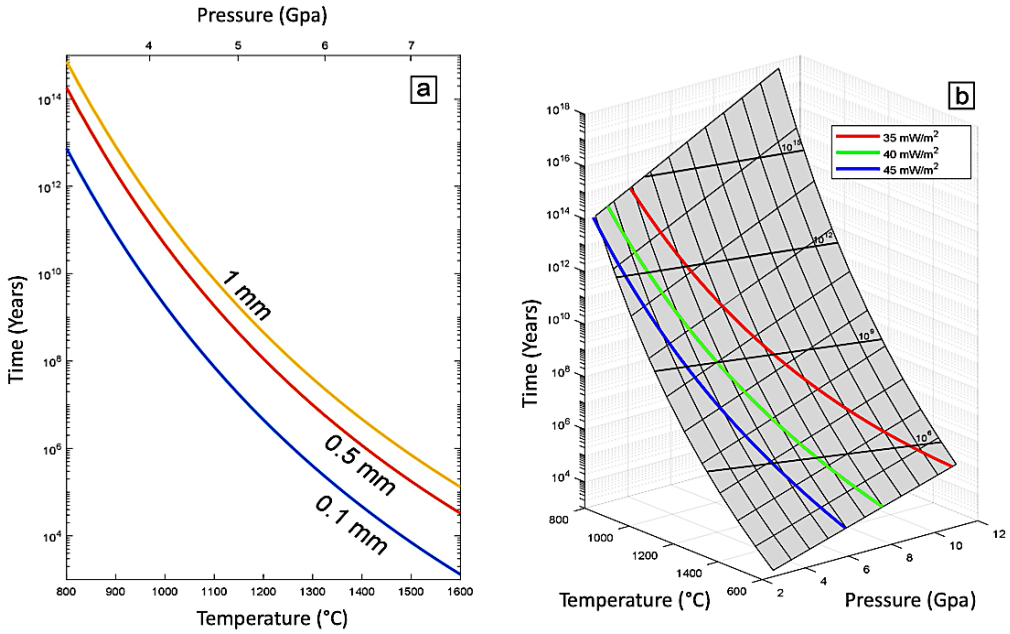


**Figure 7.1.** Model of Sm-Nd diffusive equilibration between a free-defect clinopyroxene grain with slab symmetry and a diamond-forming fluid along three different cratonic geotherms (35, 40, and 45 $mWm^{-2}$ from Hasterok and Chapman, 2011). (a) Equilibration times for clinopyroxene of different grain size (blue – 0.1 mm; red – 0.5 mm; yellow – 1 mm) as a function of temperature along 40 $mWm^{-2}$ cratonic geotherm. (b) Pressure-temperature-time diagram for 0.5 mm clinopyroxene grain.

# References


Agrosì, G., Nestola, F., Tempesta, G., Bruno, M., Scandale, E., & Harris, J. (2016). X-ray topographic study of a diamond from Udachnaya: Implications for the genetic nature of inclusions. *Lithos*, 248, 153-159.

Angel, R. J., Downs, R. T., & Finger, L. W. (2000). High-temperature–high-pressure diffractometry. *Reviews in mineralogy and geochemistry*, 41(1), 559-597.

Angel, R., Milani, S., Alvaro, M., & Nestola, F. (2015). OrientXplot: a program to analyse and display relative crystal orientations. *Journal of Applied Crystallography*, 48(4), 1330-1334.

Angel, R. J., & Nestola, F. (2016). A century of mineral structures: How well do we know them?. *American Mineralogist*, 101(5), 1036-1045.

Aulbach, S., Shirey, S. B., Stachel, T., Creighton, S., Muehlenbachs, K., & Harris, J. W. (2009). Diamond formation episodes at the southern margin of the Kaapvaal Craton: Re–Os systematics of sulfide inclusions from the Jagersfontein Mine. *Contributions to Mineralogy and Petrology*, 157(4), 525-540.

Aulbach, S., Stachel, T., Creaser, R. A., Heaman, L. M., Shirey, S. B., Muehlenbachs, K., ... & Harris, J. W. (2009). Sulphide survival and diamond genesis during formation and evolution of Archaean subcontinental lithosphere: A comparison between the Slave and Kaapvaal cratons. *Lithos*, 112, 747-757.

Aulbach, S., Stachel, T., Viljoen, S. K., Brey, G. P., & Harris, J. W. (2002). Eclogitic and websteritic diamond sources beneath the Limpopo Belt–is slab-melting the link?. *Contributions to Mineralogy and Petrology*, 143(1), 56-70.

Becker, M., & Roex, A. P. L. (2005). Geochemistry of South African on-and off-craton, Group I and Group II kimberlites: petrogenesis and source region evolution. *Journal of Petrology*, 47(4), 673-703.

Begg, G. C., Griffin, W. L., Natapov, L. M., O'Reilly, S. Y., Grand, S. P., O'Neill, C. J., ... & Bowden, P. (2009). The lithospheric architecture of Africa: Seismic tomography, mantle petrology, and tectonic evolution. *Geosphere*, 5(1), 23-50.

Boyd, S. R., Mattey, D. P., Pillinger, C. T., Milledge, H. J., Mendelssohn, M., & Seal, M. (1987). Multiple growth events during diamond genesis: an integrated study of carbon and nitrogen isotopes and nitrogen aggregation state in coated stones. *Earth and Planetary Science Letters*, 86(2-4), 341-353.

Bruno, M., Rubbo, M., Aquilano, D., Massaro, F. R., & Nestola, F. (2016). Diamond and its olivine inclusions: a strange relation revealed by ab initio simulations. *Earth and Planetary Science Letters*, 435, 31-35.

Bulanova, G. P. (1995). The formation of diamond. *Journal of Geochemical Exploration*, 53(1-3), 1-23.

Bulanova, G. P., Griffin, W. L., Ryan, C. G., Shestakova, O. Y., & Barnes, S. J. (1996). Trace elements in sulfide inclusions from Yakutian diamonds. *Contributions to Mineralogy and Petrology*, 124(2), 111-125.

Bureau, H., Frost, D. J., Bolfan-Casanova, N., Leroy, C., Esteve, I., & Cordier, P. (2016). Diamond growth in mantle fluids. *Lithos*, 265, 4-15.

Bureau, H., Remusat, L., Esteve, I., Pinti, D. L., & Cartigny, P. (2018). The growth of lithospheric diamonds. *Science Advances*, 4(6), eaat1602.

Burgess, R., Turner, G., & Harris, J. W. (1992). 40Ar-39Ar laser probe studies of clinopyroxene inclusions in eclogitic diamonds. *Geochimica et Cosmochimica Acta*, 56(1), 389-402.

Busing, W. R., & Levy, H. A. (1967). Angle calculations for 3-and 4-circle X-ray and neutron diffractometers. *Acta Crystallographica*, 22(4), 457-464.

Cameron, M., & Papike, J. J. (1981). Structural and chemical variations in pyroxenes. *American Mineralogist*, 66(1-2), 1-50.

Chakraborty, S. (2008). Diffusion in solid silicates: a tool to track timescales of processes comes of age. *Annu. Rev. Earth Planet*. Sci., 36, 153-190.

Clark, J.R., Appleman, D.E., and Papike, J.J. (1969) Crystal-chemical characterization of clinopyroxenes based on eight new structure refinements. *Mineralogical Society of America Special Paper*, 2, 31-50.

Crank, J. (1979). *The mathematics of diffusion*. Oxford university press.

Day, H. W. (2012). A revised diamond-graphite transition curve. *American Mineralogist*, 97(1), 52-62.

De Vries, D. W., Drury, M. R., De Winter, D. A. M., Bulanova, G. P., Pearson, D. G., & Davies, G. R. (2011). Three-dimensional cathodoluminescence imaging and electron backscatter diffraction: tools for studying the genetic nature of diamond inclusions. *Contributions to Mineralogy and Petrology*, 161(4), 565-579.

De Wit, M. C. J., Bhebe, Z., Davidson, J., Haggerty, S. E., Hundt, P., Jacob, J., ... & Stiefenhofer, J. (2016). Overview of diamond resources in Africa. *Episodes*, 39, 199-237.

DePaolo, D. J., & Wasserburg, G. J. (1976). Nd isotopic variations and petrogenetic models. *Geophysical Research Letters*, 3(5), 249-252.

Menzies, M. (1989). DJ DePaolo 1988. Neodymium Isotope Geochemistry. An Introduction. Minerals and Rocks Series no. 20 xi+ 187 pp. Berlin, Heidelberg, New York, London, Paris, Tokyo: Springer-Verlag. Price DM 82.00 (hard covers). ISBN 3 540 18648 4. *Geological Magazine*, 126(5), 596-597.

Dickin, A. P. (2005). *Radiogenic isotope geology*. Cambridge university press.

Dodson, M. H. (1973). Closure temperature in cooling geochronological and petrological systems. *Contributions to Mineralogy and Petrology*, 40(3), 259–274.

Ferrari, A. C., & Robertson, J. (2004). Raman spectroscopy of amorphous, nanostructured, diamond–like carbon, and nanodiamond. *Philosophical Transactions of the Royal Society of London. Series A: Mathematical, Physical and Engineering Sciences*, 362(1824), 2477-2512.

Field, M., Stiefenhofer, J., Robey, J., & Kurszlaukis, S. (2008). Kimberlite-hosted diamond deposits of southern Africa: a review. *Ore Geology Reviews*, 34(1-2), 33-75.

Frank-Kamenetskii, V. (1964). Nature of structural impurities and inclusions in minerals.

Frezzotti, M. L., Tecce, F., & Casagli, A. (2012). Raman spectroscopy for fluid inclusion analysis. *Journal of Geochemical Exploration*, 112, 1-20.

Futergendler, S. I., & Frank-Kamenetsky, V. A. (1961). Oriented inclusions of olivine, garnet and chrome-spinel in diamonds. *Zapisky Vsesoyuznogo Mineralogicheskogo obshestva*, 90, 230-236.

Ganguly, J. (2002). Diffusion kinetics in minerals: principles and applications to tectono-metamophic processes. *Notes in Mineralogy: Energy Modelling in Minerals*, 4, 271-309.

Ganguly, J., & Tirone, M. (1999). Diffusion closure temperature and age of a mineral with arbitrary extent of diffusion: theoretical formulation and applications. *Earth and Planetary Science Letters*, 170(1-2), 131-140.

Ganguly, J., & Tirone, M. (2009). *Closure temperature, cooling age and high temperature thermochronology*. In Physics and Chemistry of the Earth's Interior (pp. 89-99). Springer, New York, NY.

Goss, J. P., Briddon, P. R., Hill, V., Jones, R., & Rayson, M. J. (2014). Identification of the structure of the 3107 cm− 1 H-related defect in diamond. *Journal of Physics: Condensed Matter*, 26(14), 145801.

Gress, M. U., Howell, D., Chinn, I. L., Speich, L., Kohn, S. C., van den Heuvel, Q., ... & Davies, G. R. (2018). Episodic diamond growth beneath the Kaapvaal Craton at Jwaneng Mine, Botswana. *Mineralogy and Petrology*, 112(1), 219-229.

Griffin, W. L., O'Reilly, S. Y., Natapov, L. M., & Ryan, C. G. (2003). The evolution of lithospheric mantle beneath the Kalahari Craton and its margins. *Lithos*, 71(2-4), 215-241.

Grütter, H. S., Gurney, J. J., Menzies, A. H., & Winter, F. (2004). An updated classification scheme for mantle-derived garnet, for use by diamond explorers. *Lithos*, 77(1-4), 841-857.

Faure, G., & Mensing, T. M. (2005). *Isotopes: principles and applications*. John Wiley & Sons.

Gurney, J. J., Helmstaedt, H. H., Richardson, S. H., & Shirey, S. B. (2010). Diamonds through time. *Economic Geology*, 105(3), 689-712.

Harris, J. W. (1968). Recognition of diamond inclusions. 1. Syngenetic mineral inclusions. *Industrial Diamond Review*, 28(334), 402.

Hartman, P. (1954) A discussion on "oriented olivine inclusions in diamond." *American Mineralogist*, 39, 674–675.

Hasterok, D., & Chapman, D. S. (2011). Heat production and geotherms for the continental lithosphere. *Earth and Planetary Science Letters*, 307(1-2), 59-70.

Howarth, G. H., & Skinner, E. M. W. (2012). The geology and emplacement of the volcaniclastic infill at the Voorspoed Group II kimberlite (orangeite) pipe, Kroonstad Cluster, South Africa. *Journal of Volcanology and Geothermal Research,* 231, 24-38.

Howarth, G. H., Michael, E., Skinner, W., & Prevec, S. A. (2011). Petrology of the hypabyssal kimberlite of the Kroonstad group II kimberlite (orangeite) cluster, South Africa: Evolution of the magma within the cluster. *Lithos*, 125(1-2), 795-808.

Hunt, J. D., Kavner, A., Schauble, E. A., Snyder, D., & Manning, C. E. (2011). Polymerization of aqueous silica in H2O–K2O solutions at 25–200 C and 1 bar to 20 kbar. *Chemical Geology*, 283(3-4), 161-170.

Izraeli, E. S., Harris, J. W., & Navon, O. (2001). Brine inclusions in diamonds: a new upper mantle fluid. *Earth and Planetary Science Letters*, 187(3-4), 323-332.

Jablon, B. M., & Navon, O. (2016). Most diamonds were created equal. *Earth and Planetary Science Letters*, 443, 41-47.

Jacob, D. E., Dobrzhinetskaya, L., & Wirth, R. (2014). New insight into polycrystalline diamond genesis from modern nanoanalytical techniques. *Earth-Science Reviews*, 136, 21-35.

Jacob, D. E., Piazolo, S., Schreiber, A., & Trimby, P. (2016). Redox-freezing and nucleation of diamond via magnetite formation in the Earth's mantle. *Nature communications*, 7, 11891.

Jacobsen, S. B., & Wasserburg, G. J. (1980). Sm-Nd isotopic evolution of chondrites. *Earth and Planetary Science Letters*, 50(1), 139-155.

Johnson, K. T. (1998). Experimental determination of partition coefficients for rare earth and high-field-strength elements between clinopyroxene, garnet, and basaltic melt at high pressures. *Contributions to Mineralogy and Petrology*, 133(1-2), 60-68.

Klein-Bendavid, O., Pearson, D. G., Cantigny, P., & Nowell, G. M. (2008, October). Origins of diamond forming fluids–constraints from a coupled Sr-Nd isotope and trace element approach. In *International Kimberlite Conference: Extended Abstracts* (Vol. 9).

Klein-BenDavid, O., Pearson, D. G., Nowell, G. M., Ottley, C., McNeill, J. C., Logvinova, A., & Sobolev, N. V. (2014). The sources and time-integrated evolution of diamond-forming fluids–Trace elements and isotopic evidence. *Geochimica et Cosmochimica Acta*, 125, 146-169.

Klein-BenDavid, O., Wirth, R., & Navon, O. (2007). Micrometer-scale cavities in fibrous and cloudy diamonds—A glance into diamond dissolution events. *Earth and Planetary Science Letters*, 264(1-2), 89-103.

Koornneef, J. M., Bouman, C., Schwieters, J. B., & Davies, G. R. (2014). Measurement of small ion beams by thermal ionisation mass spectrometry using new 1013 Ohm resistors. *Analytica chimica acta*, 819, 49-55.

Koornneef, J. M., Gress, M. U., Chinn, I. L., Jelsma, H. A., Harris, J. W., & Davies, G. R. (2017). Archaean and Proterozoic diamond growth from contrasting styles of large-scale magmatism. *Nature communications*, 8(1), 648.

Kramers, J. D. (1979). Lead, uranium, strontium, potassium and rubidium in inclusion-bearing diamonds and mantle-derived xenoliths from southern Africa. *Earth and Planetary Science Letters*, 42(1), 58-70.

Krebs, M. Y., Pearson, D. G., Stachel, T., Laiginhas, F., Woodland, S., Chinn, I., & Kong, J. (2019). A common parentage-low abundance trace element data of gem diamonds reveals similar fluids to fibrous diamonds. *Lithos*, 324, 356-370.

Leost, I., Stachel, T., Brey, G. P., Harris, J. W., & Ryabchikov, I. D. (2003). Diamond formation and source carbonation: mineral associations in diamonds from Namibia. *Contributions to Mineralogy and Petrology*, 145(1), 15-24.

Logvinova, A. M., Wirth, R., Tomilenko, A. A., Afanas'ev, V. P., & Sobolev, N. V. (2011). The phase composition of crystal-fluid nanoinclusions in alluvial diamonds in the northeastern Siberian Platform. *Russian Geology and Geophysics*, 52(11), 1286-1297.

Meyer, H. O. (1987). Inclusions in diamond. *Mantle xenoliths*.

Meyer, H. O. (1985). Genesis of diamond: a mantle saga. *American Mineralogist*, 70(3-4), 344-355.

Meyer, H. O. A., & Boyd, F. R. (1972). Composition and origin of crystalline inclusions in natural diamonds. *Geochimica et Cosmochimica Acta*, 36(11), 1255-1273.

Meyer, H. O., & Tsai, H. M. (1979). Inclusions in diamond and the mineral chemistry of the upper mantle. *Physics and Chemistry of the Earth*, 11, 631-644.

Milani, S., Nestola, F., Angel, R. J., Nimis, P., & Harris, J. W. (2016). Crystallographic orientations of olivine inclusions in diamonds. *Lithos*, 265, 312-316.

Mitchell, R. S., & Giardini, A. A. (1953). Oriented olivine inclusions in diamond. *American Mineralogist*. 38, 136-138.

Navon, O. (1999). Diamond formation in the Earth's mantle, in: *Proceedings of the 7th International Kimberlite Conference*.

Navon, O., Hutcheon, I. D., Rossman, G. R., & Wasserburg, G. J. (1988). Mantle-derived fluids in diamond micro-inclusions. *Nature*, 335(6193), 784.

Nestola, F. (2015). The crucial role of crystallography in diamond research. *Rendiconti Lincei*, 26(2), 225-233.

Nestola, F., Angel, R. J., Zhao, J., Garrido, C. J., Sánchez-Vizcaíno, V. L., Capitani, G., & Mellini, M. (2010). Antigorite equation of state and anomalous softening at 6 GPa: an in situ single-crystal X-ray diffraction study. *Contributions to Mineralogy and Petrology*, 160(1), 33-43.

Nestola, F., Jacob, D. E., Pamato, M. G., Pasqualetto, L., Oliveira, B., Greene, S., ... & Sgreva, N. (2019). Protogenetic garnet inclusions and the age of diamonds. *Geology*, 47(5), 431-434.

Nestola, F., Jung, H., & Taylor, L. A. (2017). Mineral inclusions in diamonds may be synchronous but not syngenetic. *Nature communications*, 8, 14168.

Nestola, F., Nimis, P., Angel, R. J., Milani, S., Bruno, M., Prencipe, M., & Harris, J. W. (2014). Olivine with diamond-imposed morphology included in diamonds. Syngenesis or protogenesis?. *International Geology Review*, 56(13), 1658-1667.

Nestola, F., Nimis, P., Ziberna, L., Longo, M., Marzoli, A., Harris, J. W., ... & Fedortchouk, Y. (2011). First crystal-structure determination of olivine in diamond: Composition and implications for provenance in the Earth's mantle. *Earth and Planetary Science Letters*, 305(1-2), 249-255.

Nestola, F., Pasqual, D., Smyth, J. R., Novella, D., Secco, L., Manghnani, M. H., & Dal Negro, A. (2011). New accurate elastic parameters for the forsterite-fayalite solid solution. *American Mineralogist*, 96(11-12), 1742-1747.

Nestola, F., Prencipe, M., Nimis, P., Sgreva, N., Perritt, S. H., Chinn, I. L., & Zaffiro, G. (2018). Toward a robust elastic geobarometry of kyanite inclusions in eclogitic diamonds. *Journal of Geophysical Research*: Solid Earth, 123(8), 6411-6423.

Nestola, F., Zaffiro, G., Mazzucchelli, M. L., Nimis, P., Andreozzi, G. B., Periotto, B., ... & Logvinova, A. M. (2019). Diamond-inclusion system recording old

deep lithosphere conditions at Udachnaya (Siberia). *Scientific reports*, 9(1), 1-8.

Neuser, R. D., Schertl, H. P., Logvinova, A. M., & Sobolev, N. V. (2015). An EBSD study of olivine inclusions in Siberian diamonds: evidence for syngenetic growth?. *Russian Geology and Geophysics*, 56(1-2), 321-329.

Nimis, P. (2018). Trapped minerals under stress. *Geology*, 46(3), 287-288.

Nimis, P., Alvaro, M., Nestola, F., Angel, R. J., Marquardt, K., Rustioni, G., ... & Marone, F. (2016). First evidence of hydrous silicic fluid films around solid inclusions in gem-quality diamonds. *Lithos*, 260, 384-389.

Nimis, P., Angel, R. J., Alvaro, M., Nestola, F., Harris, J. W., Casati, N., & Marone, F. (2019). Crystallographic orientations of magnesiochromite inclusions in diamonds: what do they tell us?. *Contributions to Mineralogy and Petrology*, 174(4), 29.

Nolan, J. (1969). Physical properties of synthetic and natural pyroxenes in the system diopside–hedenbergite–acmite. *Mineralogical Magazine*, 37(286), 216-229.

Novella, D., Bolfan-Casanova, N., Nestola, F., & Harris, J. W. (2015). H2O in olivine and garnet inclusions still trapped in diamonds from the Siberian craton: Implications for the water content of cratonic lithosphere peridotites. *Lithos*, 230, 180-183.

Pearson, D. G. (1999). The age of continental roots. *Lithos*, 48(1-4), 171-194.

Pearson, D. G., & Shirey, S. B. (1999). Isotopic dating of diamonds. *Application of Radiogenic Isotopes to Ore Deposit Research and Exploration. Lambert DD, Ruiz J (eds) Society of Economic Geologists, Boulder, CO, United States*, 143-171.

Pearson, D. G., Shirey, S. B., Bulanova, G. P., Carlson, R. W., & Milledge, H. J. (1999). Re-Os isotope measurements of single sulfide inclusions in a Siberian diamond and its nitrogen aggregation systematics. *Geochimica et Cosmochimica Acta*, 63(5), 703-711.

Pearson, D. G., Shirey, S. B., Harris, J. W., & Carlson, R. W. (1998). Sulphide inclusions in diamonds from the Koffiefontein kimberlite, S Africa: constraints on diamond ages and mantle Re–Os systematics. *Earth and Planetary Science Letters*, 160(3-4), 311-326.

Pearson, D. G., & Wittig, N. (2008). Formation of Archaean continental lithosphere and its diamonds: the root of the problem. *Journal of the Geological Society*, 165(5), 895-914.

Phillips, D., Kiviets, G. B., Barton, E. S., Smith, C. B., Viljoen, K. S., & Fourie, L. F. (1998, April). 40Ar/39Ar dating of kimberlites and related rocks: problems and solutions. In *International Kimberlite Conference: Extended Abstracts* (Vol. 7, No. 1, pp. 690-692).

Phillips, D., Machin, K. J., Kiviets, G. B., Fourie, L. F., Roberts, M. A., & Skinner, E. M. W. (1998). A petrographic and 40Ar/39Ar geochronological study of the Voorspoed kimberlite, South Africa: Implications for the origin of Group II kimberlite magmatism. *South African Journal of Geology*, 101, 299-306.

Pollack, H. N., & Chapman, D. S. (1977). On the regional variation of heat flow, geotherms, and lithospheric thickness. *Tectonophysics*, 38(3-4), 279-296.

Prawer, S., & Nemanich, R. J. (2004). Raman spectroscopy of diamond and doped diamond. Philosophical Transactions of the Royal Society of London. Series A: Mathematical, *Physical and Engineering Sciences*, 362(1824), 2537-2565.

Ratcliffe, C. I., & Irish, D. E. (1982). Vibrational spectral studies of solutions at elevated temperatures and pressures. 5. Raman studies of liquid water up to 300. degree. C. *The Journal of Physical Chemistry*, 86(25), 4897-4905.

Raudsepp, M., Hawthorne, F. C., & Turnock, A. C. (1990). Crystal chemistry of synthetic pyroxenes on the join CaNiSi2O6-CaMgSi2O6 (diopside); a Rietveld structure refinement study. *American Mineralogist*, 75(11-12), 1274-1281.

Richardson, S. H. (1986). Latter-day origin of diamonds of eclogitic paragenesis. *Nature*, 322(6080), 623.

Richardson, S. H., & Harris, J. W. (1997). Antiquity of peridotitic diamonds from the Siberian craton. *Earth and Planetary Science Letters*, 151(3-4), 271-277.

Richardson, S. H., Chinn, I. L., & Harris, J. W. (1998, April). Age and origin of eclogitic diamonds from the Jwaneng kimberlite, Botswana. In *International Kimberlite Conference: Extended Abstracts* (Vol. 7, No. 1, pp. 734-736).

Richardson, S. H., Erlank, A. J., Harris, J. W., & Hart, S. R. (1990). Eclogitic diamonds of Proterozoic age from Cretaceous kimberlites. *Nature*, 346(6279), 54.

Richardson, S. H., Gurney, J. J., Erlank, A. J., & Harris, J. (1984). Origin of diamonds in old enriched mantle. *Nature*, 310(5974), 198.

Richardson, S. H., Pöml, P. F., Shirey, S. B., & Harris, J. W. (2009). Age and origin of peridotitic diamonds from Venetia, Limpopo Belt, Kaapvaal–Zimbabwe craton. *Lithos*, 112, 785-792.

Richardson, S. H., Shirey, S. B., & Harris, J. W. (2004). Episodic diamond genesis at Jwaneng, Botswana, and implications for Kaapvaal craton evolution. *Lithos*, 77(1-4), 143-154.

Richardson, S. H., Shirey, S. B., Harris, J. W., & Carlson, R. W. (2001). Archean subduction recorded by Re–Os isotopes in eclogitic sulfide inclusions in Kimberley diamonds. *Earth and Planetary Science Letters*, 191(3-4), 257-266.

Rutherford, E., & Soddy, F. (1902). LXIV. The cause and nature of radioactivity.—Part II. *The London, Edinburgh, and Dublin Philosophical Magazine and Journal of Science*, 4(23), 569-585.

Rutherford, E., & Soddy, F. (1902). LXXXIV.—The radioactivity of thorium compounds. II. The cause and nature of radioactivity. *Journal of the Chemical Society, Transactions*, 81, 837-860.

Schrauder, M., & Navon, O. (1993). Solid carbon dioxide in a natural diamond. *Nature*, 365(6441), 42.

Shirey, S. B., Cartigny, P., Frost, D. J., Keshav, S., Nestola, F., Nimis, P., ... & Walter, M. J. (2013). Diamonds and the geology of mantle carbon. *Reviews in Mineralogy and Geochemistry*, 75(1), 355-421.

Shirey, S. B., Smit, K., Pearson, D. G., Walter, M., Aulbach, S., Brenker, F., ... & Weiss, Y. (2019). Diamonds and the Mantle Geodynamics of Carbon: Deep Mantle Carbon Evolution from the Diamond Record. In B. Orcutt, I. Daniel, & R. Dasgupta (Eds.), *Deep Carbon: Past to Present* (pp. 89-128). Cambridge: Cambridge University Press.

Shiryaev, A. A., Izraeli, E. S., Hauri, E. H., Zakharchenko, O. D., & Navon, O. (2005). Chemical, optical and isotopic investigation of fibrous diamonds from Brazil. *Russian Geology and Geophysics,* 46(12), 1185-1201.

Skinner, E. M. W. (1986, September). Contrasting Group 1 and Group 2 kimberlite petrology: towards a genetic model for kimberlites. In *International Kimberlite Conference: Extended Abstracts* (Vol. 4, pp. 202-204).

Smith, E. M., Kopylova, M. G., Frezzotti, M. L., & Afanasiev, V. P. (2014). N-rich fluid inclusions in octahedrally-grown diamond. *Earth and Planetary Science Letters*, 393, 39-48.

Smith, E. M., Kopylova, M. G., Frezzotti, M. L., & Afanasiev, V. P. (2015). Fluid inclusions in Ebelyakh diamonds: Evidence of CO2 liberation in eclogite and the effect of H2O on diamond habit. *Lithos,* 216, 106-117.

Smith, E. M., Kopylova, M. G., Nowell, G. M., Pearson, D. G., & Ryder, J. (2012). Archean mantle fluids preserved in fibrous diamonds from Wawa, Superior craton. *Geology*, 40(12), 1071-1074.

Smit, K. V., & Shirey, S. B. (2019a). How Old Are Diamonds? AreThey Forever?. *Gems & Gemology,* 55(1), 102–109.

Smit, K. V., & Shirey, S. B. (2019b). Kimberlites: Earth's Diamond Delivery System. *Gems & Gemology*, 55(2), 270–276.

Smit, K. V., Shirey, S. B., Richardson, S. H., le Roex, A. P., & Gurney, J. J. (2010). Re–Os isotopic composition of peridotitic sulphide inclusions in diamonds from Ellendale, Australia: Age constraints on Kimberley cratonic lithosphere. *Geochimica et Cosmochimica Acta*, 74(11), 3292-3306.

Smith, E. M., Shirey, S. B., Richardson, S. H., Nestola, F., Bullock, E. S., Wang, J., & Wang, W. (2018). Blue boron-bearing diamonds from Earth's lower mantle. *Nature*, 560(7716), 84.

Smit, K. V., Shirey, S. B., Stern, R. A., Steele, A., & Wang, W. (2016). Diamond growth from C–H–N–O recycled fluids in the lithosphere: Evidence from CH4 micro-inclusions and δ13C–δ15N–N content in Marange mixed-habit diamonds. *Lithos*, 265, 68-81.

Sobolev, N. V., Kaminsky, F. V., Griffin, W. L., Yefimova, E. S., Win, T. T., Ryan, C. G., & Botkunov, A. I. (1997). Mineral inclusions in diamonds from the Sputnik kimberlite pipe, Yakutia. *Lithos,* 39(3-4), 135-157.

Stachel, T. (2014). Diamonds. *Geology of Gem Deposists Edition, 2*, 1-28.

Stachel, T., Aulbach, S., Brey, G. P., Harris, J. W., Leost, I., Tappert, R., & Viljoen, K. F. (2004). The trace element composition of silicate inclusions in diamonds: a review. *Lithos*, 77(1-4), 1-19.

Stachel, T., & Harris, J. W. (2008). The origin of cratonic diamonds—constraints from mineral inclusions. *Ore Geology Reviews*, 34(1-2), 5-32.

Stachel, T., & Harris, J. W. (2009). Formation of diamond in the Earth's mantle. *Journal of Physics: Condensed Matter*, 21(36), 364206.

Stachel, T., & Luth, R. W. (2015). Diamond formation—Where, when and how?. *Lithos*, 220, 200-220.

Sun, C., & Liang, Y. (2014). An assessment of subsolidus re-equilibration on REE distribution among mantle minerals olivine, orthopyroxene, clinopyroxene, and garnet in peridotites. *Chemical Geology*, 372, 80-91.

Sunagawa, I. (2007). *Crystals: growth, morphology, & perfection*. Cambridge University Press.

Tappert, R., & Tappert, M. C. (2011). *Diamonds in nature: a guide to rough diamonds*. Springer Science & Business Media.

Taylor, L. A., Anand, M., & Promprated, P. (2003a, June). Diamonds and their inclusions: are the criteria for syngenesis valid?. In *International Kimberlite Conference: Extended Abstracts* (Vol. 8).

Taylor, L. A., Anand, M., Promprated, P., Floss, C., & Sobolev, N. V. (2003b). The significance of mineral inclusions in large diamonds from Yakutia, Russia. *American Mineralogist*, 88(5-6), 912-920.

Taylor, L. A., Snyder, G. A., Crozaz, G., Sobolev, V. N., Yefimova, E. S., & Sobolev, N. V. (1996). Eclogitic inclusions in diamonds: evidence of complex mantle processes over time. *Earth and Planetary Science Letters*, 142(3-4), 535-551.

Taylor, L. A., Logvinova, A. M., Howarth, G. H., Liu, Y., Peslier, A. H., Rossman, G. R., ... & Sobolev, N. V. (2016). Low water contents in diamond mineral inclusions: Proto-genetic origin in a dry cratonic lithosphere. *Earth and Planetary Science Letters*, 433, 125-132.

Thomassot, E., Cartigny, P., Harris, J. W., Lorand, J. P., Rollion-Bard, C., & Chaussidon, M. (2009). Metasomatic diamond growth: A multi-isotope study

(13C, 15N, 33S, 34S) of sulphide inclusions and their host diamonds from Jwaneng (Botswana). *Earth and Planetary Science Letters*, 282(1-4), 79-90.

Timmerman, S., Koornneef, J. M., Chinn, I. L., & Davies, G. R. (2017). Dated eclogitic diamond growth zones reveal variable recycling of crustal carbon through time. *Earth and Planetary Science Letters*, 463, 178-188.

Tomilenko, A. A., Chepurov, A. I., Pal'yanov, Y. N., Pokhilenko, L. N., & Shebanin, A. P. (1997). Volatile components in the upper mantle (from data on fluid inclusions). *Russian Geology and Geophysics c/c of Geologiia i Geofizika*, 38, 294-303.

Tomlinson, E. L., Jones, A. P., & Harris, J. W. (2006). Co-existing fluid and silicate inclusions in mantle diamond. *Earth and Planetary Science Letters*, 250(3-4), 581-595.

Tomlinson, E. L., & Müller, W. (2009). A snapshot of mantle metasomatism: trace element analysis of coexisting fluid (LA-ICP-MS) and silicate (SIMS) inclusions in fibrous diamonds. *Earth and Planetary Science Letters*, 279(3-4), 362-372.

Van Orman, J. A., Grove, T. L., & Shimizu, N. (2001). Rare earth element diffusion in diopside: influence of temperature, pressure, and ionic radius, and an elastic model for diffusion in silicates. *Contributions to Mineralogy and Petrology*, 141(6), 687-703.

Van Orman, J. A., Grove, T. L., Shimizu, N., & Layne, G. D. (2002). Rare earth element diffusion in a natural pyrope single crystal at 2.8 GPa. *Contributions to Mineralogy and Petrology*, 142(4), 416-424.

Viljoen, K. S., Perritt, S. H., & Chinn, I. L. (2018). An unusual suite of eclogitic, websteritic and transitional websteritic-lherzolitic diamonds from the Voorspoed kimberlite in South Africa: Mineral inclusions and infrared characteristics. *Lithos*, 320, 416-434.

Viljoen, K. F., Dobbe, R., Smit, B., Thomassot, E., & Cartigny, P. (2004). Petrology and geochemistry of a diamondiferous lherzolite from the Premier diamond mine, South Africa. *Lithos*, 77(1-4), 539-552.

Wasserburg, G. J., Jacobsen, S. B., DePaolo, D. J., McCulloch, M. T., & Wen, T. (1981). Precise determination of SmNd ratios, Sm and Nd isotopic abundances in standard solutions. *Geochimica et Cosmochimica Acta*, 45(12), 2311-2323.

Weiss, Y., Griffin, W. L., & Navon, O. (2013). Diamond-forming fluids in fibrous diamonds: the trace-element perspective. *Earth and Planetary Science Letters,* 376, 110-125.

Weiss, Y., Kessel, R., Griffin, W. L., Kiflawi, I., Klein-BenDavid, O., Bell, D. R., ... & Navon, O. (2009). A new model for the evolution of diamond-forming fluids: Evidence from microinclusion-bearing diamonds from Kankan, Guinea. *Lithos*, 112, 660-674.

Weiss, Y., Kiflawi, I., Davies, N., & Navon, O. (2014). High-density fluids and the growth of monocrystalline diamonds. *Geochimica et Cosmochimica Acta*, 141, 145-159.

Weiss, Y., Navon, O., Goldstein, S. L., & Harris, J. W. (2018). Inclusions in diamonds constrain thermo-chemical conditions during Mesozoic metasomatism of the Kaapvaal cratonic mantle. *Earth and Planetary Science Letters*, 491, 134-147.

Weiss, Y., McNeill, J., Pearson, D. G., Nowell, G. M., & Ottley, C. J. (2015). Highly saline fluids from a subducting slab as the source for fluid-rich diamonds. *Nature*, 524(7565), 339.

White, R. S. (1997). Mantle plume origin for the Karoo and Ventersdorp flood basalts, South Africa. *South African Journal of Geology*, 100(4), 271-282.

Whitney, D. L., & Evans, B. W. (2010). Abbreviations for names of rock-forming minerals. *American mineralogist*, 95(1), 185-187.

Windl, W., Pavone, P., Karch, K., Schütt, O., Strauch, D., Giannozzi, P., & Baroni, S. (1993). Second-order Raman spectra of diamond from ab initio phonon calculations. *Physical Review B*, 48(5), 3164.

Zhang, Y. (2010). Diffusion in minerals and melts: theoretical background. *Reviews in Mineralogy and Geochemistry*, 72(1), 5-59.

Zhang, B., & Wu, X. (2012). Calculation of self-diffusion coefficients in diamond. *Applied Physics Letters*, 100(5), 051901.

Zotov, N., & Keppler, H. (2002). Silica speciation in aqueous fluids at high pressures and high temperatures. *Chemical Geology*, 184(1-2), 71-82.

# Acknowledgments

A conclusione del presente elaborato di tesi desidero dedicare le ultime pagine alle persone che hanno svolto un ruolo fondamentale durante la scrittura dello stesso, nonché in questi anni di studio, nell'auspicio che loro presenza possa continuare ad affiancarmi anche in futuro.

In primis, ringrazio il mio relatore, il professor *Fabrizio Nestola*, per aver stimolato in me l'interesse per l'argomento di tesi ivi discusso, per avermi mostrato aspetti dello stesso che senza di lui avrei ignorato, ma soprattutto per la fiducia che ha sempre riposto nei miei confronti e l'entusiasmo che mi ha trasmesso. Avrò sempre a cuore i suoi insegnamenti, altrettanto preziosi come lo sono i diamanti oggetto di studio. Tra le altre figure accademiche, ringrazio soprattutto il mio correlatore, il *Dr. Leonardo Pasqualetto*, dottorando di ricerca presso il Dipartimento di Geoscienze dell'Università di Padova, il quale mi ha seguita in tutta la fase di stesura, aiutandomi a condurre le analisi su cui si basa la presente tesi. In particolare, gli sono grata per i saggi consigli di cui mi ha fatto dono, senza i quali non sarei mai riuscita a correggermi e migliorarmi.

Ringrazio anche tutti i professori del *Dipartimento di Geoscienze* per l'esempio che mi hanno dato in questi anni, e che io considero indimenticabile, di come sia possibile amare lo studio delle scienze geologiche, disciplina unica nella sua capacità di far viaggiare nel tempo e nello spazio, alla scoperta degli arcani segreti del nostro pianeta. Vorrei ringraziare anche tutto il personale dello stesso dipartimento e della biblioteca, i quali hanno sempre mostrato gentilezza e disponibilità nei miei confronti. Ringrazio i compagni e amici di corso, con i quali ho condiviso gioie e dolori di questi anni di studio.

Un ringraziamento speciale va alla mia *famiglia*, per il sostegno economico, ma soprattutto morale, che ha fatto sì che questo giorno potesse arrivare. In particolare, ringrazio i miei *genitori*, che nella loro dolcezza e premurosità, mi hanno insegnato il valore dello studio e della conoscenza, accompagnandomi nei momenti più difficili di questi anni. Rivolgo un ultimo e importante ringraziamento al mio fidanzato *Andrea*, che con il suo amore e la sua pazienza lungimirante ha sempre creduto in me, aiutandomi ad affrontare le mie innumerevoli debolezze e ad esaltare le mie capacità.

Padova, 4.XII.2019.

*Pia Antonietta Antignani*

# Appendix A

# Modeling of Sm-Nd diffusion in clinopyroxene

The numerical model used in this thesis work to constrain the equilibration times between clinopyroxene and diamond-forming fluid/melt has been elaborated by Jacob D.E. and her scientific team (Department of Earth and Planetary Science, Macquarie University, Australia).

The model considered a free-defect grain of clinopyroxene with slab symmetry in contact with melt, assuming that the extent of Nd re-equilibration within each mineral grain depends on diffusive mass-flux along a concentration gradient of thermodynamic potentials, according to the *Fick's first law* (A. Fick, 1885):

$$F = -D \frac{\partial C_s}{\partial x}, \qquad \text{(A.1)}$$

where $F$ is the diffusive mass flow of Nd (mol/m$^2$ s), $C_s$ is the concentration (mol/m$^3$) of Nd along the $x$-direction of mineral grain ($s$ refers to solid), $D$ is the diffusion coefficient (m$^2$/s), and $\partial C/\partial x$ is the concentration gradient (mol/m$^2$).

The diffusion coefficient indicates the "rate" of diffusion, and, hence, is fundamental in quantifying diffusion. The diffusion coefficient for clinopyroxene used in the numerical model follows the Arrhenius relation and is the slowest reported in the literature for Sm and Nd in clinopyroxene [7.94 x $10^{-5}$ m$^2$/s ($\log_{10}D_{Nd}$= -2.94 ± 2.64); from Van Orman et al., (2001,2002)], which was corrected for the effect of pressure on the activation volume of ~ 9 cm$^3$/mol (Van Orman et al. 2001, 2002).

The model calculations also assumed that the grain-boundary is always in equilibrium with the surrounding medium, such that the concentration of Nd in the melt and mineral grain is linked by the partition coefficient *K* between the mineral and melt. If *K* is the partition coefficient between the clinopyroxene and melt (Sun and Liang, 2014), it results that:

$$C_s\,(R,\,t) = K\,Cm(t), \tag{A.2}$$

where *R* is the representative crystal size of the mineral grain along *x*-direction, *m* refers to melt, and *t* is time.

The equilibration times were obtained by solving the one-dimensional partial differential equation that describes how a concentration profile would evolve with time *t*, given the initial concentration distribution of Nd between the mineral/melt interface, namely the diffusion equation, also known as *Fick's second law*. This law is stated as follow:

$$\frac{\partial C_s(x,t)}{\partial t} = D\,\frac{\partial {C_s}^2(x,t)}{\partial x^2}, \quad 0 \le x \le R. \tag{A.3}$$

The analytical solution of the equation A.3 was proposed by Crank (1975) for different geometries and can be iterate by using a numerical model in MATLAB until the concentration gradient vanished and the system homogenizes.

Accordingly, the model used in this thesis work was run until the concentration profile of Nd reached the required equilibration level, defined by the following equations:

$$tol = \frac{int_{t=\infty} - int_t}{int_{t=\infty} - int_{t=0}}, \tag{A.4}$$

$$int_t = \int_0^R C(x,t)dx. \tag{A.5}$$

In the following table are reported all the equilibration times calculated with the diffusion model explained above, as a function of pressure, temperature, and grain size.

**Table A-1.** Calculated maximum times for equilibration of clinopyroxene grains of different size with a diamond-forming fluid at pressure-temperature conditions corresponding to 35, 40, and 45 $mWm^{-2}$ cratonic geotherms from Hasterok and Chapman (2011).

| **Geotherm temperature** | **Clinopyroxene grain size** | | |
|---|---|---|---|
| | *0.1 mm* | *0.5 mm* | *1 mm* |
| ***35 mWm$^{-2}$*** | | | |
| 900°C | 2.0 x $10^{11}$ yrs | 5.0 x $10^{12}$ yrs | 2.0 x $10^{13}$ yrs |
| 1000°C | 4.8 x $10^{9}$ yrs | 1.2 x $10^{11}$ yrs | 4.8x $10^{11}$ yrs |
| 1100°C | 2.0 x $10^{8}$ yrs | 5.1 x $10^{9}$ yrs | 2.0 x $10^{10}$ yrs |
| 1200°C | 1.3 x $10^{7}$ yrs | 3.4 x $10^{8}$ yrs | 1.3 x $10^{9}$ yrs |
| 1300°C | 1.3 x $10^{6}$ yrs | 3.2 x $10^{7}$ yrs | 1.3 x $10^{8}$ yrs |
| 1400°C | 1.6 x $10^{5}$ yrs | 4.0 x $10^{6}$ yrs | 1.6 x $10^{7}$ yrs |
| ***40 mWm$^{-2}$*** | | | |
| 900°C | 7.6 x $10^{10}$ yrs | 1.9 x $10^{12}$ yrs | 7.6 x $10^{12}$ yrs |
| 1000°C | 1.7 x $10^{9}$ yrs | 4.3 x $10^{10}$ yrs | 1.7 x $10^{11}$ yrs |
| 1100°C | 6.8 x $10^{7}$ yrs | 1.7 x $10^{9}$ yrs | 6.8 x $10^{9}$ yrs |
| 1200°C | 4.2 x $10^{6}$ yrs | 1.1 x $10^{8}$ yrs | 4.2 x $10^{8}$ yrs |
| 1300°C | 3.7 x $10^{5}$ yrs | 9.3 x $10^{6}$ yrs | 3.7 x $10^{6}$ yrs |
| 1400°C | 4.4 x $10^{4}$ yrs | 1.1 x $10^{6}$ yrs | 4.4 x $10^{6}$ yrs |
| ***45 mWm$^{-2}$*** | | | |
| 900°C | 3.5 x $10^{10}$ yrs | 8.7 x $10^{11}$ yrs | 3.5 x $10^{12}$ yrs |
| 1000°C | 7.6 x $10^{8}$ yrs | 1.9 x $10^{10}$ yrs | 7.6 x $10^{10}$ yrs |
| 1100°C° | 2.9 x $10^{7}$ yrs | 7.2 x $10^{8}$ yrs | 2.9 x $10^{9}$ yrs |
| 1200°C | 1.7 x $10^{6}$ yrs | 4.3 x $10^{7}$ yrs | 1.7 x $10^{8}$ yrs |
| 1300°C | 1.4 x $10^{5}$ yrs | 3.6 x $10^{6}$ yrs | 1.4 x $10^{7}$ yrs |
| 1400°C | 1.6 x $10^{4}$ yrs | 4.1 x $10^{5}$ yrs | 1.6 x $10^{6}$ yrs |

# Appendix B

# Collected UB matrices

The UB matrices of each analyzed host- inclusion pair are reported below, using a similar format used to write the input data file required by the OrientXplot software (Angel et al., 2015, see § 4.2). Three columns of matrices are given, in which each line reports first the UB matrices of the diamond hosts respect to which the UB matrices of the clinopyroxene inclusions of the next line is referenced. Therefore, a couple of UB matrices characterizes each host-inclusion pair. The numbers and labels accompanying the UB matrices of each host-inclusion pair are the same reported in Table 5-1 in § 5.1.

HOST 1 DIA Lot41stone1_inc1
-0.066737 0.130444 0.138277
-0.185905 -0.058447 -0.032980
0.018355 -0.139745 0.140787

HOST 2 DIA Lot41stone1_inc2
0.136642 0.067912 -0.128509
-0.033386 0.184760 0.059774
0.139766 -0.018204 0.139885

HOST 3 DIA Lot41stone1_inc3
0.124988 -0.066640 -0.135912
-0.061080 -0.184855 0.033604
-0.138768 0.016993 -0.137611

INC 1 CPX Lot41stone1_inc1
0.038317 -0.062225 0.072217
-0.057341 -0.011389 0.061335
-0.034412 -0.050002 -0.103293

INC 2 CPX Lot41stone1_inc2
0.042485 -0.042732 -0.066925
0.038253 0.067003 -0.016278
0.051475 -0.014524 0.121813

INC 3 CPX Lot41stone1_inc3
-0.036787 -0.043372 0.076563
-0.013332 -0.057749 -0.097544
0.066522 -0.035663 0.064664

HOST 4 DIA Lot41stone1_inc4
0.118156 0.115582 -0.110353
-0.069966 0.156085 0.091362
0.141157 -0.020807 0.133978

HOST 5 DIA Lot41stone2_inc1
-0.060077 -0.095947 0.158770
-0.002964 -0.165139 -0.102715
0.187765 -0.033889 0.052540

HOST 6 DIA Lot41stone2_inc2
0.198086 -0.006162 0.009052
0.001807 0.205200 -0.004690
0.001789 0.006294 0.201758

INC 4 CPX Lot41stone1_inc4
-0.040648 -0.056681 0.045146
-0.001687 -0.044208 -0.113902
0.065512 -0.036337 0.067675

INC 5 CPX Lot41stone2_inc1
-0.071380 0.027208 -0.048013
0.001809 0.026132 0.129152
0.026774 0.070317 -0.029105

INC 6 CPX Lot41stone2_inc2
-0.070998 -0.021803 -0.059881
0.019843 -0.013936 -0.118850
0.015616 -0.077333 0.038492

HOST 7 DIA Lot41stone2_inc3

0.114645 0.084188 -0.138898
-0.020968 -0.163848 -0.104271
-0.159566 0.075358 -0.086535

HOST 8 DIA Lot41stone2_inc4

-0.061357 -0.142757 0.114799
0.009577 -0.127335 -0.149732
0.186651 -0.035466 0.045886

HOST 9 DIA Lot34stone2_inc1

0.035581 -0.139407 -0.128492
0.064615 0.132802 -0.129938
0.180275 -0.017273 0.083276

INC 7 CPX Lot41stone2_inc3

0.074628 -0.001394 0.004213
-0.018431 -0.003002 -0.140985
0.000604 0.080030 -0.005195

INC 8 CPX Lot41stone2_inc4

-0.072299 -0.009974 0.004225
0.022421 0.005452 0.141154
-0.011811 0.079043 -0.008386

INC 9 CPX Lot34stone2_inc1

0.010275 0.062185 0.088234
-0.043131 -0.035694 0.072709
0.061898 -0.035592 0.085749

HOST 10 DIA Lot34stone2_inc2

0.138703 0.134451 -0.038910
-0.124602 0.142524 0.050344
0.056144 -0.018078 0.183982

HOST 11 DIA Lot34stone2_inc3

-0.050983 -0.157847 -0.099641
-0.152612 -0.028282 0.119432
-0.105278 0.109659 -0.134131

HOST 12 DIA Lot34stone18_inc1

0.131390 0.140366 -0.033593
-0.111174 0.129505 0.098582
0.091403 -0.047974 0.167619

INC 10 CPX Lot34stone2_inc2

-0.019953 0.070531 0.043275
0.050363 0.034626 -0.058353
-0.054567 0.006800 -0.123894

INC 11 CPX Lot34stone2_inc3

-0.001223 -0.026671 0.127462
0.000748 -0.075270 -0.044786
0.076426 0.000272 0.041691

INC 12 CPX Lot34stone18_inc1

-0.064576 0.041378 -0.014987
-0.009739 0.002118 -0.138922
-0.039484 -0.067825 -0.013198

HOST 13 DIA Lot34stone18_inc2

-0.027412 0.084279 0.174028
0.032586 0.178114 -0.086183
-0.185390 0.016696 -0.044296

HOST 14 DIA Lot34stone18_inc3

0.130153 0.140702 -0.030234
-0.111779 0.130691 0.099455
0.094008 -0.046446 0.166945

HOST 15 DIA Lot34stone18_inc4

0.043932 0.190804 0.031669
-0.169733 0.020433 0.098592
0.094373 -0.046219 0.166918

INC 13 CPX Lot34stone18_inc2

0.025600 0.066550 0.069540
-0.066334 0.008441 0.033339
0.027769 -0.042691 0.117512

INC 14 CPX Lot34stone18_inc3

0.049650 0.060114 0.030790
0.041092 -0.042281 0.108904
0.040263 -0.031853 -0.082227

INC 15 CPX Lot34stone18_inc4

-0.050850 0.034107 0.057831
0.008755 0.069191 -0.061010
-0.056351 -0.019386 -0.112127

HOST 16 DIA Lot34stone21_inc1

-0.015007 -0.002647 0.193139
-0.002983 -0.201092 -0.006358
0.196291 -0.011361 0.008991

HOST 17 DIA Lot34stone22_inc1

-0.060470 -0.187847 0.004953
0.155144 -0.045623 -0.105284
0.113495 -0.026470 0.160961

HOST 18 DIA Lot34stone22_inc2

0.100429 -0.167653 0.013002
-0.071499 -0.061143 -0.174185
0.147702 0.086305 -0.095330

INC 16 CPX Lot34stone21_inc1

-0.043961 -0.037018 0.069339
0.044865 -0.064511 0.014850
0.043259 0.028915 0.121423

INC 17 CPX Lot34stone22_inc1

-0.054010 0.013579 -0.122491
0.000919 0.076877 0.030254
0.054818 0.012191 -0.067492

INC 18 CPX Lot34stone22_inc2

0.002751 0.060382 0.089706
-0.074394 0.013470 -0.057750
-0.016825 -0.050295 0.092448

HOST 19 DIA Lot34stone22_inc3

0.036175 -0.169282 -0.093387
-0.157882 -0.077486 0.080000
-0.107711 0.051232 -0.162142

HOST 20 DIA Lot34stone22_inc4

-0.009800 -0.182702 -0.064042
0.168908 0.021200 -0.094986
0.104881 -0.062033 0.153734

HOST 21 DIA Lot22stone36_inc1

0.144642 0.082349 -0.104514
-0.044224 0.173162 0.076854
0.123087 -0.035670 0.148398

INC 19 CPX Lot34stone22_inc3

0.049500 0.005707 0.127963
0.033447 -0.067861 -0.023266
0.047614 0.041732 -0.054649

INC 20 CPX Lot34stone22_inc4

-0.025105 0.073897 -0.036172
-0.012923 -0.019301 -0.135968
-0.070933 -0.022548 -0.002657

INC 21 CPX Lot22stone36_inc1

-0.033229 0.019608 0.100077
0.043943 -0.051569 0.088687
0.052116 0.056315 0.047060

HOST 22 DIA Lot22stone36_inc2

0.097879 0.088747 -0.143719
0.046501 -0.174319 -0.074962
-0.164762 0.005014 -0.110318

HOST 23 DIA Lot22stone36_inc3

0.146484 -0.087445 -0.100235
0.075956 0.176256 -0.045918
0.111046 -0.001782 0.161890

HOST 24 DIA Lot22stone36_inc4

0.122897 0.133830 -0.079225
-0.085298 0.138757 0.111035
0.131489 -0.036477 0.143074

INC 22 CPX Lot22stone36_inc2

0.047841 0.050011 -0.041805
0.060029 -0.033516 0.095027
0.006984 -0.053671 -0.097681

INC 23 CPX Lot22stone36_inc3

-0.020421 -0.004812 -0.139970
0.052079 0.054095 -0.006806
0.051021 -0.057773 0.005745

INC 24 CPX Lot22stone36_inc4

-0.011119 0.058868 -0.094653
0.010910 -0.051408 -0.096494
-0.074726 -0.015518 -0.038619

HOST 25 DIA Lot22stone36_inc5

0.078007 -0.134965 -0.126728
-0.111786 -0.142012 0.085653
-0.144110 0.038839 -0.131266

HOST 26 DIA Lot22stone36_inc6

0.100771 0.087488 -0.146490
0.048845 -0.175367 -0.075270
-0.164954 0.002518 -0.112589

HOST 27 DIA Lot22stone36_inc7

0.144962 -0.087672 -0.098685
0.074789 0.173981 -0.046379
0.112454 -0.004289 0.166237

INC 25 CPX Lot22stone36_inc5

-0.025992 -0.051903 -0.104141
0.029443 0.043392 -0.085430
0.065232 -0.040683 0.041643

INC 26 CPX Lot22stone36_inc6

-0.039935 0.056867 0.041737
0.054312 0.005723 0.122416
0.035640 0.055458 -0.056465

INC 27 CPX Lot22stone36_inc7

0.024028 0.022335 0.134394
0.060412 -0.047843 0.018690
0.039455 0.059872 -0.034220

HOST 28 DIA Lot22stone36_inc8

0.147624 -0.087135 -0.099794
0.074650 0.176001 -0.046323
0.115604 -0.006817 0.166076

HOST 29 DIA Lot22stone36_inc9

0.101267 0.087240 -0.146775
0.046160 -0.178781 -0.078037
-0.166902 0.004192 -0.113436

HOST 30 DIA Lot22stone36_inc10

0.102468 0.086285 -0.145524
0.046052 -0.175775 -0.076984
-0.165310 0.003868 -0.111253

INC 28 CPX Lot22stone36_inc8

0.024464 -0.022652 -0.111706
0.060754 0.047757 0.042542
0.039849 -0.060204 0.074884

INC 29 CPX Lot22stone36_inc9

-0.020528 -0.004920 -0.140456
0.052583 0.054619 -0.007013
0.051351 -0.058163 0.005561

INC 30 CPX Lot22stone36_inc10

-0.029429 -0.073621 -0.016699
-0.059825 0.025590 0.041446
-0.037487 0.015137 -0.135013

HOST 31 DIA Lot22stone36_inc11

0.144829 -0.088815 -0.102653
0.075356 0.174656 -0.044756
0.110933 -0.002982 0.165729

HOST 32 DIA Lot10stone21_inc1

-0.128729 0.131267 0.064984
0.137687 0.144984 -0.012180
-0.055069 0.043904 -0.188432

HOST 33 DIA Lot10stone21_inc2

-0.129056 0.128617 0.067149
0.136838 0.142495 -0.010227
-0.053721 0.039450 -0.184715

INC 31 CPX Lot22stone36_inc11

0.048445 -0.052854 0.078172
0.058002 0.035211 -0.034969
0.009917 0.048175 0.111749

INC 32 CPX Lot10stone21_inc1

-0.048693 0.004544 0.078080
0.011063 0.078767 0.012016
-0.057506 0.011331 -0.116425

INC 33 CPX Lot10stone21_inc2

0.042308 0.015253 -0.087461
-0.004875 0.078074 0.022550
0.062955 -0.004037 0.107825

HOST 34 DIA Lot8stone_4_inc1

-0.123674 -0.058528 0.145409
0.008549 0.178838 0.081615
-0.155875 0.057763 -0.108008

HOST 35 DIA Lot8Stone4_inc2

0.083883 0.170994 -0.054041
-0.070936 0.083283 0.157414
0.161353 -0.043445 0.096481

HOST 36 DIA Lot8Stone4_inc3

0.054555 -0.168488 -0.079874
-0.163300 -0.087334 0.072953
-0.095744 0.046456 -0.164090

INC 34 CPX Lot8stone4_inc1

0.056712 -0.040978 0.085250
-0.033157 -0.066159 -0.056293
0.038412 0.004056 -0.098382

INC 35 CPX Lot8Stone4_inc2

-0.048320 0.059838 -0.038870
0.056621 0.046693 -0.011712
-0.011520 -0.021444 -0.133074

INC 36 CPX Lot8Stone4_inc3

0.010946 -0.071231 0.058627
-0.067033 -0.023586 -0.081350
0.032903 -0.024202 -0.096891

HOST 37 DIA Lot8Stone4_inc5

0.081485 0.168295 -0.056180
-0.072214 0.086440 0.159099
0.164291 -0.046156 0.096237

INC 37 CPX Lot8Stone4_inc5

0.023097 0.024770 0.131400
-0.039025 -0.058081 0.039771
0.060506 -0.047241 0.020953

# Appendix C

# Collected micro-Raman spectra

Raman spectra of the samples investigated with micro-Raman confocal spectroscopy are reported below. In Figure C.1 are reported the Raman spectra collected out on the rims of clinopyroxene inclusions, while in Figure C.2 are shown those obtained from the clinopyroxene inclusions. Data relative to the observed Raman-active fluid films around the inclusions are reported in Table 5-2 in § 5.2.

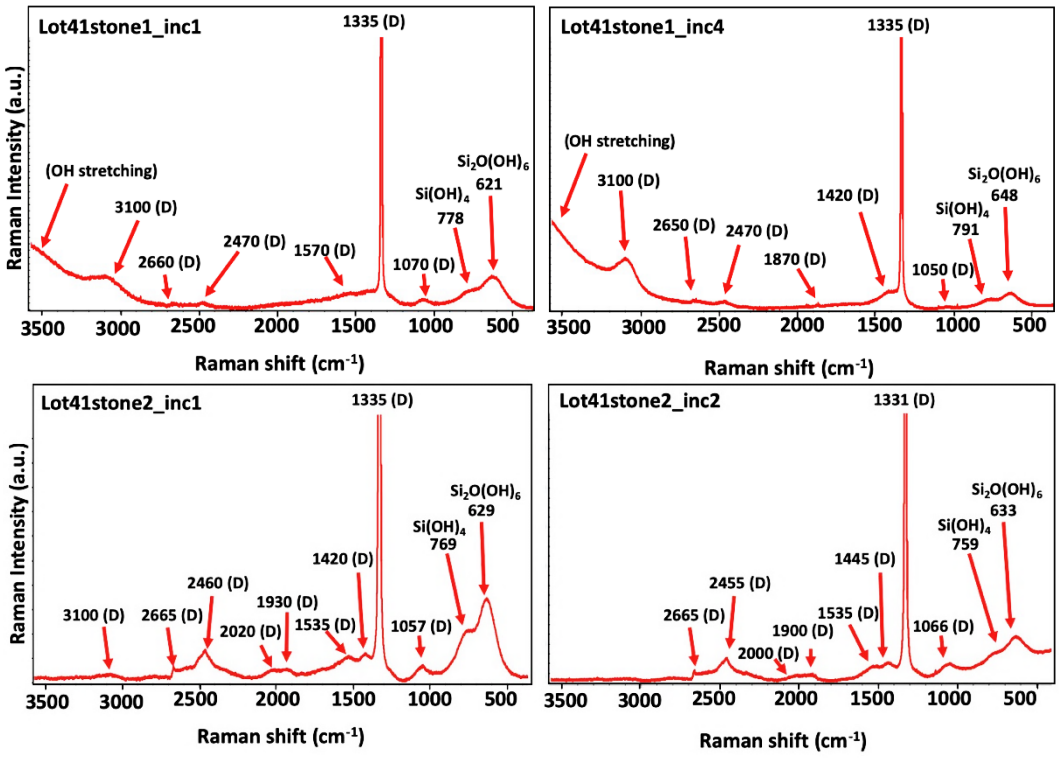


**Figure C.1**. Raman spectra collected out on the rims of the investigated clinopyroxene inclusions. D = diamond. The diamond peaks at ~ 1333 $cm^{-1}$ are truncated. The two peaks at 617-659 $cm^{-1}$ and 759-805 $cm^{-1}$ are relative to $Si_2O(OH)_6$ dimers and $Si(OH)_4$ monomers in aqueous fluid, respectively; (*continued on next pages*).

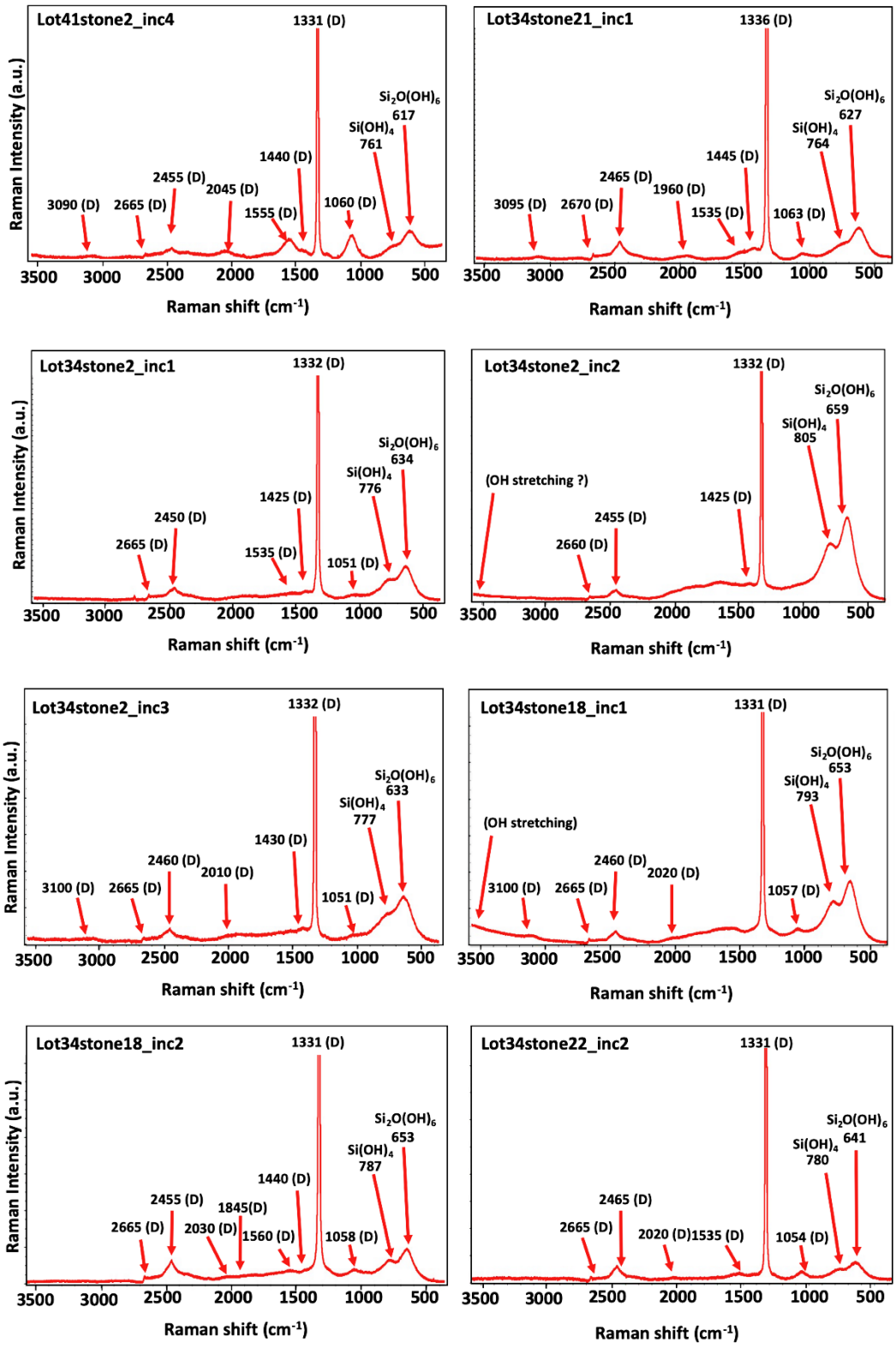


**Figure C.1** (*continued*).

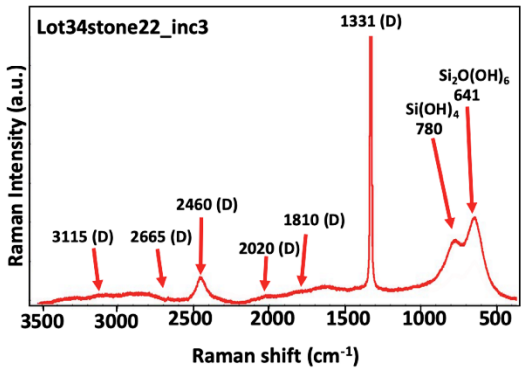


**Figure C.1** (*continued*).

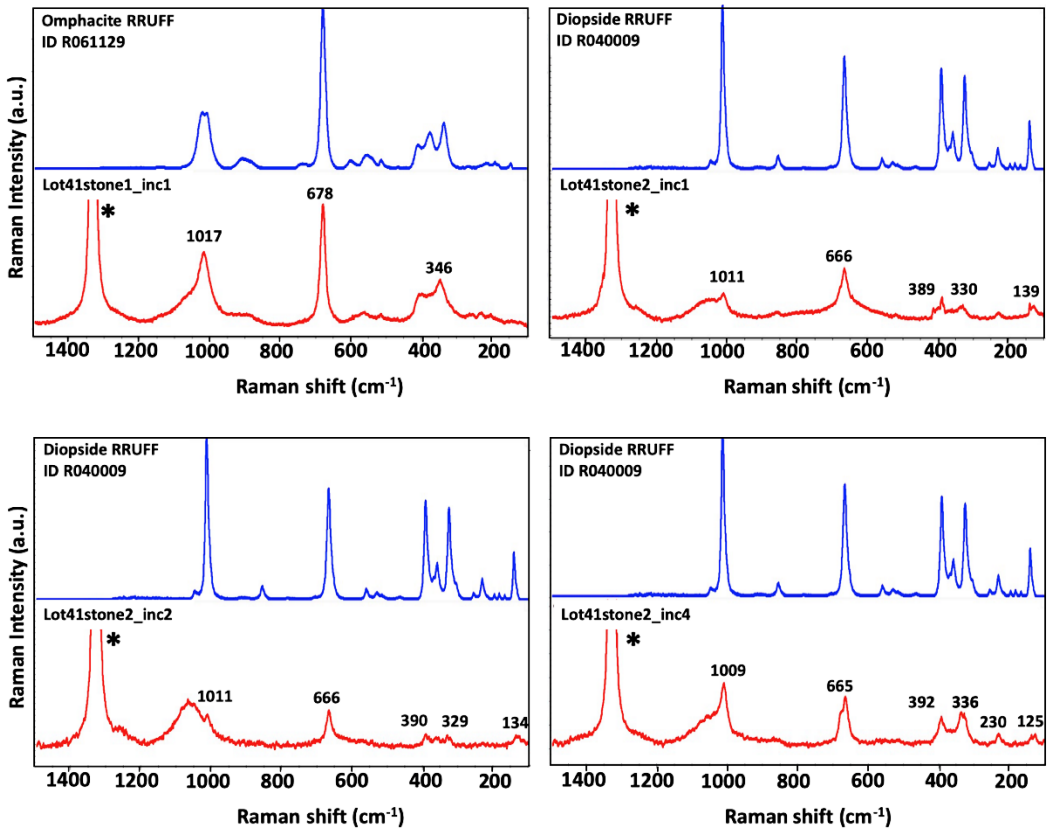


**Figure C.2.** Raman spectra collected from clinopyroxene inclusions. The upper reference Raman spectra are from the RRUFF Raman minerals database. Raman peaks of diamond host at ~ 1333 $cm^{-1}$ are marked with asterisk and are truncated; (*continued on next pages*).

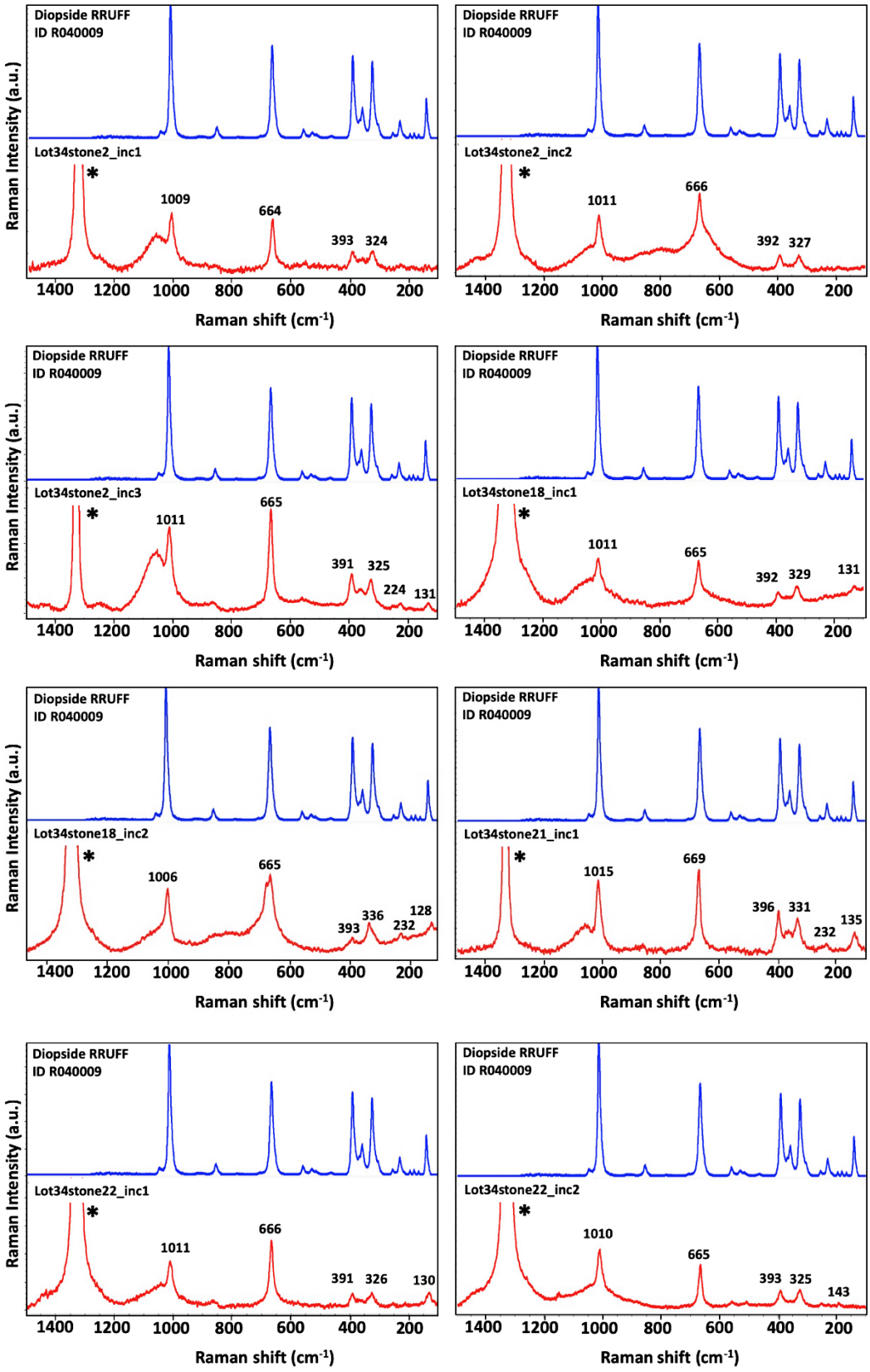


**Figure C.2** (*continued*).

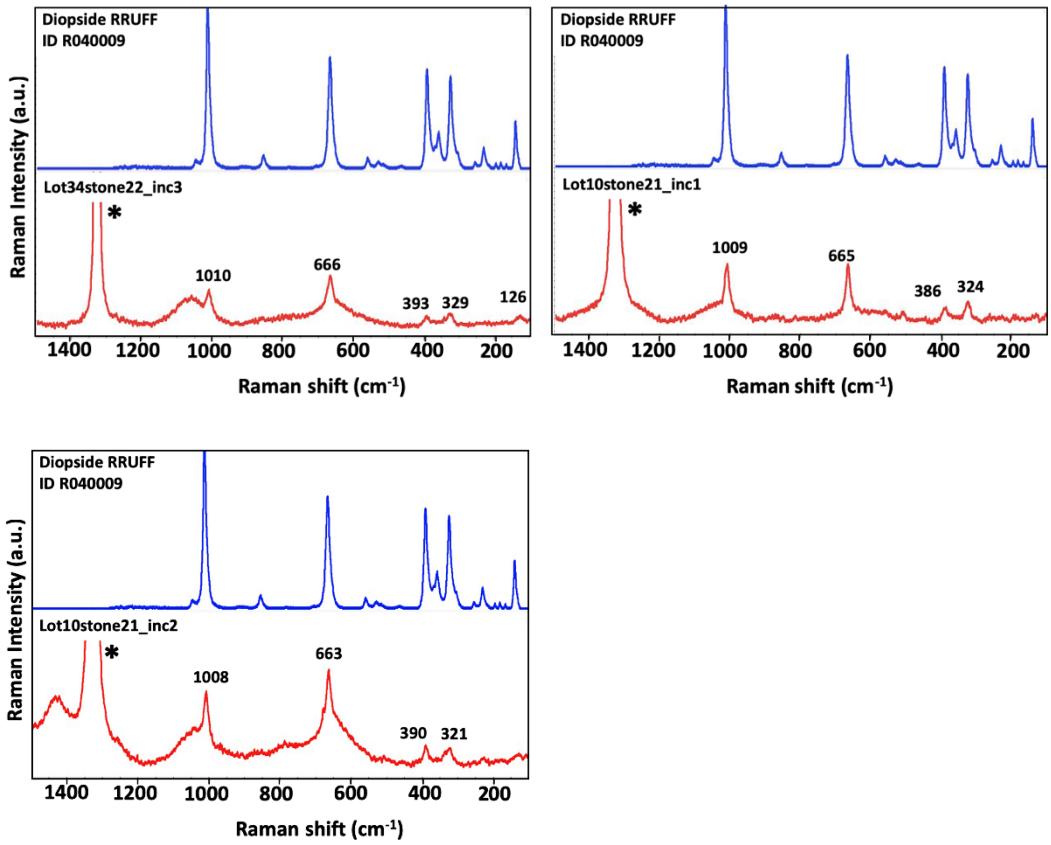


**Figure C.2** (*continued*).